UiT
THE ARCTIC UNIVERSITY OF NORWAY

Faculty of Science & Technology

Department of Geosciences

Sedimentary environment and seismic anomalies of the upper Brygge and Kai formations on the northern part of the Mid-Norwegian Continental Shelf

Suchada Y. Krokmyrdal

Master thesis in Geology, GEO-3900

May 2017

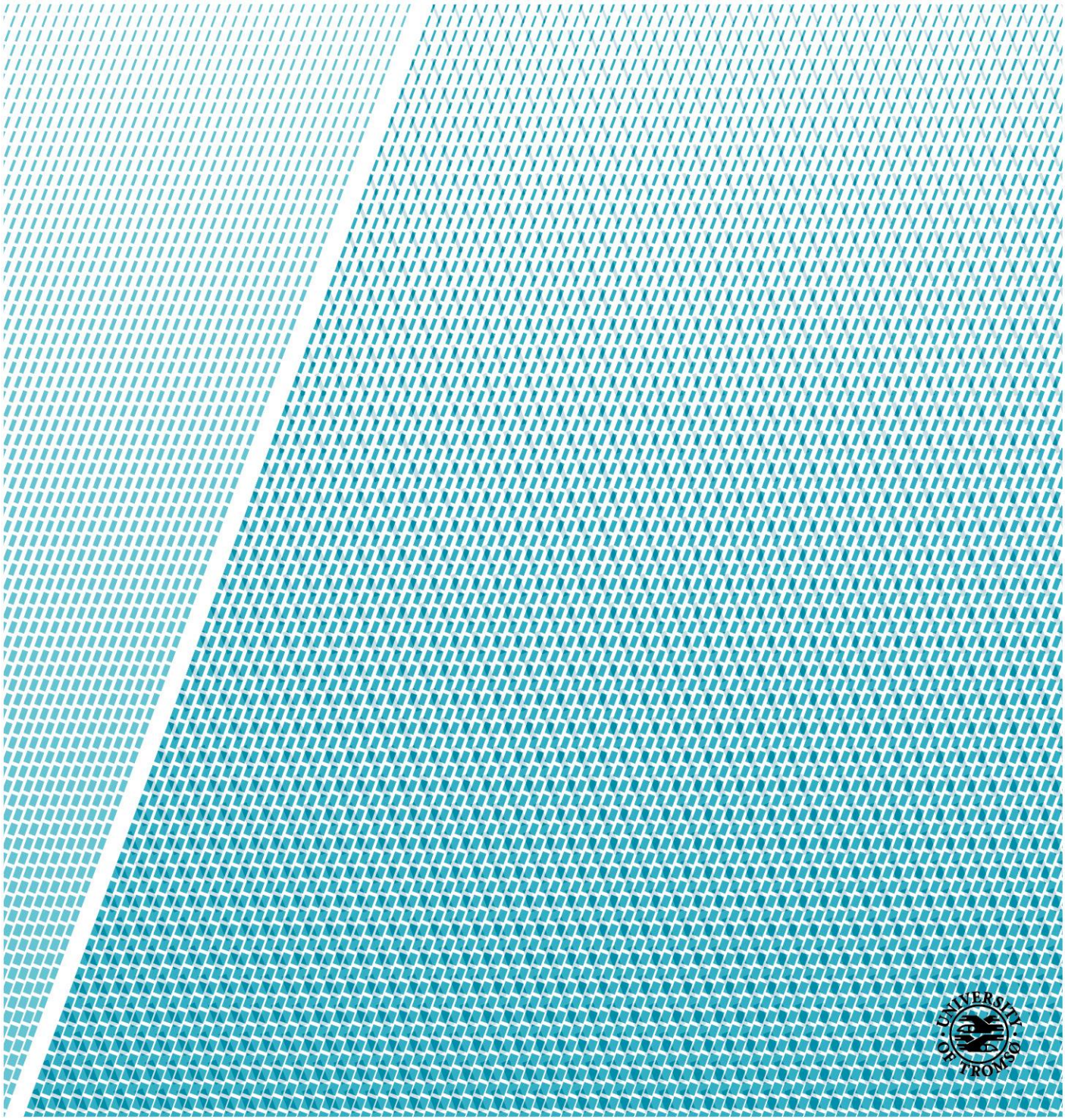

Abstract

The sedimentary environment and seismic anomalies of the upper Brygge and Kai formations on the northern part of the Mid-Norwegian Continental Shelf is analysed from 3D seismic data and the exploration well 6604/2-1. This was done in order to give a better understanding of the paleo-climatic development in the period before the establishment of the large-scale ice sheets of the Northern Hemisphere, and to provides a better insight in the relationship to fluid and/or gas migration from different levels in the subsurface. Based on a seismic stratigraphic analysis, correlation to well logs and previous work in the area, five seismic sub-units were recognized: B1-B2 of the upper Brygge Formation (pre-mid Miocene), and K1-K3 of the Kai Formation (mid Miocene-early Pliocene). The geometry and internal seismic reflection facies, as well as the morphology of buried surfaces have been described and discussed in relation to the depositional environment and the development of the ocean circulation pattern in the Norwegian Sea.

Based on the seismic analysis, a signature characteristic of contourite deposits was identified in the study area. Mounded elongated contourite drifts formed by ocean current-controlled deposition was observed in the upper Brygge Formation. After a period of tectonic uplift in the mid-Miocene, local anticlinal highs were developed, including the Helland-Hansen and Modgunn arches. These features probably played a major role in controlling the flow pattern of the ocean currents, associated with the deposition of the Kai Formation sediments. The ocean currents were entering the study area from the south, resulting in erosion in the southern part and deposition in the northern part. During the late Miocene-early Pliocene time, a change of the ocean current pattern led to erosion in the northern part, and deposition in the southeastern part of the study area.

Seismic attribute analysis revealed seismic anomalies, including circular forms. These are classified into three types, based on their stratigraphic distribution and dimensions, and association with fluid and/or gas migration from deep to shallow strata. The cluster of high amplitude anomalies, including bright spots and acoustic pipes indicate fluid flow originating from deep stratigraphic levels to terminate at or near the top of the Kai Formation. Paleo-pockmarks resulted from fluid migration along major faults from a deep thermogenic source, and eventually fluid expulsion from the polygonal fault system.

Acknowledgement

For 5 år siden sto det klart for meg at jeg ville ta mere utdanning, selvfølgelig i geologi. For jeg hadde blitt fascinert av det norske landskapet og jeg hadde massevis av spørsmål om det. Tenk som tiden går, plutselig sitter jeg på siste dagen ved institutt for geovitenskap, UiT. Det er litt trist å tenke på at jeg allerede er ferdig med studietiden.

Først vil jeg takke min hovedveileder, Professor Jan Sverre Laberg for at du ga meg muligheten til å jobbe med oppgaven som jeg hadde lyst på. Tusen hjertelig takk for innsats, kunnskap, oppfølging, veiledning og for at din kontordør alltid var åpen for meg når det dukket opp spørsmål. Dette er fantastisk og jeg setter veldig stor pris på det.
Tusen takk til mine biveiledere, Førsteamanuensis Tom Arne Rydningen for god veiledning om oppgaveskriving og for støttende ord, og senior geolog, Bjarne Rafaelsen for god veiledning og gode tekniske råd i Petrel programmet. Takk til rådgiver Ivar Martens for hjelp med overføring av brønndata til Petrel programmet.

Takk til mine medstudenter Katrine og Anna for at dere alltid spredte godt humør og for de koselige kaffepauser vi hadde sammen. Spesielt takk til Katrine for gode faglige diskusjonene og for oppdatering av nyttige studie nyheter.

Takk til mine gode venner både i Tromsø, Oslo og i Thailand som igjennom årene alltid har støttet meg opp. Takk til Taweerat og Pranee for god thaimat og hyggelige avvekslinger både fra jobb og studiet.

Takk til min familie i Thailand, mamma og min søster som alltid har støttet meg, og har kommet med gode råd når jeg har trengt det.

Takk til min kjære mann, Tor-Ketil og mine to barn Bjørn-Tore og Sigve, at dere bestandig er glad i meg og støtter meg. Selv om har jeg tilbrakt mye tid på kontoret det siste året, er vi fortsatt lykkelig sammen.

Suchada Yaiying Krokmyrdal

Tromsø, 15. mai 2017

Table of Contents

1 INTRODUCTON AND OBJECTIVES

The aims of this thesis are to 1) describe the sedimentary environment and the seismic anomalies of the Kai and the upper part of the Brygge Formations deposited on the Mid-Norwegian continental margin by using 3D seismic and well data, 2) discuss the origin of the deposits and the seismic anomalies, and 3) derive the paleo-environment during deposition.

The Brygge Formation is dominated by clay on the present-day shelf, and ooze-dominated sediments in the distal part, and deeper marine deposits in the Møre and Vøring Basins, and dated to early Eocene-early Miocene time (Eidvin et al., 2007). After the reginal uplift in mid Miocene, mud-dominated sediments belonging to the Kai Formation were deposited on the outer and middle parts of the Mid-Norwegian margin and dated to mid Miocene-early Pliocene (Eidvin et al., 2007). Base on a seismic stratigraphic analysis, the deposits of the Brygge and Kai formations will be divided into seismic sub-units. The geometry and internal seismic reflection facies will then be described and discussed, as well as the morphology of buried surfaces. Using available well data from the Norwegian Petroleum Directorate (NPD) web page, their lithology will also be described and discussed.

Furthermore, the sedimentary environment will be discussed in relation to the development of the oceanic circulation in the Norwegian Sea to provide an increased understanding of the paleo-climatic development in the period before the establishment of the large-scale ice sheets of the Northern Hemisphere.

Seismic anomalies are observed in the study area, and they will also be describes and discussed. This includes their relationship to geological features and their possible association to fluid and/or gas migration from deep to shallow strata.

1.1 Study Area

The study area comprises the Vøring Plateau on the northern part of the Mid-Norwegian continental margin. The 3-D seismic cube used is located between ~66°23'- 67°07 N and 3°47'- 5°34' E (Fig. 1.1.1).

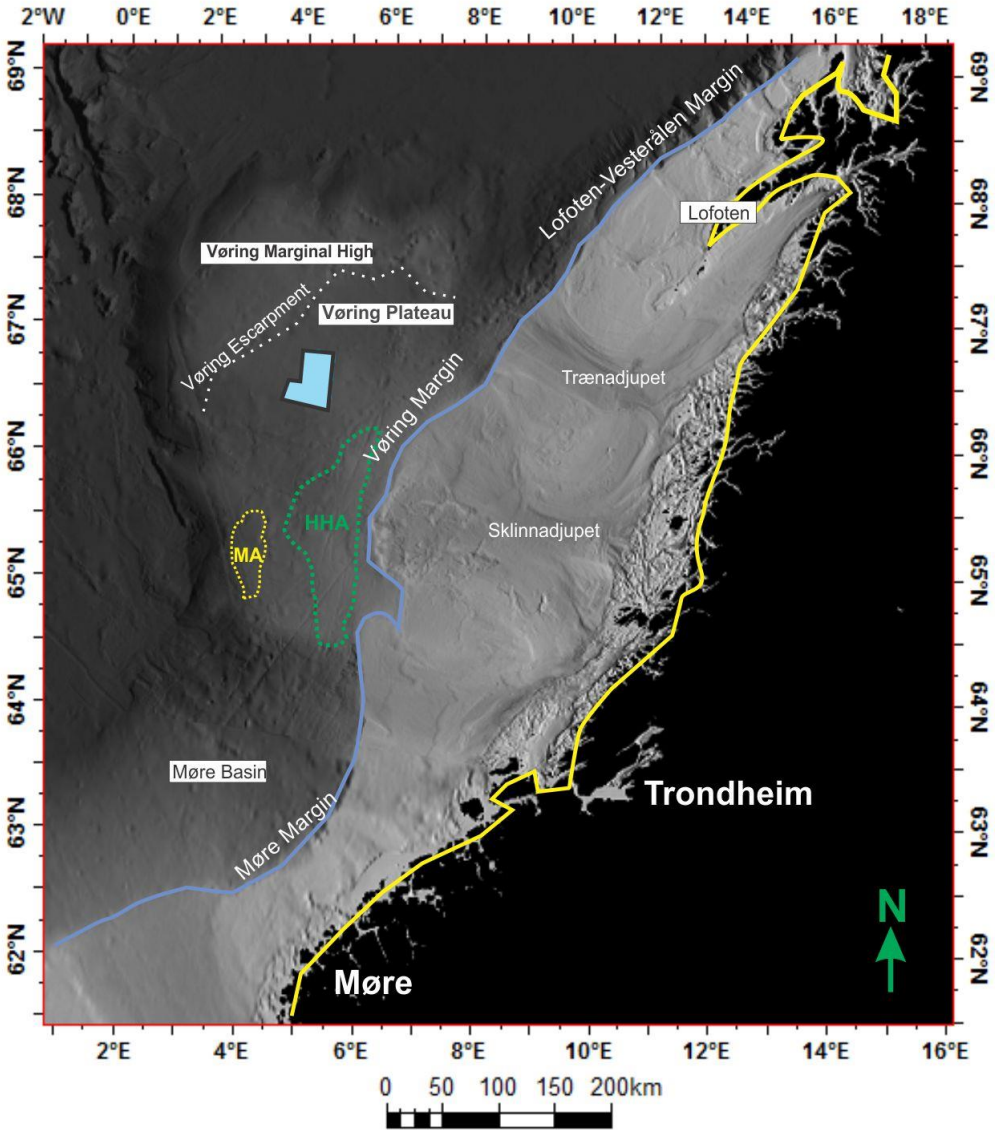

Figure 1.1.1: *Overview map of the Mid-Norwegian Continental margin. The location of 3D seismic cube used for this study is indicated as a blue polygon is located on the Vøring Plateau. Blue line displaying the Shelf edge, and yellow line indicating the Norwegian coastline.*

2 GEOLOGICAL BACKGROUND

2.1 Tectonic setting of the Mid-Norwegian continental margin

The tectono-magmatic evolution of the Mid-Norwegian margin can be divide to three parts (Faleide et al. 2008): (1) lithospheric extension during rifting in late Cretaceous-Palaeocene leading to break up and separation of the Eurasian and Greenland/North American tectonic plates, (2) During late rifting, the central rift was uplifted and increased igneous activity commenced, and after breakup voluminous basaltic lavas poured out in the early Eocene, (3) Change to normal sea-floor spreading with subsequent continental margin subsidence and maturation from mid Eocene to present day.

2.1.1 Opening of the Norwegian – Greenland Sea

2.1.1.1 Pre-breakup basin evolution

From the late Jurassic to Early Cretaceous rifting affected the NE Atlantic-Arctic region. The period of lithospheric extensions was followed by subsidence and resulted in the development of major Cretaceous sedimentary basins, such as the Møre and Vøring basins off mid-Norway (Hjelstuen et al., 1999; Faleide et al., 2008, 2015). As a result, the base Cretaceous is deeply buried in the most of the Vøring Basin (Morgensen et al., 2000). After the mid-Cretaceous, the post-rifted sediments have been deposited in the basin with a maximum thickness of 6-8 km, and these consist mainly fine-grained clastic sediments (Hjelstuen et al., 1999; Faleide et al., 2008).

2.1.1.2 Breakup-related tectonism and magmatism

The breakup in the NE Atlantic followed the rifting in the late Cretaceous-Palaeocene period. This included the main period of brittle faulting in Campanian time that resulted in low-angle detachment structures, lava intrusion and the formation of deep basins (Faleide et al., 2008, 2015). The extensional rifting was oriented in NW-SE direction. This extensional faulting took place by reactivation of the older NE-SW oriented Palaeozoic and/or Mesozoic faults of the area (Caledonian trend) (Mogensen et al., 2000; Faleide et al., 2008, 2015). The western part of these deep basins comprise thick accumulations of Paleocene sediments which were sourced from the uplifted rift zone in the west (Hjelstuen et al., 1999; Faleide et al., 2015).

This area of relative uplift during volcanic margin formation could be an importance source area for sediment accumulation in the basins in this period (Hjelstuen et al., 1999) such as the uplifted and eroded zone in the northwestern part of southern Norway, that resulted in sediment accumulation in the northeast North Sea and the southeastern Møre Basin (Faleide et al., 2015).

The final breakup occurred near the Paleocene-Eocene transition, at ~ 54-55 Ma ago (Planke and Alvestad, 1999; Faleide et al., 2008, 2015) (Fig. 2.1.1). The breakup started in the south and progressed northward. It included massive magmatic activity and lasted ca 3-6 m.y. before the final breakup and the initiation of seafloor spreading (Faleide et al., 2015). At the outer Møre- and Vøring margins dykes and sill intrusions penetrated the Cretaceous strata (Faleide et al., 2015). At the Vøring Basin, intrusive dykes and sills were identified as subaerially and/or neritically erupted basalt (Faleide et al., 2008). These includes characteristic unit of SDRs (seaward dipping reflectors sequences), which are seismic reflectors diagnostic of volcanic margins (Planke and Alvestad, 1999; Faleide et al., 2015).

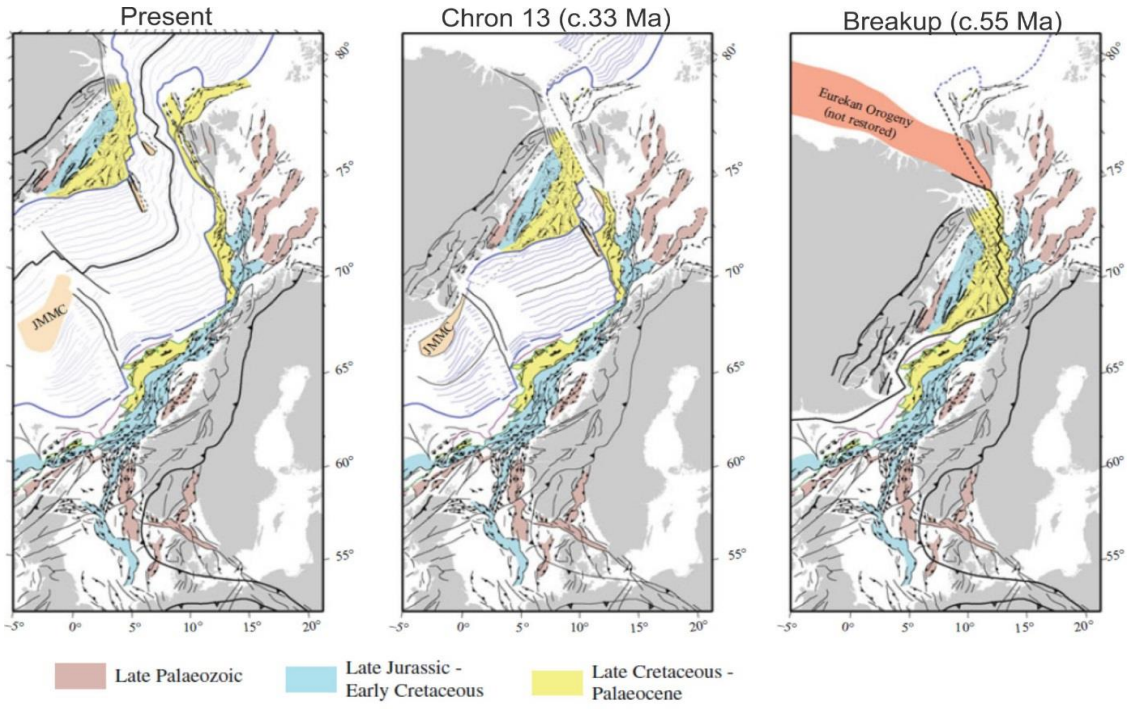

Figure 2.1.1*: A three stage model of the opening of the Norwegian -Greenland Sea from ca.55-54 Ma until present-day. The figure is adapted from Faleide et al., 2015*.

2.1.1.3 Post-breakup margin evolution

Since middle Eocene time, the mid-Norwegian margin evolved into a passive rifted margin bordering the oceanic Norwegian-Greenland Sea. The Vøring margin subsided rapidly in Eocene time, where the central Vøring Marginal High and the outer Vøring Basin subsided around 1000 m during Eocene (Eldholm et al., 1989; Hjelstuen et al., 1999). Along the subsiding margin, relatively moderate sedimentation occurred, until late Pliocene time when the Northern Hemisphere Glaciations greatly increased the Plio-Pleistocene deposition rates (Faleide et al., 2008). This led to rapid progradation offshore Mid-Norway (Faleide et al., 2008).

The ocean circulation has had a major influence on the sedimentary environment following the opening for the Fram Strait, in Miocene, and the increasing exchange of deep water though the Faroe Conduit (Southern gateway) because of the subsidence of the Greenland-Scotland Ridge (Stoker et al., 2005a). These conditions probably had the overall control on the deposition of the Miocene succession, which was dominated by excessive contourite sediment drifts and deposited in deep water condition (Laberg et al., 2005a). During an episode of middle Miocene compressional tectonism, large anticlines, synclines and elongated domes were formed in the deep-water areas of the Norwegian Sea and the outer part of the continental shelf (Stoker et al., 2005b; Eidvin et al., 2014). In late Miocene, sediment progradation on the inner continental shelf (Molo Formation) was caused by a regional uplift of Fennoscandia (Faleide et al., 2008).

2.2 Physiographic provinces (Møre, Vøring and Lofoten margins)

The present-day morphology of the mid-Norwegian continental shelf is dominated by a prograding sediment wedge, the Naust formation, deposited over the last 3 million years (Rise et al., 2005) (Fig. 2.2.1). The Møre and Vøring basins are presently buried under this wedge (Stoker et al., 2005b). During the deposition of the Naust formation, the middle and outer parts of the shelf have subsided, whereas the inner shelf and the mainland have been uplifted. The timing of the Neogene uplift phase is unclear, the Norwegian mountain range may already have been uplift before the large ice sheet spread to the coastal area around 2.8 million years ago (Ottensen et al., 2009). There are several hypotheses as to explain the timing and causes of the Cenozoic uplift (Henriksen and Vorren, 1996; Ottesen et al., 2009).

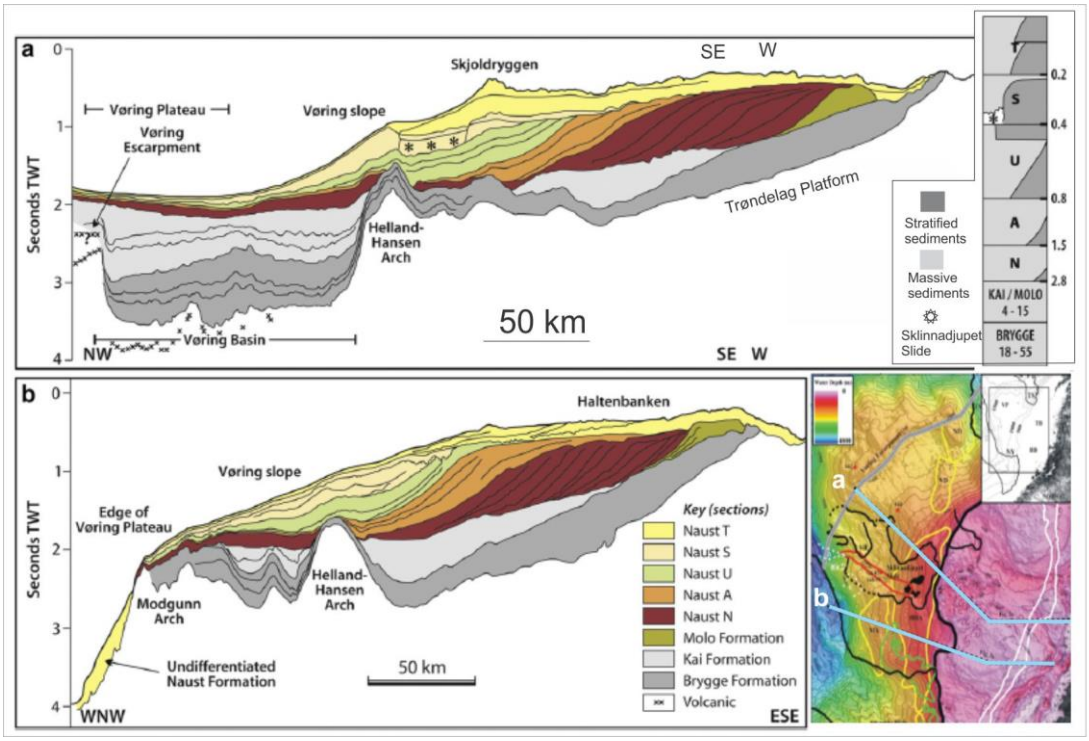

Figure 2.2.1: *Two interpreted seismic sections showing the general stratigraphy of the region. The age of the Naust sequences in million years is indicated. The location of the region and two seismic lines shown in the right corner. The figure is modified from Rise et al. (2010).*

The Møre margin, characterised by a narrow shelf and wide and gentle slope, is underlain by the wide and deep Møre Basin, which formed by rifting in late Jurassic-Early Cretaceous time (Fig. 2.2.2). The deep Møre basin is characterised by a thick Cretaceous successions (Eidvin

et al., 2014), which consists of several sub-basins separated by intra-basinal highs. The thickest part of the sedimentary succession (15-16 km) is in the western part of the basin and decreases landwards (Faleide et al., 2015).

The Vøring margin, formed in Late Jurassic-Early Cretaceous, resulted in the development of the Cretaceous Vøring Basin, up to 6-8 km deep (Hjelstuen et al., 1999) including sub-basins and highs, mainly caused by variations in the vertical movement of tectonic events (Faleide et al., 2015). The Vøring Marginal High is created along the continent-ocean transition, and located to the west of the basin and has had a major impact of the Cenozoic depositional environment (Hjelstuen et al., 1999; Laberg et al., 2005a; Faleide et al., 2015) (Fig. 2.2.2). Within the Vøring Basin, the Surt lineament separates the sedimentary succession in the south from a northern region (Hjelstuen et al., 1999). The Vøring escarpment have a marked at the northern Vøring Plateau and the Vøring Marginal High (Faleide et al., 2015).

Lofoten-Vesterålen margin has a narrow shelf and a steep slope. The main basins are asymmetric half-graben structures (Fig. 2.2.2). The sedimentary basins are narrower and shallower than the Møre and Vøring basins (Faleide et al., 2015). The seafloor morphology of the shelf is strongly influenced by glacial erosional and depositional processes. Numerous glacially eroded troughs, separated by relatively shallow banks cut across the shelf (Vorren, 2003). The continental crust on the Lofoten-Vesterålen margin has experienced moderate extension, opposite to the greatly extended crust in the Vøring Basin (Faleide et al., 2015).

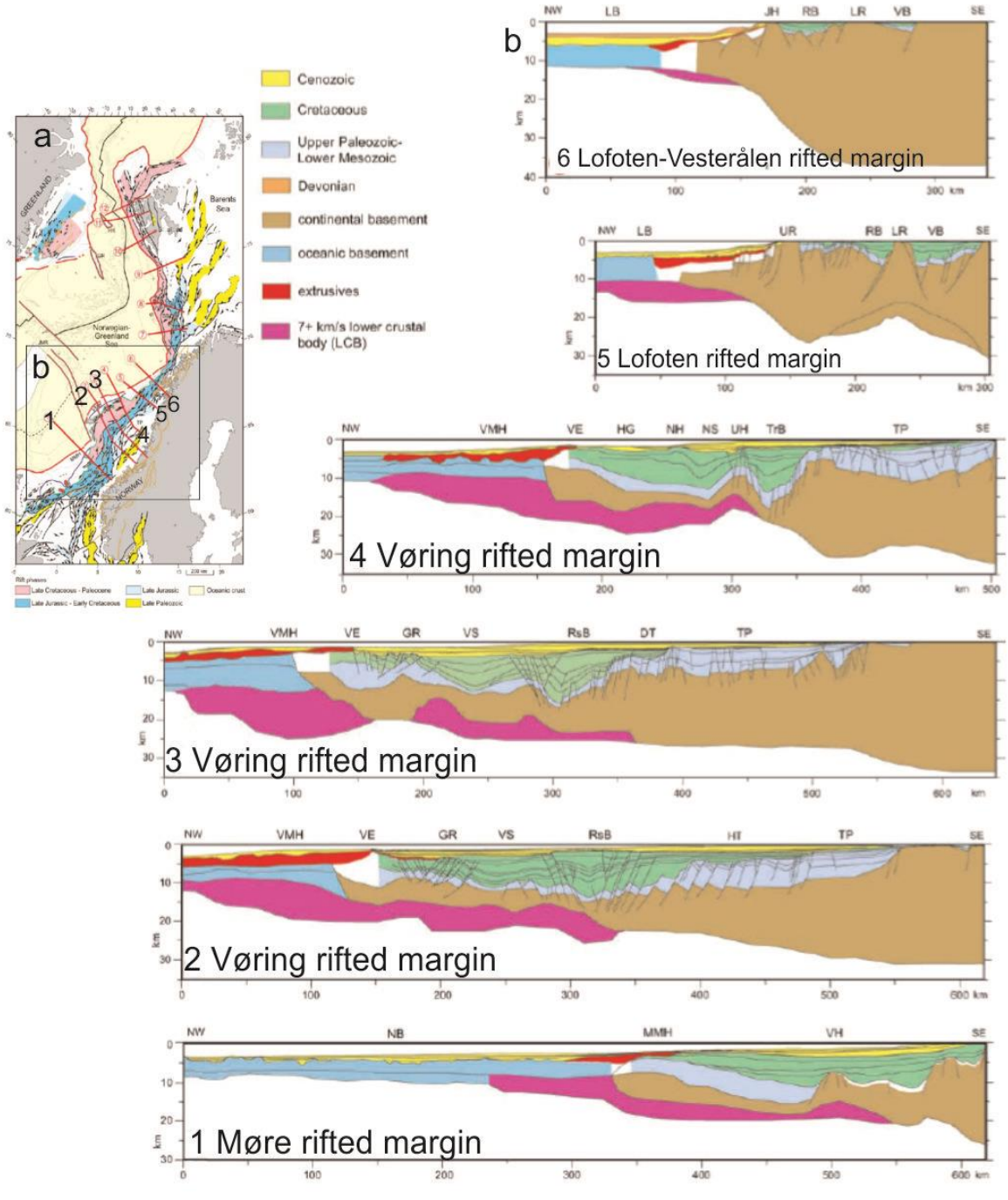

***Figure 2.2.2**: Regional structure map of Norway. **a)** Structural element related to different rift phases and seismic lines 1-6 in the black block will be shown structures in figure b. **b)** Crustal transects across the rifted continental margin off mid-Norway. Location of profiles in figure a) GR: Gjallar Ridge, HT: Halten Terrace, HG: Hel Graben, LB: Lofoten Basin, LR: Lofoten Ridge, MMH: Møre Marginal High, NB: Norway Basin, NH: Nyk High, NS: Någrind Syncline, RB: Ribban Basin, RsB: Rås Basin, TrB: Træn Basin, TP: Trøndelag Platform, UH: Utgrad High, UR: Utrøst Ridge, VB: Vestfjorden Basin, VE: Vøring Escarpment, VH:Vigra High, VMH: Vøring Marginal High, VS: Vigrid Syncline. The figure is modified from Faleide et al., 2008.*

2.3 Cenozoic stratigraphy of the Mid-Norwegian margin

The Brygge Formation comprise sediments deposition from early Eocene to early Miocene, the Kai/Molo Formation from mid Miocene to early Pliocene (~ 14-4 Ma) and the Naust Formation from late Pliocene to the present (<2.8 Ma). The Nordland Group comprises the Kai/Molo and Naust formations, illustrated in Figure 2.3.1 (Eidvin et al., 2014). The dominant sedimentary environment on the central shelf area is hemipelagic sedimentation, while the Møre and Vøring basins comprise depocentres dominated by pelagic biogenic sedimentation (biogenic ooze) (Ottesen et al, 2009; Eidvin et al., 2014).

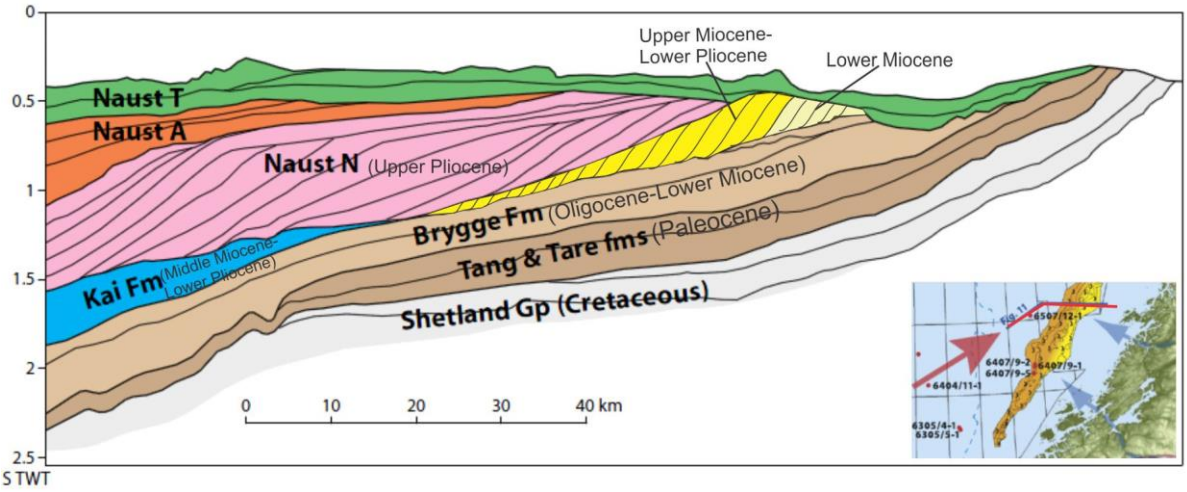

***Figure 2.3.1**: Geoseismic cross-section showing the Molo and Kai Formation and the underlying Brygge Formation. The Middle Miocene unconformity is in between them. Figure is modified from Eidvin et al. (2007 and 2014).*

Along the Vøring margin (summarized in Table 2.3), the Kai Formation is separated from the underlying Brygge Formation by the base Kai unconformity and from the overlying Naust Formation by the intra-Pliocene unconformity (the base Naust unconformity). Another unconformity, the middle Miocene unconformity separates the Kai Formation into an upper and a lower part (Stoker et al., 2005a). This angular unconformity is related to a major mid-Miocene expansion of contourite drift sedimentation on the both sides of the Greenland-Scotland Ridge (Laberg et al., 2005b).

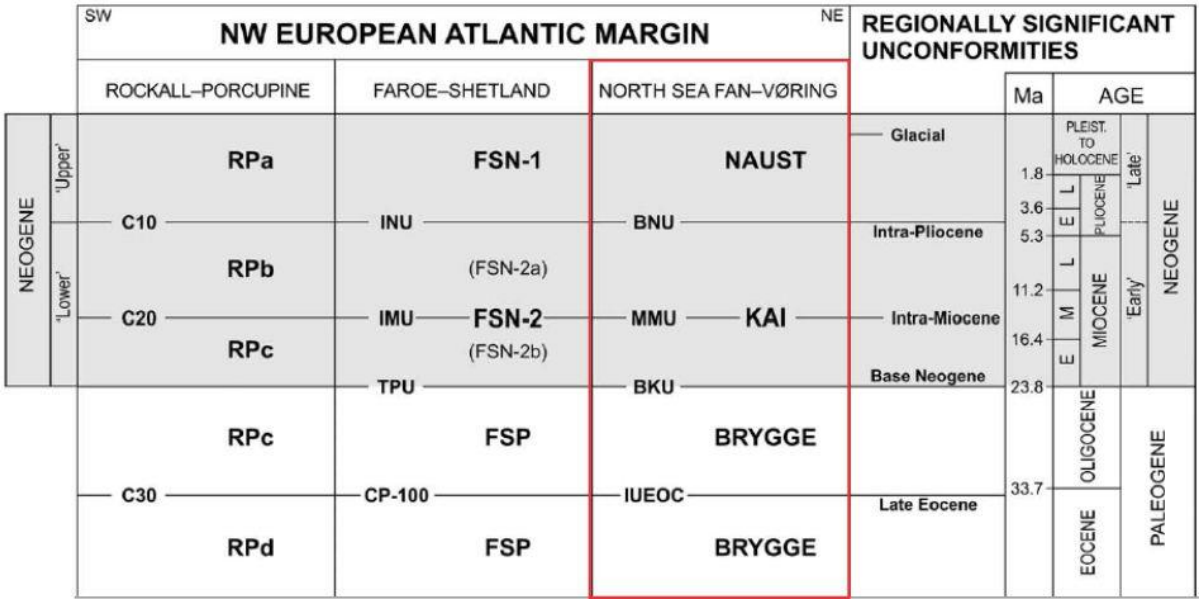

***Table 2.3**: Stratigraphic nomenclature for the Cenozoic succession on the NW European Atlantic margin with focus on the North Sea Fan-Vøring region (red rectangle). BNU, Base Naust Unconformity; MMU, Middle Miocene Unconformity; BKU, base Kai Unconformity; IUEOC, Intra-Upper Eocene Unconformity. The table is added from Laberg et al. (2005b).*

2.3.1 The Brygge Formation

The Brygge Formation is dominated by clay and ooze sediments deposited from early Eocene to early Miocene time, and is dated to c. 55-18 Ma (Eidvin et al., 2007). The thickness of this sediment successions is 600-1000 m in the Møre Basin and 500-700 m in the outer part of the Vøring Basin (Eidvin et al., 2007). The Brygge Formation consists mainly of clay on the present-day shelf and ooze-dominated sediments in the distal part, and deeper marine deposits in the Møre and Vøring basins (Eidvin et al., 2007, 2010; Rise et al., 2010). The Brygge formation is characterised by small-scale polygonal faulting. These faults could have been caused by compaction and fluid flow out (Eidvin et al., 2010). Other indications of fluid remobilization, as liquefaction and vertical squeezing were found in crater-like forms within the Storegga Slide area (Riis et al., 2005), and this reactivation could have occurred during or after deposition of the glacigenic Naust Formation (Eidvin et al., 2010).

2.3.2 The Molo Formation

Along the inner continental shelf of Norway north of 66º N, progradation of the Molo Formation started in the early Oligocene (Eidvin et al., 2014). The Molo Formation is mainly sandy and deposited by coastal progradation as a consequence of regional onshore uplift and forced sea-level regression. From the coast off Møre to the Lofoten Islands (a distance of ca. 500 km) sandy coastal plains and deltas of the Molo Formation was deposited during the late Miocene to early Pliocene (Eidvin et al., 2014). In the outer part of the Vøring Plateau, deposits were dominantly fine-grained clastic sediment, deposited by contouritic currents (Laberg et al., 2005b). The Molo Formation can be interpreted as the shallow-water comparable to the Kai Formation. Eidvin et al. (2014) describes the Molo Formation to comprise mainly glauconitic and quartzose sand of Burdigalian age (early Miocene).

A few indication of hiatus within the Molo Formation was found at Trøndelag platform, separating the early Oligocene to early Miocene part from middle Miocene to early Pliocene part (Eidvin et al., 2104). This is the middle Miocene unconformity, which related to non-deposition between the base of the Molo and the Brygge formations. Associated with climate retrogression and a low global sea level in the late Miocene, progradation of clayey hemipelagic sediments continued along the inner continental shelf of the Norwegian Sea which resulted in deposition of pelagic ooze of the Kai Formation on the slope and rise (Eidvin et al., 2014).

2.3.3 The Kai Formation

After the middle Miocene, tectonism caused a major regression along the Norwegian continental margin between 62º and 69º N. The forced regression caused the subsidence of the Kai Formation 50-150 km seaward of the present coastline (Eidvin et al., 2014). The sediments related to the Kai Formation are dominantly clayey and located on the middle-outer parts of the margin (Fig. 2.2.1). The maximum thickness of the Kai Formation is in the central part of Trøndelag Platform and thins eastward towards the Molo Formation and westward towards the Nordland Ridge (Eidvin et al., 2014). The clay-dominated deposits of the Kai Formation contain fine-grained pelagic and hemipelagic sediment that have been dated to middle Miocene-early Pliocene. In the Vøring Basin the Kai Formation contains fine-grained

calcareous and siliceous ooze (Stoker et al., 2005a; Rise et al., 2010) and the sediment were deposited in a deep-marine environment, as in the outer part of the Vøring Plateau, where the Kai Formation was dominantly fine-grained clastic sediment and redeposited by contouritic currents (Laberg et al., 2005a, 2005b) (Fig. 2.3.2). Polygonal faulting is characteristic for the Kai Formation, similar to the fault pattern of the Brygge Formation (Eidvin et al., 2014).

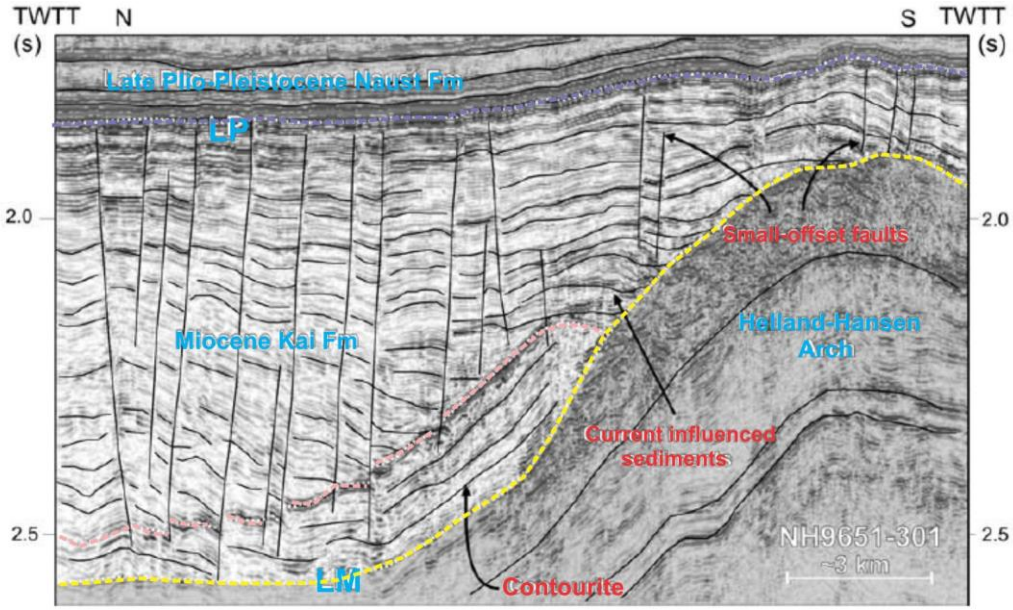

***Figure 2.3.2**: Seismic facies of the Miocene Kai Formation and late Pliocene Naust Formation showing characteristic depositional pattern of current influenced sediments on the Vøring Plateau. LM: Low Miocene; LP: late Plio-Pleistocene. The figure is added from Laberg et al. (2005b).*

Large domes were formed as a result of middle Miocene compressional tectonism, influencing the pattern of sedimentation. As a result, fine-grained sediments were redistributed along the flank of the domes (Eidvin et al., 2014).

2.3.4 The Naust Formation

In late Pliocene the climate started to be colder and large-scale ice sheets started to build up in the Northern Hemisphere. In combination with the late Neogene tectonic uplift of the mainland this resulted in the large sediment accumulation of prograding wedges along the margin (Dahlgren et al., 2005; Rise et al., 2005, 2010). The prograding wedges comprise fine-grained, mostly clay and silt from various sources (Rise et al., 2010). The Naust Formation

was mostly deposited on the mid-outer shelf (Evan et al., 2000; Ottesen et al., 2009; Rise et al., 2010). The wedges are normally low angle, prograding clinoforms, thinning westward and deposited on the underlying Kai and Molo formations (downlap onto the top of underlying Kai Formation) (Rise et al., 2005). The base of the wedge on the middle to upper slope and shelf is dated to late Pliocene (3.0-2.5 Ma), whereas in the deep-water areas the Naust deposits are younger (Evan et al., 2000). The wedges of the Naust Formation have a wide distribution and a maximum total thickness over 1500 m. The volume of the Naust Formation is estimated to around 80,000 km^3 (Evan et al., 2000).

The Naust Formation was divided into five sequences (Figs 2.3.3; 2.3.4); Naust N (oldest), A, U, S, and T (youngest) (Fig 2.3.3). Naust N - S represent the dominating prograding wedges, which has the character of the four oldest units, while as Naust T comprises mainly horizontal aggradational units (Rise et al., 2005).

Naust N and A sequences (Fig. 2.3.4 E) are westerly prograding, wedge-formed units and located below the present shelf. Their deposits were various types of mass movements and down-slope gravity currents, these can be reliable for recycling of sediments beyond the palaeo-shelf edge (Rise et al., 2005, 2010). Naust N is dated to be c. 2.8-1.5 Ma (Eidvin et al., 2007).

The Naust U sequence was deposited between c. 0.8-0.4 Ma. This sequence is thickest on the slope, and interpreted as glacial debris redistributed downslope from the grounding line of the ice sheets at or near the paleo-shelf break (Ottesen et al., 2009; Rise et al., 2010) with a depocenter located in the Nyegga area (Rise et al., 2010).

Naust S was deposited between c.0.4-0.2 Ma, and is up to 300 m thick on the slope west of Skjoldryggen (Rise et al., 2005, 2010; Ottesen et al., 2009). The sediments are inferred to be glacial debris deposited by the Fennoscandian Ice Sheet which drained westward to the shelf edge in the Skinnadjupet palaeo-trough (Rise et al., 2005, 2010).

Naust T comprise sediments deposited in period of the last c. 200,000 years (Rise et al., 2005). These sediments were deposited on the shelf and the uppermost slope during the two last glacial-interglacial cycles and comprise two large units of till and glacial debris deposited during the Saalian and Weichselian glaciations. Along the shelf edge, a large marginal moraine ridge, called Skjoldryggen was formed during the Late Weichselian glacial maximum (Fig. 2.3.3) (Rise et al., 2010).

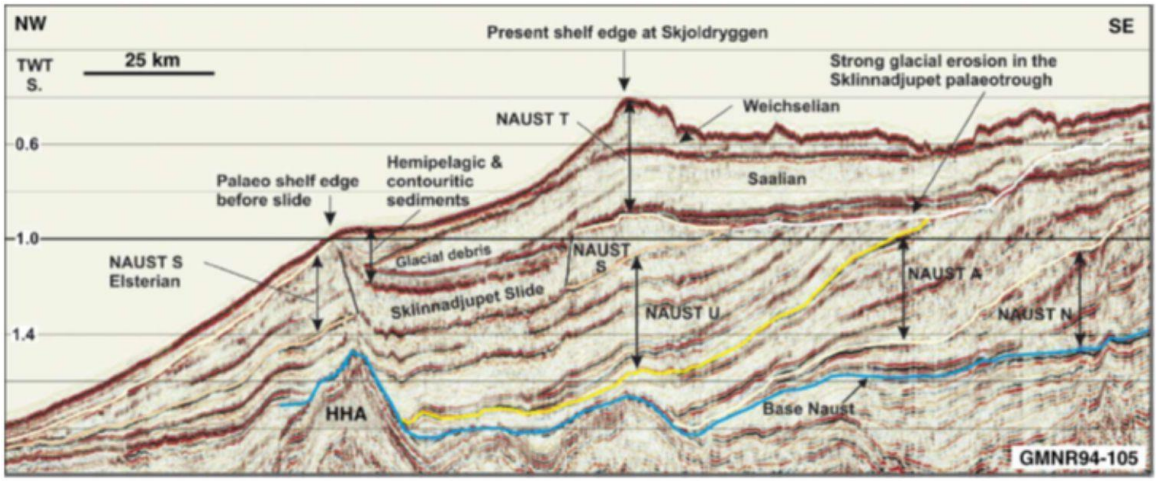

***Figure 2.3.3**: A regional seismic section showing the prograding Naust Formation. The seismic line is located across the northern part of the Sklinnadjupet slide scar. The figure is added from Rise et al. (2010).*

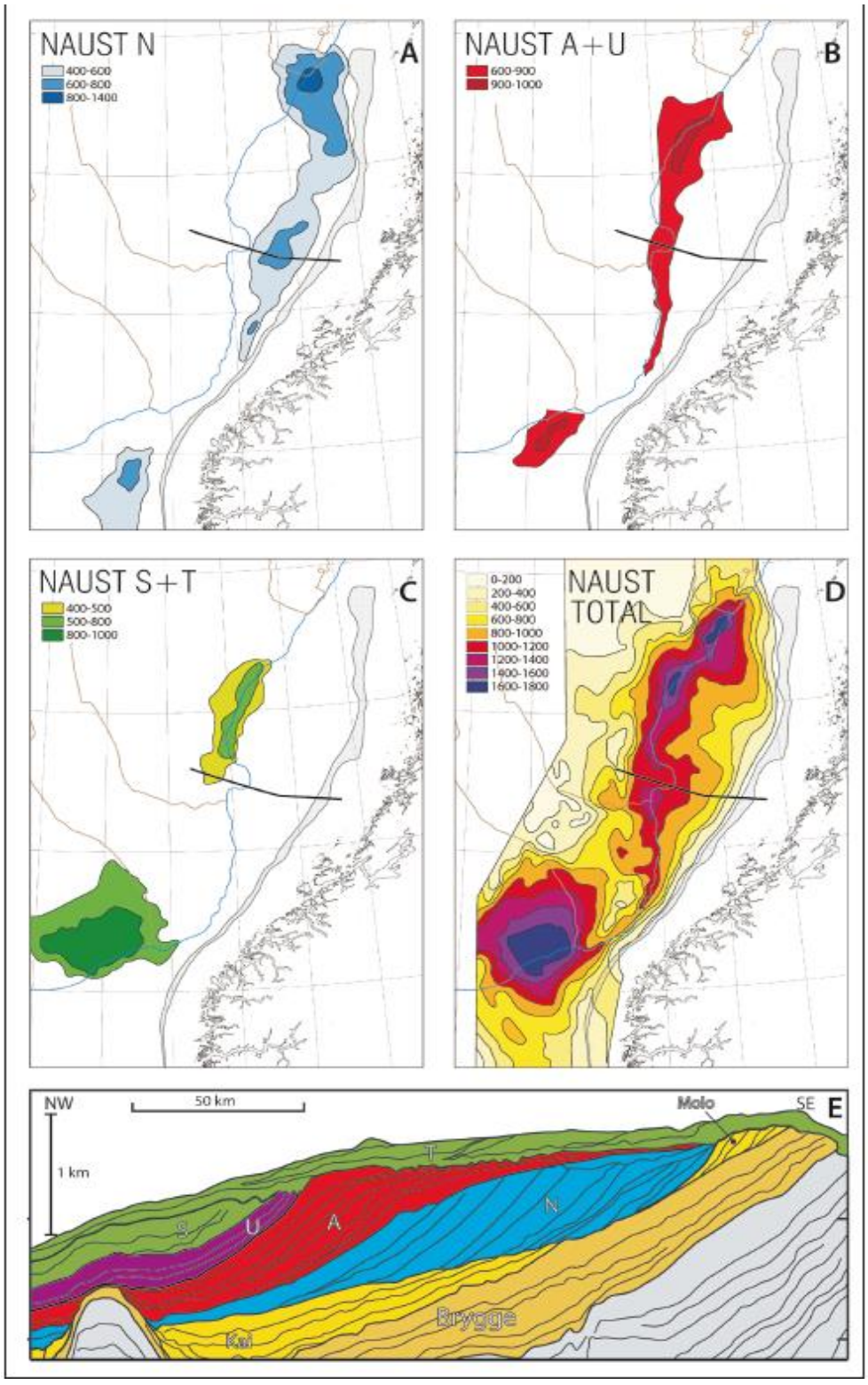

***Figure 2.3.4**: A-D:Ttime thickness maps in milliseconds (two-way travel time) of the Naust sequences (A-D). E: Geoseismic section across the Naust sequences. The figure is added from Ottesen et al. (2009)*

2.4 Glacial history of Fennoscandia

The first indications of glaciers reaching the coast occurs in the late middle Miocene, at the same time as tills and glacimarine diamict were deposited on the east Greenland continental shelf (Hjelstuen et al., 2005). This could be observed from cores on the Vøring Plateau (Fig. 2.4.1), which shows the first occurrence of ice-rafted debris (IRD) at about 12.7 Ma and a dramatically increasing IRD flux dated at around 2.7 Ma (Hjelstuen et al., 2005), most likely reflecting a significant ice volume expansion around the Nordic Seas with reference to the onset of the Northern Hemisphere glaciations.

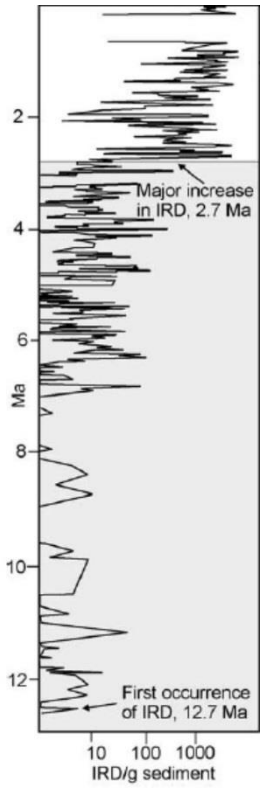

***Figure 2.4.1**: Complied IRD records from the Vøring Plateau.The figure is added from Hjelstuen et al. (2005).*

Dahlgren et al. (2005) relates the onset of glaciations to the deposition of the major prograding wedges on the Vøring Plateau. These prograding wedges were dated to late Plio-Pleistocene and is characterized by units of till/diamicton deposited from around 2.74 Ma. However, the size of ice sheets were mostly moderate until about 1.1 Ma when there was a shift of climate, which caused glacial periods of longer duration and warmer interglacial periods (Hjelstuen et al., 2005).

The glacial sediments were transported westward from the mainland and deposited mainly as a prograding wedge into a basin of intermediate depth offshore Mid Norway (Rise et al., 2005). The glacial sediments are defined as the Naust Formation and deposited rapidly as compared to the underlying units, and the thickness is more than one kilometer covering a large area (Ottesen et al., 2009; Rise et al., 2010; Mangerud et al, 2011). Rise et al. (2005) identified till from boreholes penetrating the oldest part of the Naust Formation on Haltenbanken.

Hjelstuen et al., 2005 suggest that the first major ice sheet reached the shelf edge at the mouth of the Norwegian Channel on the southern part of the mid-Norwegian continental shelf at around 1.1 Ma. Glacial and inter-glacial periods occurred though the early Pleistocene, but did not include any ice sheet reaching the continental shelf (Fig. 2.4.2). The Mangerud et al.

(2011) found the oldest identified till unit from the Norwegian Channel, the Fedje till, to be dated to about marine isotope stage MIS 12 (Fig. 2.4.2). The North Sea Fan was the main depocenter of glacial sediments from southern Scandinavia (Sejrup et al., 2005; Nygård et al., 2005).

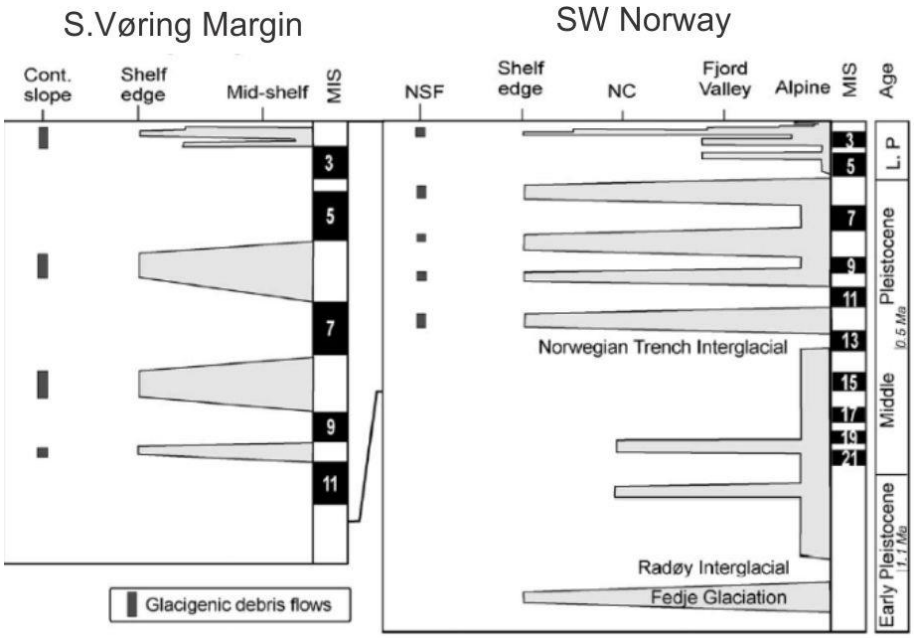

Figure 2.4.2: *The glacial time-distance curves from the south Vøring Margin and the southwest Norway. MIS: Marine Isotope Stage; NC: Norwegian Channel; NSF: North Sea Fan. The figure is added from Hjelstuen et al. (2005).*

The cold glacial condition was disrupted by the warmer Radøy interglacial (MIS 13 age) in the latest early Pleistocene to middle Pleistocene (Hjelstuen et al., 2005; Mangerud et al., 2011). During the late middle Pleistocene (0.5-0.13 Ma, MIS 12 to MIS 6) packages of GDFs (Glacigenic debris flow, which represent the building blocks of the trough-mouth-fans) were deposited on the North Sea Fan during each glacial maximum stage. These occurred at least four times, during MIS12, 10, 8 and 6 the Norwegian Channel Ice Stream enlarged to reach the mouth of the Norwegian Channel (Hjelstuen et al., 2005; Mangerud et al., 2011). At the same time, on the southern Vøring margin the ice sheet reached the continental shelf break both during MIS 10 and MIS 8 but not during MIS 6 (Hjelstuen et al., 2005). Another study suggested that the ice sheet reached its maximum during MIS 10 and MIS 6 along the northern part of Vøring margin (Hjelstuen et al., 2005).

2.5 Bathymetry and geomorphology

The 400-500 km long mid-Norwegian continental margin can be divided into three main provinces; the Møre (south), Vøring and Lofoten-Vesterålen margin (north) , separated by the Jan Mayen Fracture Zone and the Bivrost Lineament/Transfer Zone, respectively (Faleide et al., 2015) (Fig. 2.5.1).

The continental shelf is less than 100 km wide at the Møre margin, widening to more than 200 km at the Vøring margin, before it narrows northwards to the Lofoten-Vesterålen margin, which is 60-80 km wide on average (Ottesen et al., 2009). The mid-Norwegian continental shelf morphology is characterised by shallow banks (50 to 300 m water depth) alternated by deeper cross-shelf troughs (150-550 m water depth). These troughs were the pathways for palaeo ice-streams flowing across the shelf during repeated glaciations (Ottesen et al 2005; Rise et al., 2005; Sejrup et al., 2005).

The water depth varies from about 300 m at the shelf break to more than 3000 m in the abyssal Lofoten Basin (Laberg et al., 2005a). The Vøring Plateau is a flat area and located at water depths between 1200-1600 m (Dahgren and Vorren, 2003; Laberg et al., 2005a; Ottesen et al., 2009). The continental slope has relatively gentle gradient and dips less than 1º towards the Vøring Plateau, whereas the slope on the Lofoten-Vesterålen margin has a gradient up to 5º (Dahgren and Vorren, 2003).

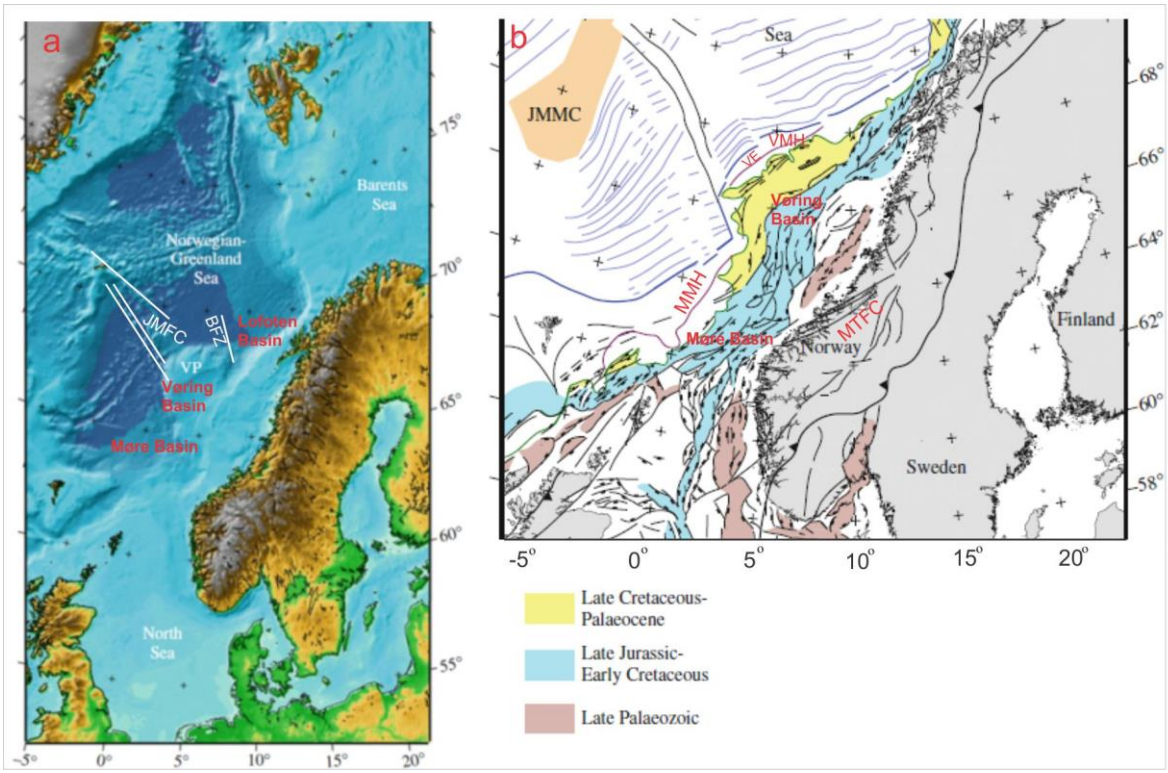

Figure 2.5.1: *Overview regional setting.* ***a)*** *Bathymetry and topography of the Norwegian Continental Shelf and adjacent areas. VP: Vøring Plateau; JMFC: Jan Mayen fracture zones; BFZ: Bivrost Lineament/Transfer Zone* ***b)*** *Main structure elements of the mid-Norwegian margin; MMH: Møre Marginal High, MTFC: Møre-Trøndelag Fault Complex, VE: Vøring Escarpment, VMH: Vøring Marginal High. The figure is modified from Faleide et al., 2015.*

2.6 Present-day oceanography and paleoceanography

The Mid-Norwegian Continental margin is at present overlain by the Atlantic Water of the Norwegian Current. The Norwegian Atlantic Current (NwAC) consists of three distinct branches; two surface current systems flow along the inner, upper continental slope and on the outer Vøring Plateau and the third is the Norwegian Coastal Current (NCC) flowing along the coast (Hjelstuen et al.,2005; Laberg et al., 2005b) (Fig. 2.6.1a).

The North Atlantic Current (NAC) is divided into two main branches, which flows separately across the Iceland-Faroe Ridge and the Faroe Shetland Channel, respectively (Fig. 2.6.1 b). The north-eastern branch moves through the Faroe Shetland Channel and follows along the Norwegian continental margin and is called the Norwegian Atlantic Current, whereas the western branch passes though the Iceland-Faroe Ridge and enters into the area of the outer

continental slope of the Vøring Plateau and then continue northward to the Jan Mayen area (Hjelstuen et al., 2005) (Fig. 2.6.1).

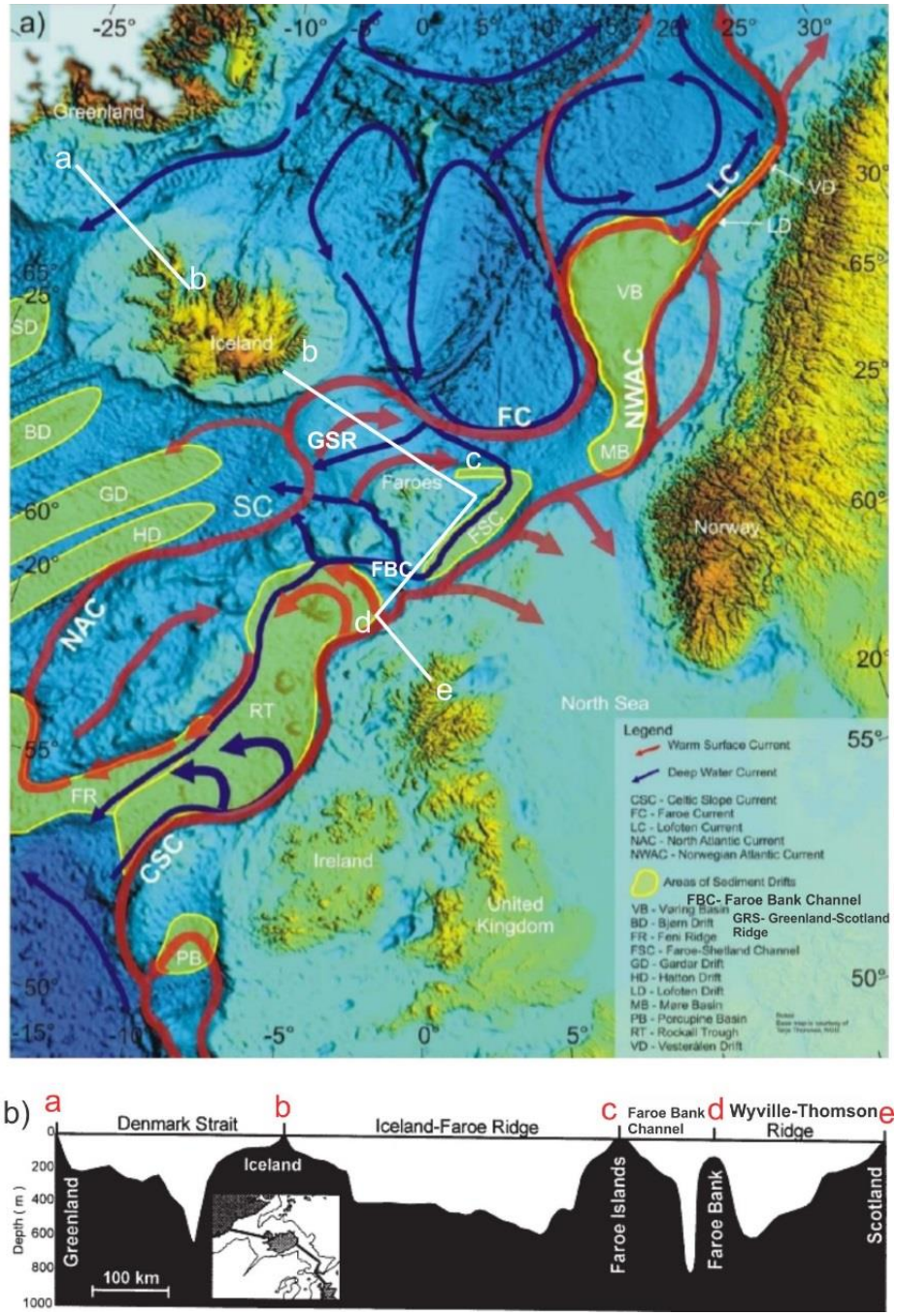

Figure 2.6.1: a) *Map displaying the modern ocean circulation and the general location of contouritic sediments on the NW Europe of the Atlantic margin. The pattern of the warm, saline Atlantic surface water is indicated by red arrows, whereas the cold and dense deep water by blue arrows. The white line is shown in b). The figure is modified from Laberg et al., 2005b.* ***b)*** *Water depth across the Norwegian-Greenland Sea. The figure is modified from Hansen and Østerhus, 2000.*

The North Atlantic Current (NAC) is divided into two main branches, which flows separately across the Iceland-Faroe Ridge and the Faroe Shetland Channel, respectively (Fig. 2.6.1 b). The north-eastern branch moves through the Faroe Shetland Channel and follows along the Norwegian continental margin and is called the Norwegian Atlantic Current, whereas the western branch passes though the Iceland-Faroe Ridge and enters into the area of the outer continental slope of the Vøring Plateau and then continue northward to the Jan Mayen area (Hjelstuen et al., 2005) (Fig. 2.6.1).

The Norwegian Atlantic Current consist of warm and saline Atlantic surface water, which is gradually cooling when moving northward causing the water mass to sink in the Norwegian-Greenland Sea in form of cold, dense, intermediate and deep waters, which are turned southward into the North Atlantic Ocean, partly as surface outflow along the Greenland coast and partly as deeper water mass across the Greenland-Scotland Ridge, as Denmark Strait and the Faroe Conduit (the Faroe-Shetland Channel together with the Faroe Bank Channel)(Hansen and Østerhus, 2000; Laberg et al., 2005b; Stoker et al., 2005b).

The Cenozoic evolution of the continental margins and deep-sea basins has had an important influence on the palaeoceanographic circulation and associated deep-water sedimentation patterns (Laberg et al., 2005b). From the late Oligocene to mid Miocene, two gateways, the Fram Strait to the north and the Greenland-Scotland Ridge to the south opened and this strongly affected the ocean circulation of the Norwegian – Greenland Sea. From the early Miocene the ocean currents mainly affected sedimentation on the inner high, while renewed influence of ocean current controlled sedimentation on the outer slope of the Vøring Plateau (Laberg et al., 2005a).

During the early and middle Miocene there was an extensive biogenic opal depocenter in the Norwegian-Greenland Sea caused by silica supply from chemical weathering of the mainland and additionally oceanic condition with low water masses exchange, resulting in increasing isolation of the deep-water. In contrast, more carbonate-dominated accumulation occurred in the late Miocene to early Pliocene, when the surface water and deep water circulation increased (Eidvin et al., 2004; Laberg et al., 2005a).

2.6.1 Bottom Current

In the present-day bottom current generated by cooling and sinking surface water at high latitude that sink in to the deep ocean water, are influence by thermohaline and the wind-driven circulation pattern. They are naturally semi-permanent with a net flow alongslope, but very variable in direction and velocity, and contour current is widely used in term of synonym to bottom current (Stow et al., 2002). Rebesco et al. (2001) suggest that bottom current is water mass move though out the ocean basins, as a generally persistent water current near the seafloor.

Antarctic Bottom Water (AABW) is coldest, densest and deepest water in the oceans, formed under ice-shelves around Antarctica. AABW flows down on the continental slope and eastward around continent, further flows northwards though gateways into Pacific, Atlantic and Indian Oceans. In the Norwegian and Greenland Seas, Arctic Bottom Current forms by subpolar surface water gyre and then flows southward across the Greenland–Scotland Ridge (GSR), as the Southern Oceanic Gateway, into Rockall, Scotland and Greenland basins (Stow et al., 2002). Topographic barrier, as the mid-ocean ridges and aseismic ridge systems play partly roll for bottom current flowing (Stow et al., 2002).

Bottom water flows normally very slowly with velocity 1-2 cm/s. It can be highly variable in velocity, direction in their locations at any one time. Bottom currents are effected by the Coriolis force, which controls water mass to flows against the continental slops on western margin of ocean basins and here the bottom currents will gain velocity up to 10-20 cm/s (Stow et al., 2002). The influence of bottom current in the deep-water creates sediment deposition and erosion at the deep seafloor, the sediment deposition leads to development of contourite drift, whereas erosion in long-term creates hiatuses and several erosive features. (Stow et al., 2002, 2009). The depositional and erosional bedform were affected by the action of bottom currents could give information about flow direction, variability, continuity and velocity in that time (Stow et al., 2009). The details of bedform in relationship current velocity, which is affected by bottom current system in deep water are classified by Stow et al. (2009) (Fig. 2.6.2), for bedform scale summarized to table 2.6

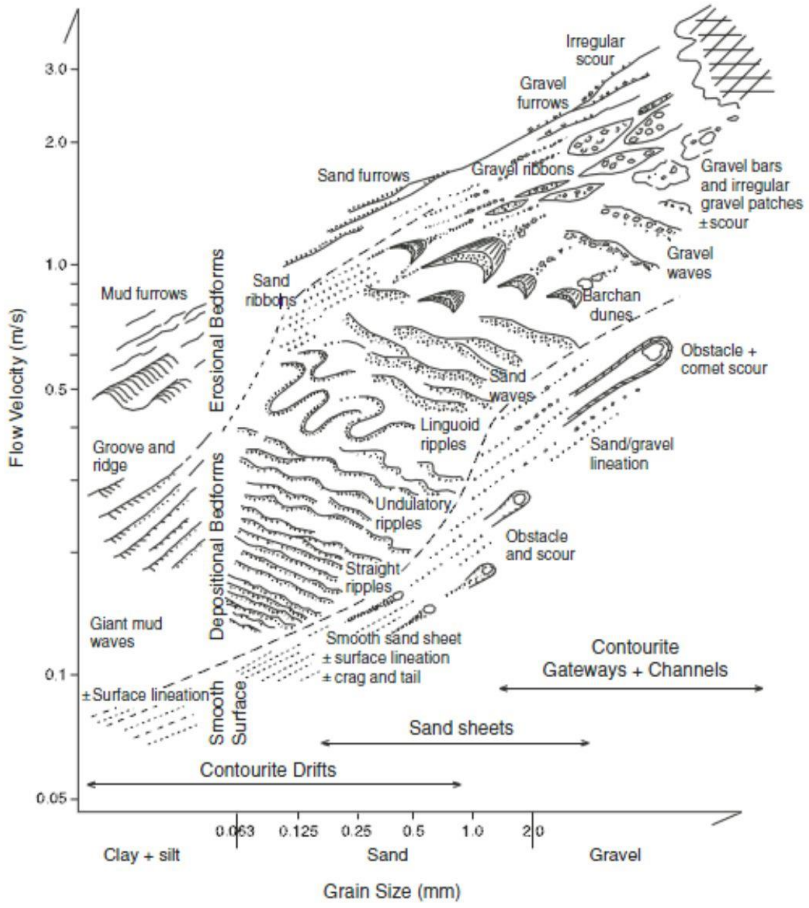

Figure 2.6.2: *The classification of bedform-velocity matrix* for deep-water bottom current system, showing in relationship between grain size of sediment and flow velocity. The figure is added from Stow et al. (2009).*
**The principal physical parameters that control development of bedforms include flow velocity and depth, fluid density and viscosity, particle density and size, sediment supply, and bed roughness (Stow et al., 2009).*

According to Laberg, et al. (2005b) along the NW European Atlantic is found the first indications for bottom current circulation have been dated from late Eocene time, and has had a major influence to the Cenozoic deep-water sedimentation patterns, as well as an indication of late Eocene unconformity on the North Sea Fan-Vøring margin that represent a deepening of the continental margin, and origination of bottom current activity along the margin (Laberg et al., 2005b; Stoker et al., 2005b).

Bedforms type	Characteristic	Ranging of bedform scale
Linear form		
• **Surface lineation**	Elongate, parallel to flow direction with low-relief linear streaks	Small scale; millimeter, decimeter
• **Groove and ridge**	straight to sinuous in planform. Groove are narrower and shape crests	Decimeter up to 1-5 meter
• **Crag and tail**	Elongate mound, deposited rapidly downstream of a obstacle (crag) in the path of flow (tail)	Tail; centimeter to decimeter
• **Obstacle and scour**	crescentic to elongate scour	Scour; meter to 100-m. but decimeter within crag and tail structure
• **Ribbon mark**	elongate mounded fi laments, parallel to slightly sinuous planform	Large scale; width 10–100 m, length 5–50 km
• **Furrow**	elongate, primarily erosional features, with regular to irregular spacing and a parallel to slightly sinuous planform.	Large scale; width 5–150 m, length 1–10 km
Transverse Bedforms	Undulation, oriented transverse to flow direction, symmetry in planform. Unidirectional flow asymmetrical in cross section with a steeper, shorter lee side (downstream) and more gentle, longer stoss side (facing upstream).	Transverse bedform
• **Ripple**	straight-crested, undulatory (sinuous crested), and linguoid (3-D) types in plan form, asymmetrical with sharp to rounded crestlines.	smallest-scale; wavelength 0.1–0.6 m, height 0.02–0.1 m
• **Dune**	sinuous-crested and barchanoid (3-D) dune planforms.	wavelength 0.6–10 m, height 0.1–1 m.
• **Sand wave**	A longer wavelength, flatter bedform compared with dunes, and generally sinuous crested (2-D) in planform.	wavelength 5–100 m, height 0.1–1 m
• **Giant sediment waves (or mudwaves**	regular, transverse to oblique bedforms (under long-term stable current condition)	wavelength 0.5–10 km, height 10–80 m

***Table 2.6**: Summarized the detail of bedform and flow velocity, and is provided by coverage of the range of bedforms that could be observed in deep-water affected by active bottom current systems (Stow et al., 2009).*

2.6.2 Contourites

Contourites are defined as sediments deposited in the deep sea from and affected by thermohaline-induced geotrophic ocean currents (Stow et al., 2002). Contourites occur along continental slopes and deep-sea areas and the sediments are partly reworked by the persistent action of the bottom current (Rebesco et al., 2001).

The contourite accumulations can be divided into 6 types by Stow et al. (2002), based on morphology and the overall setting of which they occur; i) contourite sheet drifts; ii) elongated mounded drifts; iii) channel-related drifts; iv) confined drifts; v)infill drifts, and vi) modified drift-turbidite systems.

The occurrence of these six main types are controlled by five factors (Stow et al., 2002), as i) the morphology and topography; ii) the current velocity and variability; iii) at both short-period and longer timescale the amount and type of sediment available; iv) the length of the time over which the bottom current has been generated, and v) modification by interaction with downslope process and their deposit.

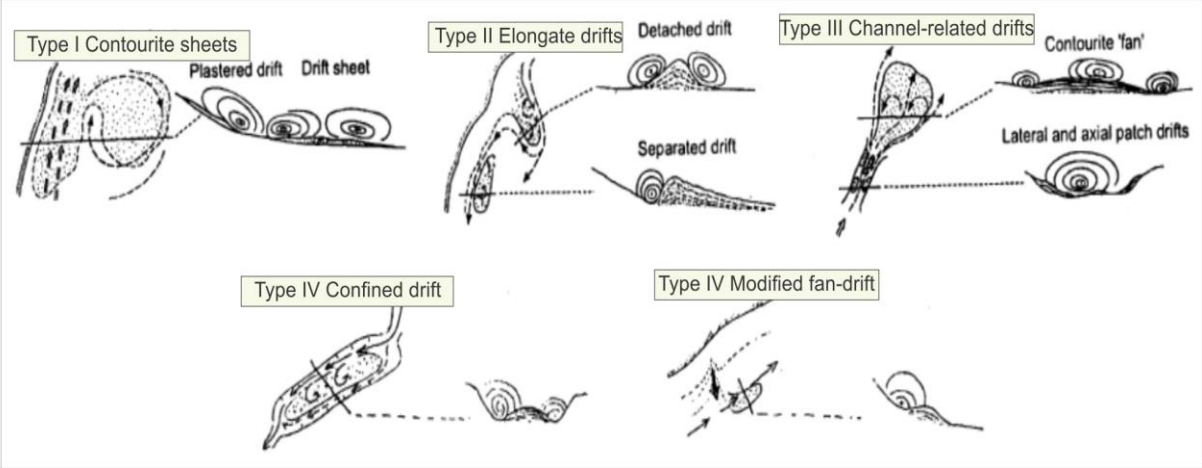

***Figure 2.6.3**: contourite drift models with illustrations of the deposition around the drifts. The figure is modified from Stow et al. (2002).*

Laberg et al. (2005a) have identified two contourite drifts on the continental margin offshore Lofoten and Vesterålen; the Lofoten Drift and the Vesterålen Drift, both drifts which are located on the lower part of the continental slope, and identified as mounded elongated drifts. The Lofoten drift has originated sometime during the Miocene based on correlation to the regional seismic stratigraphy of the area and consist of sediments of the Miocene - mid Pliocene Kai and late Pliocene-Pleistocene Naust Formations.

2.7 Gravity-driven resedimentation processes

2.7.1 Slides

On the Mid-Norwegian continental margin, seven large-scale slides from pre-Holocene, having a size of more than 2,000 km^2, has been mapped within the area of the Storegga Slide Complex (located between 0 - 6ºE and 62 - 67ºN, Fig. 2.7.1) (Bryn et al., 2005a). The scale of these slides is comparable in size with the Storegga Slide (Fig. 2.7.2) (Solheim et al., 2005). The main sliding activity occur from about 0.5 Ma, shortly after the Fennoscandian Ice Sheet started to reach the continental shelf break during peak glacials (Solheim et al., 2005). The large-scale sliding occurred after extensive shelf glaciations with glide planes being developed within the stratified clay-rich hemipelagic and/or contouritic sediments (Bryn et al., 2005a; Solheim et al., 2005; Rise et al., 2006a).

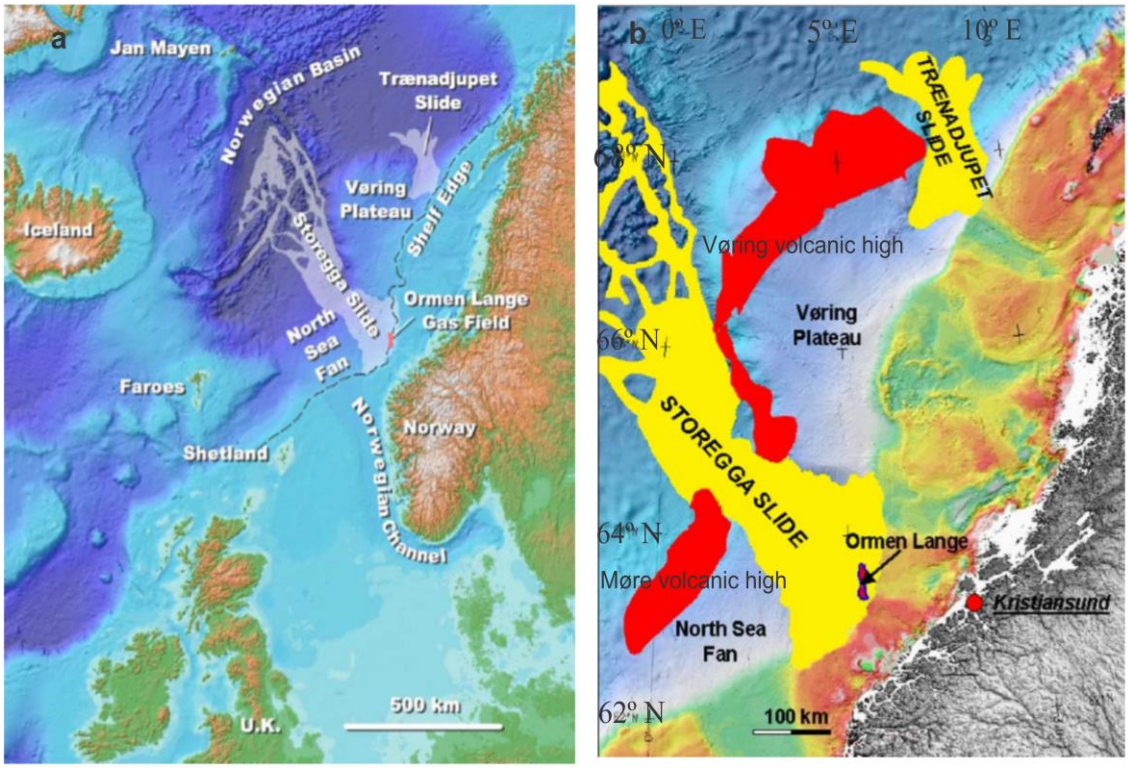

***Figure 2.7.1**: A location map showing **a)** the Storegga and Trænadjupet submarine slides on the mid-Norwegian margin **b)** The Møre- and Vøring volcanic highs are marked in red color. The figure is modified from Bryn et al. (2005a).*

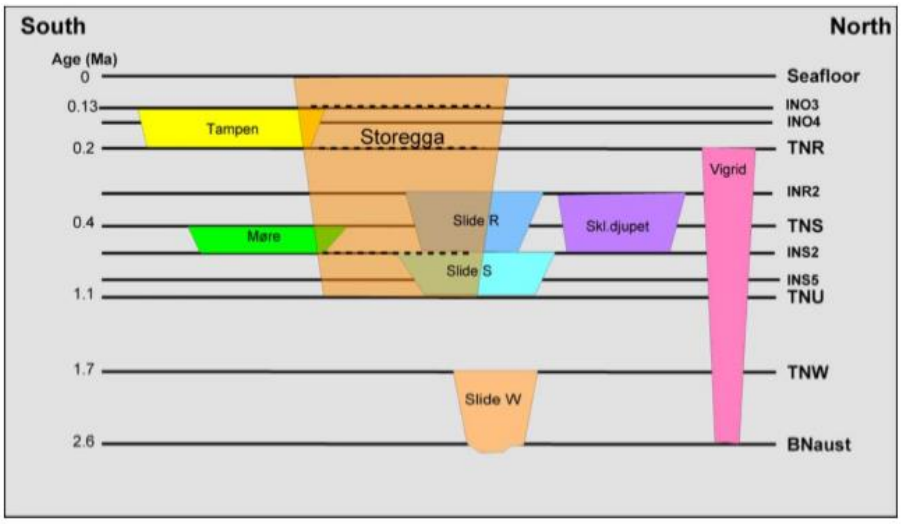

***Figure 2.7.2**: A schematic slide stratigraphy of the mid-Norwegian margin. Stippled within the Storegga Slide indicate the most important slide planes for this Holocene slide. The figure is added from Solheim et al. (2005).*

According Solheim et al. (2005) Slide W and the Vigrid Slide are overlying deposits of the Kai Formation. This could involve instability of partly biogenic ooze sediment deposits, as well as the underlying polygonal faults of the Kai Formation indicates that fluid flow may have affected the stability of the sediments in this area.

At present the shelf and upper slope offshore Norway is winnowed by the Norwegian Atlantic Current (NwAC) and sediments from this winnowing are deposited in the slide scars of the slope, forming the post-slide sediments of the Storegga (Bryn et al., 2003) and Trænadjupet Slide Scars (Laberg and Vorren 2000; Laberg et al., 2005a).

A submarine slide development involve sediment transition from solid to liquefied state, as have been described for the Storegga slide. The development of the slide includes three main phases: (i) initial failure, including formation of blocks and slabs; (ii) transition into debris flows; and (iii) further sediment remoulding and development into turbulent flows, turbidity currents (Bryn et al., 2005a) (Fig. 2.7.3).

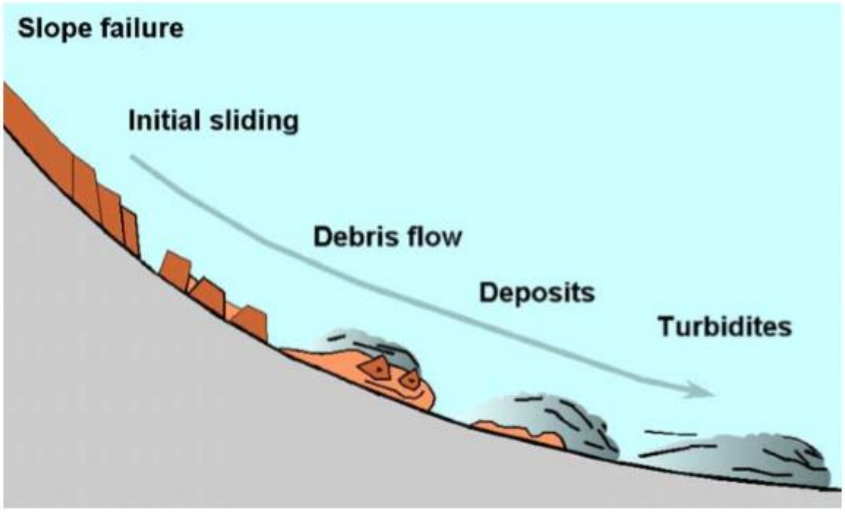

***Figure 2.7.3**: A schematic presentation of the three main phases of slide development from slope failure to turbidity currents. The figure is added from Bryn et al. (2005a).*

2.8 Polygonal faults and their relation to fluid flow

Polygonal fault systems tend to develop in fine-grained sedimentary successions (Cartwright et al., 2003; Berndt et al., 2003). They are normal faults with modest throw values, typically 10-100 m and has in plain view a characteristic form of a polygon with variations in planform pattern (Cartwright et al., 2003). Their shape implies a lack of dominant strike direction meaning that strikes are almost randomly oriented (Cartwright et al., 2003; Berndt et al., 2003). The mechanism by which fluids move up through the sedimentary column to the surface is widely debated (Cartwright et al., 2003; Gay & Berndt, 2007). During burial, the sediment porosity decreases because of loading by overlying sediments, and a set of process allow the sediment particles to reorientation and fluid to expulse, resulting in a decrease of space between particles (Berndt et al., 2003; Gay & Berndt, 2007).

The development of the polygonal fault system is explained by Cartwright et al. (2003) in four steps: i) as initial deposition of clay, followed by ii) the development of local seals, which prevent the uniform dewatering under increasing burial loads iii) then the density gradient reverses and generate sealing of clay-units, which leads to folding of sediment and finally iv) resulting in fracturing and dewatering of the sediments (Fig. 2.8.1).

The Kai Formation is composed of fine-grained hemipelagic sediments (Eidvin et al., 2007; Ottesen et al., 2009) characterized by frequent steeply dipping, densely spaced planar faults in most of the Vøring Basin (Fig. 2.8.2) (Berndt et al., 2003). Berndt et al. (2003) suggested that the polygonal fault systems contain fluid expulsion from the host rock and that this occurred in the uppermost Brygge and the Kai formations. The fault frequency trend to be higher in the Brygge Formation compared to the upper part of the Kai Formation. The faults do not necessary occur at the same stratigraphic level. No clear faults are observed in the overlying Naust Formation, but Berndt et al. (2003) suggest that the most of the faulting happen before the deposition of the Naust Formation, developed and were activated sometime in the Miocene.

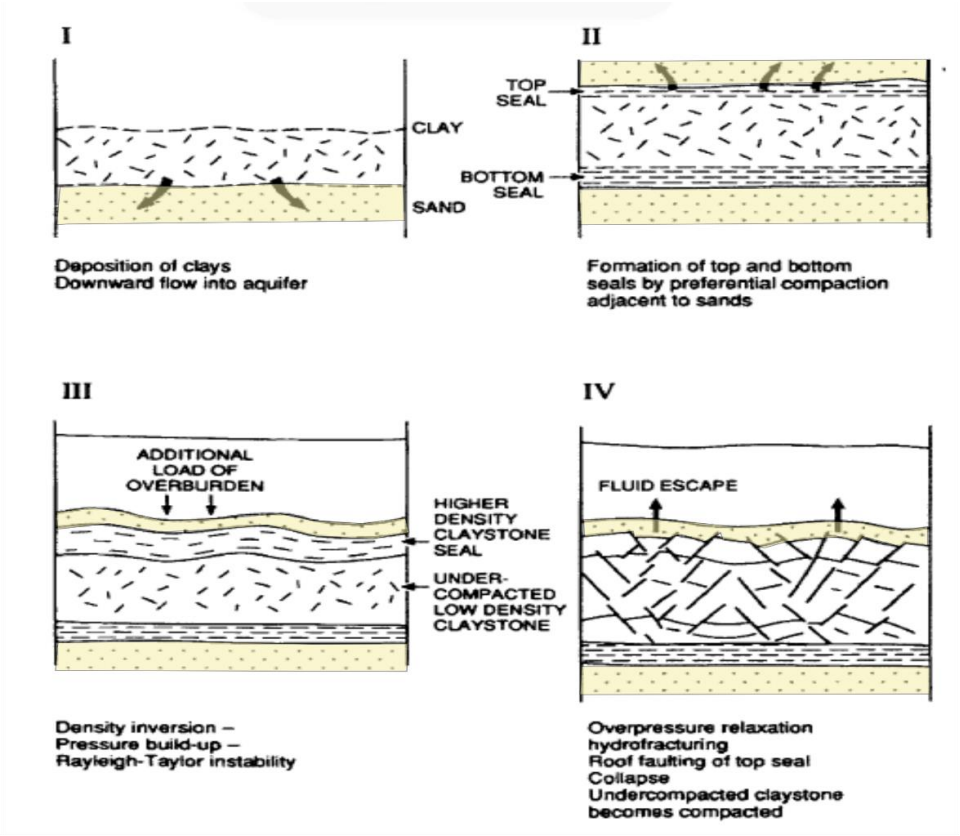

Figure 2.8.1*: The development of polygonal fault system in 4 steps. I: Deposition of clay. II: Sealing of the top and bottom of clay layers generating overpressure. III: Density inversion folding. IV: Collapse of fault and pore pressure results in fluid escape. The figure is modified from Cartwright et al (2003).*

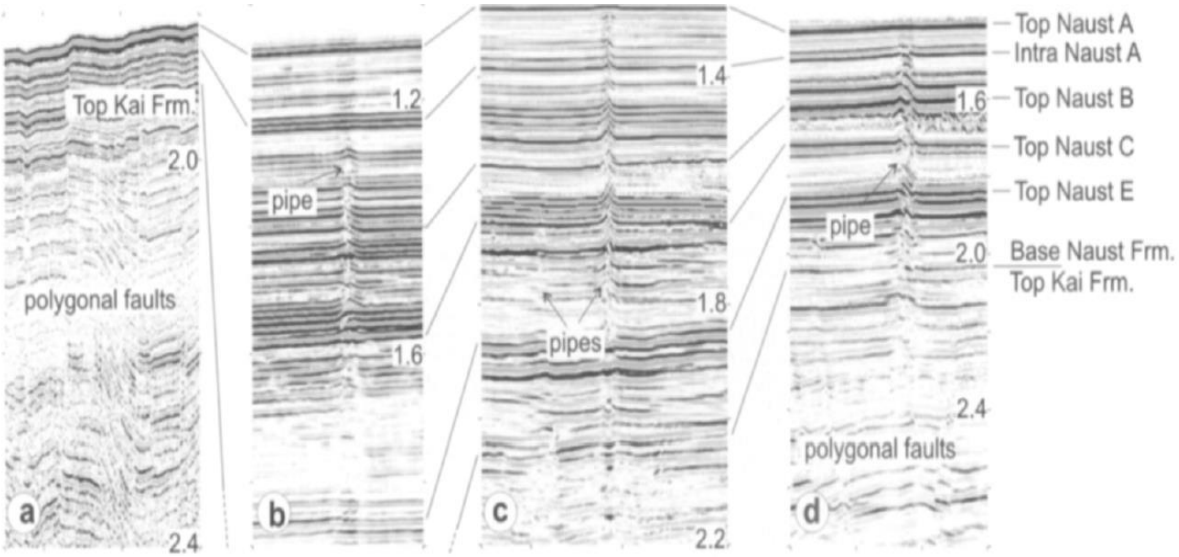

Figure 2.8.2*: Seismic observations of prolonged polygonal fault system development. The figure is added from Berndt et al. (2003).*

3 MATERIAL AND METHOD

3.1 Seismic dataset

The seismic data is used to this study area consist of a 3D seismic cube BG12M02 which has been provided through the DISKOS data base (Fig. 3.1.1). The data cube is located in the Vøring Basin, northwest of the Helland-Hansen Arch in the northern part of the Mid-Norwegian continental shelf. The seismic survey consists of 2,424 inlines, 1,990 crosslines and covers an area of ~3,000 km^2.

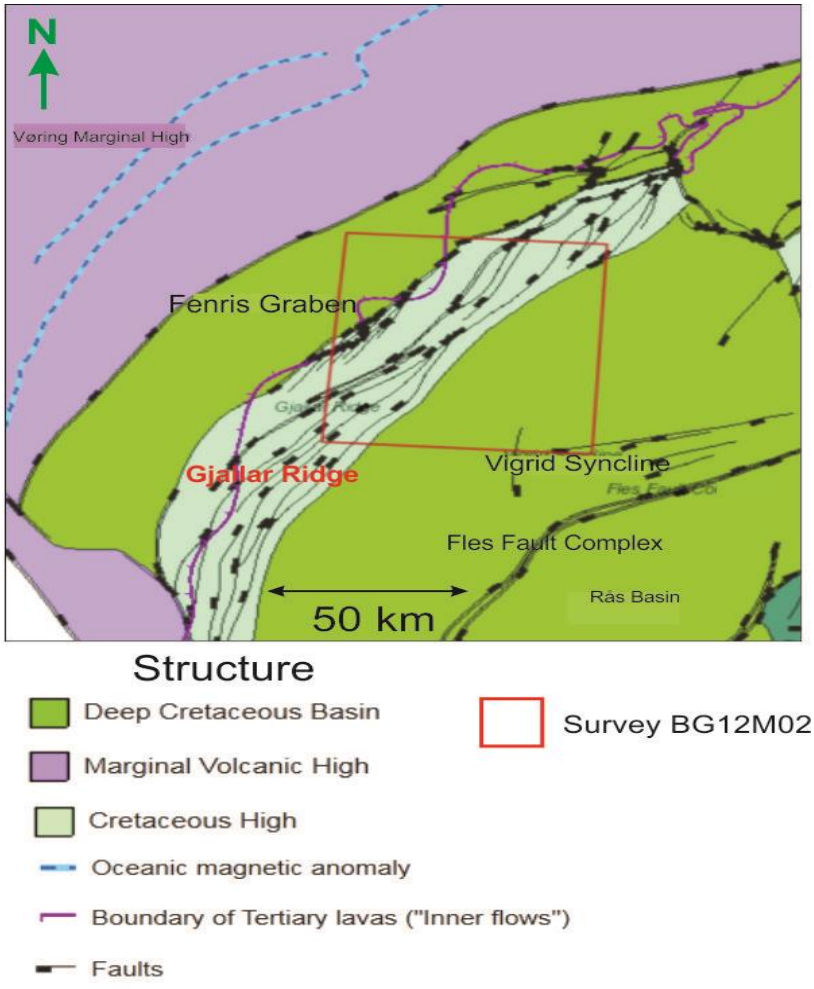

***Figure 3.1.1**: The location of 3D seismic data from Survey BM12M02 (Red square). The figure is modified from NPD FactMaps, 2017.*

3.1.1 Polarity

The polarity and phase of the Survey BG12M02 seismic signal is a zero-phase signal with a normal polarity (SEG) using the definition of Sheriff (2006) (Fig 3.1.2). The seafloor reflection (Fig 3.1.2 a) was used as a reference because it always produces a positive acoustic impedance contrast (Reflection Coefficient, RC+). According to Sheriff (2006) the zero-phase pulse with normal polarity consist of a central peak and two lobes of opposite sign with lesser amplitude, that are represented as two white troughs (Fig 3.1.2 b).

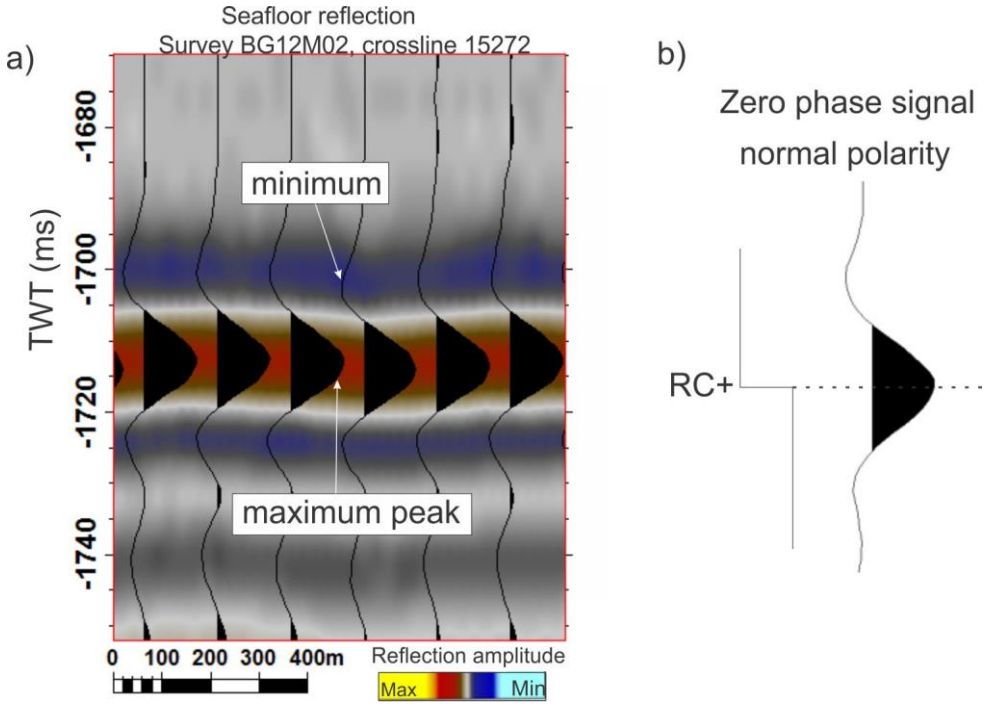

***Figure 3.1.2**: Zero-phase pulses with normal polarity using the convention of Sheriff (2006) **a)** Seafloor reflection from the study area shows normal polarity with wavelet. Notice that in this study positive amplitudes are red, and negative amplitudes are blue. **b)** Zero-phase signal with normal polarity convention. The figure is modified from Sheriff (2006).*

3.1.2 Seismic data quality

The quality of the seismic dataset is overall very high with little noise in the studied interval. The frequency of the seismic signal is mostly between 30-50 Hz. The 3D seismic cube has been cut and modified at -4250 ms (TWT) to display only the focused area.

3.1.3 Seismic resolution

Seismic resolution is the ability to distinguish two nearby features, and is commonly known as the minimum distance between two features. Seismic interpretation is related to resolution in two directions, as vertical (in two-way traveltime) and horizontal (trace to trace), as the resolution can be detected for both vertical and horizontal aspects (Sheriff 1977, 1985; Brown 1999).

The resolution of seismic data is measured in terms of the seismic wavelength, which is provided by the velocity and frequency (Fig 3.1.3). The velocity is denoted by v (m/s), frequency is given by f (Hz), and wavelength is denoted by λ (m). Seismic velocity increases with depth due to compaction. This is opposite to the frequency, which decreases with depth because the higher frequencies in the seismic signal are more quickly attenuated, resulting in the increase of the wavelength with depth, and this is resulting in lower resolution (Brown 1999).

$$\lambda = \frac{v}{f} \qquad (3.1)$$

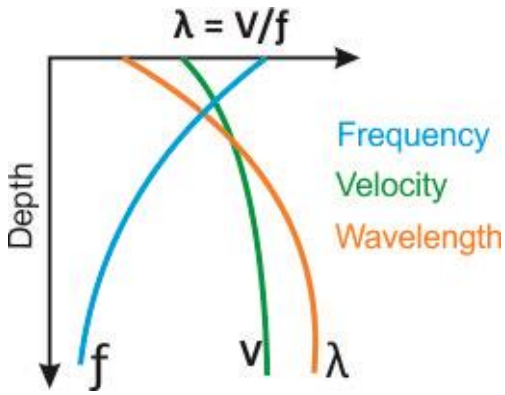

Figure 3.1.3: *Relationship between frequency, velocity, and wavelength as they propagate downward through the subsurface. Velocity increases with depth, as frequency decreases. This results in increasing wavelength of the seismic signal. Illustration modified from Brown (1999).*

3.1.3.1 Vertical resolution

The vertical resolution is the minimum thickness of a layer where the reflections from the top and the bottom of the layer can be separated. According to Brown (1999) the vertical resolution is resulting from the interaction of the reflection from the interfaces. It has two limits; the limit of separability and limit of visibility. The limit of separability is equal to ¼ of the wavelength, the same as half a period (Sheriff, 1985; Brown, 1999; Reynolds, 2011). This is simply the bed thickness related to the closest separation of two wavelets of a given bandwidth. It means we can identify the top and bottom of a layer, as long as the bed thickness is equal or bigger than the ¼ of wavelength, λ/4. For thinner intervals than λ/4, the amplitude is progressively attenuated until the limit of visibility is reached. The limit of visibility depends on the acoustic contrast of layers related to signal-to-noise ratio in the data, the phase of the data or the shape of the seismic wavelets. The vertical resolution is given here as Vr (m) and wavelength is denoted by λ (m);

$$Vr = \frac{\lambda}{4} \qquad (3.2)$$

3.1.3.2 Horizontal Resolution

The horizontal resolution for unmigrated seismic data can be defined by the size of the Fresnel zone (Sheriff, 1977). This represents the smallest horizontal distance from two reflections points that can be recognized as two separated points rather than one. Seismic waves propagate spherically from the source to the reflector along a ray path. When the wavefront reaches a reflecting interface part of it will be reflected and some of it will continue. Figure 3.1.4 illustrates the first energy reaching the receiver from a plane reflector and the ¼ region of the wavelength behind the wavefront is called the first Fresnel zone. The wavefront returning to the geophone/hydrophone within half cycle or ¼ of the wavelength is known as *the Fresnel zone* (Sheriff, 1977, 1985).

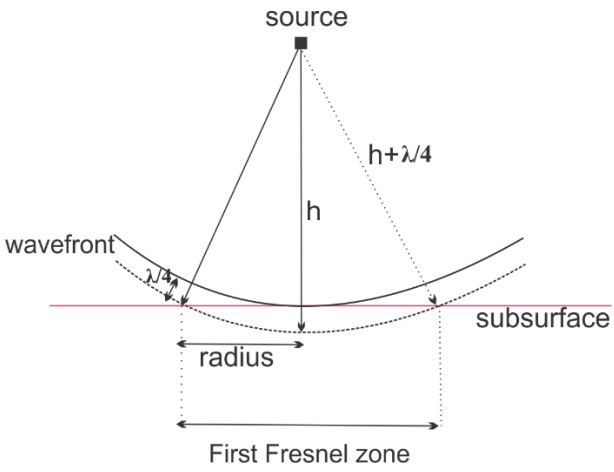

***Figure 3.1.4**: Illustration of the First Fresnel zone on the reflector at the depth (h). The figure is modified from Sheriff (1977).*

The size of the Fresnel zone before migration can be calculated by the relationship;

$$r(f) = \frac{V}{2}\sqrt{\frac{t}{f}} \qquad (3.3)$$

The radius of the Fresnel zone is denoted as r (f), the average propagating speed of the incident wave is given as V (m/s), where two-way travel time is t, and f is the frequency. From the equation above it is shown that the Fresnel zone radius is increasing with depth as the velocity is increasing downward (Brown, 1999).

The horizontal resolution can be improved by migration (Fig 3.1.5). For 2-D migration, the Fresnel zone will be collapsed in only one direction, the other direction will be reduced to an ellipse perpendicular to the seismic line. For 3D migration, the Fresnel zone will be reduced in all directions to a small circle (Sheriff, 1977; Brown, 1999) (Fig 3.1.5).

The horizontal resolution of migrated seismic data is given by Sheriff (1977) and Reynolds (2011) as:

$$Hr = \frac{\lambda}{4} \text{ or } \frac{V}{4f} \qquad (3.4)$$

The Fresnel zone after migration is denoted as Hr, the wavelength is given as λ, V is velocity and f is the frequency.

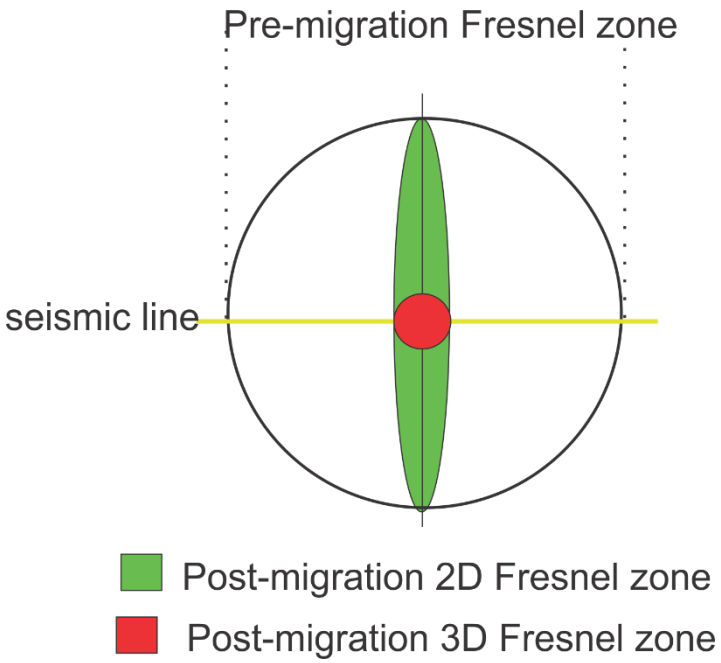

Figure 3.1.5: *Illustration of Fresnel zone size and shape before and after migration. The green ellipse illustrates that the Fresnel zone is reduced perpendicular to the seismic line for 2-D migration. The red circle displays that the Fresnel zone will reduced to a small circle for 3-D migration. Figure is modified from Brown (1999).*

3.1.3.3 Resolution of the dataset in this study

The vertical- and horizontal resolution of the dataset from the Survey BG12M02 can be calculated. The P-sonic well log will be used to identify resolution to the upper Brygge Formation, due to velocity values. While it is absent velocity values in the P-sonic well log in the Kai Formation. Therefore, the closest velocity model, which have been found from the inner part of the southern Vøring margin will be used (Storvoll et al., 2006) (Fig. 3.1.6).

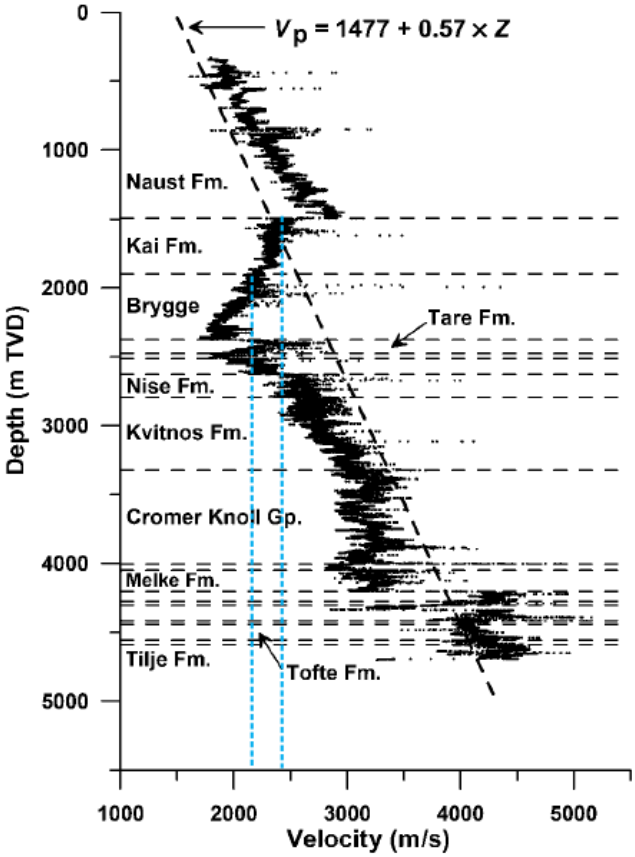

Figure 3.1.6: *Velocity model based on studied wells, correlated by data from various publications. The figure is modified from Storvoll et al. (2006).*

The velocity is approximately 2,400 m/s for the top of the Kai Formation, and 2,200 m/s at the base of the formation. For the Intra Brygge 1 and 2 will be calculated by applying the equation 3.5 with using the slowness from the P-sonic log. Normally, the velocity in sediment will increase downward in relation to compaction. This velocity model trend between the Kai Formation is atypical pattern. It will not show the same increase in velocity in depth because it has different clay minerals in these sediment packages, which has a connection to a different density decrease with depth (Storvoll et al., 2006). The frequency of the seismic data has earlier been given in 30-50 Hz. For simplicity the frequency will be given by using inspector mode in the Petrel program. The resolution of the data set will be calculated by applying the equation 3.1-3.4., and have shown in Appendix 8.1. The table 3.1 summarizes the resolution of the dataset in this study.

Surface boundaries	Velocity (m/s)	Frequency (Hz)	Two-way travel time (s)	Vertical resolution (m)	Horizontal resolution, Pre-migration (m)	Horizontal resolution, Post-migration(m)
Top Kai	2,400	38.16	1959	15.72	272	15.72
Base Kai	2,200	40.46	2187	13.60	255.7	13.60
Intra Brygge 2	1,927	41.45	2583	11.63	240.52	11.62
Intra Brygge 1	2,111	45.39	2648	11.63	259.94	11.63

***Table 3.1**: Summary table of the resolution from the dataset of the study.*

3.1.4 Artifacts and noise

It is important to be able to recognize artefacts and eliminate them from seismic dataset because they may obscure the true structures and lead to false interpretations. From the generated horizon surfaces in this study some artefacts were found at the top layer of the Kai Formation. X Several parallel lines located in NW-SE orientation are referred to inlines, and another lines located in NE-SW orientation, identified as crosslines (Fig 3.1.7). However, it was not easy to observe clearly artefacts, this should have a mention that these were noted in order to avoid misinterpretation.

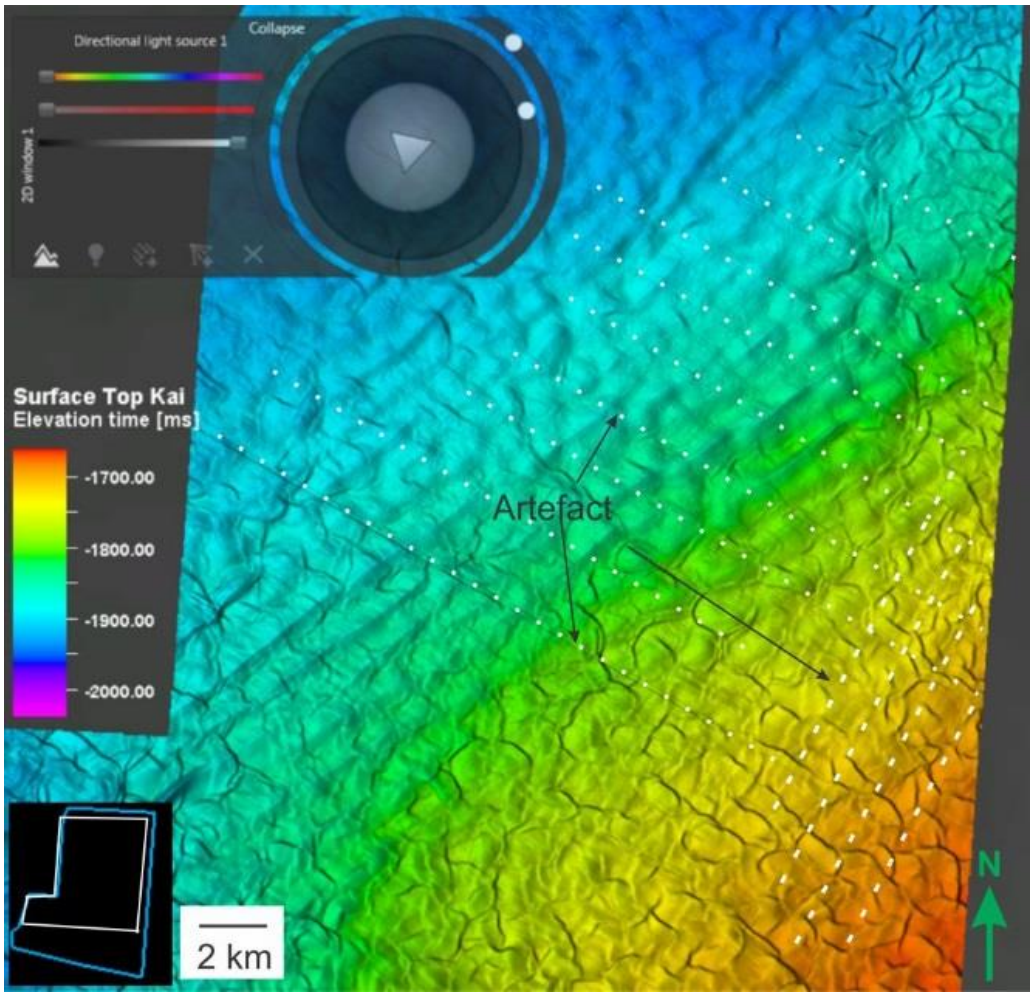

Figure 3.1.7: *Artefacts shown in the horizon surface of the top of the Kai Formation. Artefacts marked with long parallel dotted lines are referred to inlines, and another dash lines are in perpendicular referred to crosslines. The vertical exaggeration is 20x and the light source is from ENE direction*

3.2 Methods of seismic interpretation

3.2.1 Seismic stratigraphic analysis

Stratigraphy can be considered as the relationship between rocks and time, and the events that are recorded in those rocks can be determined by their stratigraphic relationship, which can been associated with events of climate change, tectonic movements of the crust and their sedimentary characteristics (Nichols, 2009).

The interpretation of the sedimentary successions in terms of their depositional environment is one of the main aims of sedimentology (Collinson et al., 2005). Seismic stratigraphy is the study of the stratigraphy and depositional facies of seismic data, and is often used for correlation of depositional sequences (Mitchum et al., 1977). Deposition of the stratigraphic sequences is associated with cycles of regional and global changes of sea level, and are defined as genetically related strata and bounded by unconformities and their correlative conformities (Mitchum et al., 1977; Vail, 1987). Seismic stratigraphy analysis can be divided into two different steps; (1**) seismic sequence analysis** by subdividing the seismic section into packages of concordant reflections, which are separated by surfaces of discontinuity, and interpreting them as depositional sequences; and (2**) seismic facies analysis** by analysing the configuration, continuity, amplitude, frequency, and interval velocity of seismic reflection patterns within seismic sequences. These patterns are interpreted in terms of environmental setting and estimates of lithology (Mitchum et al., 1977).

3.2.1.1 Seismic sequence analysis

A seismic sequence is defined by Mitchum et al. (1977) as a depositional sequence identified on a seismic section. The principal criteria for recognition of seismic sequence boundaries are reflection terminations, which is marked at tops and bases by surfaces of discontinuity. Figure 3.3.1 illustrates the types of reflection terminations within seismic sequences. The termination included within Figure 3.2.1 can be classified into two main types of discordance, as top-discordant and base-discordant. Discordance is the main physical criterion used in the determination of sequence boundaries, and discordant relation is the best indicator of an unconformity resulting from erosion or non-deposition (Mitchum et al., 1977).

A Top-discordant relation includes: (1) *erosional truncation* meaning that parts of the strata have been removed along an unconformity surface; and (2) *toplap* is the terminal reflections interpreted as strata terminating against an overlying surface because of non-deposition (sedimentary bypassing) and only slight erosion (Mitchum et al., 1977).

A Base-discordant relationship includes: (1) *onlap* which is a lapout at the lower boundary of a depositional sequence, where an initially horizontal stratum laps out against an initially inclined surface, or inclined stratum laps out updip against a surface of greater initially inclination; and (2) *downlap* that is a lapout at the lower boundary of a depositional sequence, where an initially inclined stratum terminates downdip against an initially horizontal or inclined surface. *Offlap* is a term used for seismic reflection patterns from strata prograding into basins (Mitchum et al., 1977) (Fig. 3.2.1).

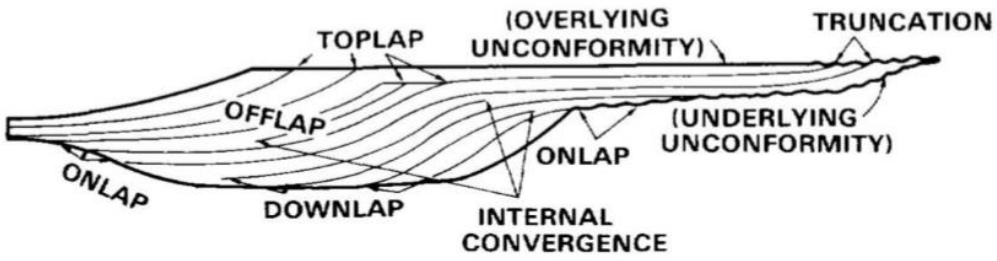

Figure 3.2.1*: The main reflection terminations that use to be identify within seismic sequence. The figure is added from Mitchum (1997).*

3.2.1.2 Seismic facies analysis

Seismic facies units are in 3D seismic units composed of groups of reflections whose parameters vary from those of adjacent facies units. Seismic facies analysis is interpreted and described by these parameters; configuration, continuity, amplitude, frequency and interval velocity (Mitchum et al., 1977; Veeken et al., 2013). Table 3.2.1 summarize the geological interpretation based on the reflection parameters. Each parameter provides essential information of the geological subsurface (Mitchum et al., 1977).

SEISMIC FACIES PARAMETERS	GEOLOGIC INTERPRETATION
REFLECTION CONFIGURATION	• BEDDING PATTERNS • DEPOSITIONAL PROCESSES • EROSION AND PALEOTOPOGRAPHY • FLUID CONTACTS
REFLECTION CONTINUITY	• BEDDING CONTINUITY • DEPOSITIONAL PROCESSES
REFLECTION AMPLITUDE	• VELOCITY-DENSITY CONTRAST • BED SPACING • FLUID CONTENT
REFLECTION FREQUENCY	• BED THICKNESS • FLUID CONTENT
INTERVAL VELOCITY	• ESTIMATION OF LITHOLOGY • ESTIMATION OF POROSITY • FLUID CONTENT
EXTERNAL FORM & AREAL ASSOCIATION OF SEISMIC FACIES UNITS	• GROSS DEPOSITIONAL ENVIRONMENT • SEDIMENT SOURCE • GEOLOGIC SETTING

***Table 3.2.1**: An overview of the different seismic reflection parameters and geologic interpretation, which have association with each reflection parameter. These seismic reflection parameters are used in seismic stratigraphy. Table is modified from Mitchum et al. (1977).*

The overall geometry of a seismic unit consists of the external form and the internal reflection configuration of the unit (table 3.2.2); both must be described to understand the geometric interrelation and depositional setting of the units. First, initially analysis will start with a 2D mode of a single seismic section, and these apparent reflection configurations will be then approved in a 3-D grid of a seismic section (Mitchum et al., 1977). When the internal reflection parameters, the external form, and the 3-D associations of these seismic facies units are accurately represented the units can be interpreted in terms of environment setting, depositional processes and lithology (Mitchum et al., 1977; Vail, 1987).

REFLECTION CONFIGURATIONS (WITHIN SEQUENCES)		EXTERNAL FORMS (OF SEQUENCES AND SEISMIC FACIES UNITS)
PRINCIPAL STRATAL CONFIGURATION		SHEET
PARALLEL		SHEET DRAPE
SUBPARALLEL		WEDGE
DIVERGENT		BANK
PROGRADING CLINOFORMS		LENS
SIGMOID		MOUND
OBLIQUE		FILL
COMPLEX SIGMOID-OBLIQUE		
SHINGLED		
HUMMOCKY CLINOFORM		
CHAOTIC		
REFLECTION-FREE		
MODIFYING TERMS		
EVEN	HUMMOCKY	
WAVY	LENTICULAR	
REGULAR	DISRUPTED	
IRREGULAR	CONTORTED	
UNIFORM		
VARIABLE		

***Table 3.2.2**: Geological interpretation of seismic facies parameters. Notice that within a given external form, one or several internal reflection configurations may occur. The table is modified from Mitchum et al. (1977)*

3.2.2 Seismic expression of contourites.

Seismic reflection characteristic is useful for identify and map contourite deposits and allow us to predict lithology and reconstruct the geological and (paleo-) oceanographic history (Rebesco and Stow, 2001; Nielsen et al., 2008). Laberg et al. (2005a) have studied and identified the deposits of the Kai formation that has been interpreted to be contourites (Laberg, Dahlgren, & Vorren, The Eocene-late Pliocene paleoenvironment in the Vøring Plateau area,. Norwegian Sea- paleoceanographic implications, 2005a). Nielsen et al. (2008) divide the characteristic of contourites into three orders of seismic elements, called large-, medium- and small scale, where increasing order represent an increasing level of seismic interpretation details, as illustrated in figure 3.2.2.

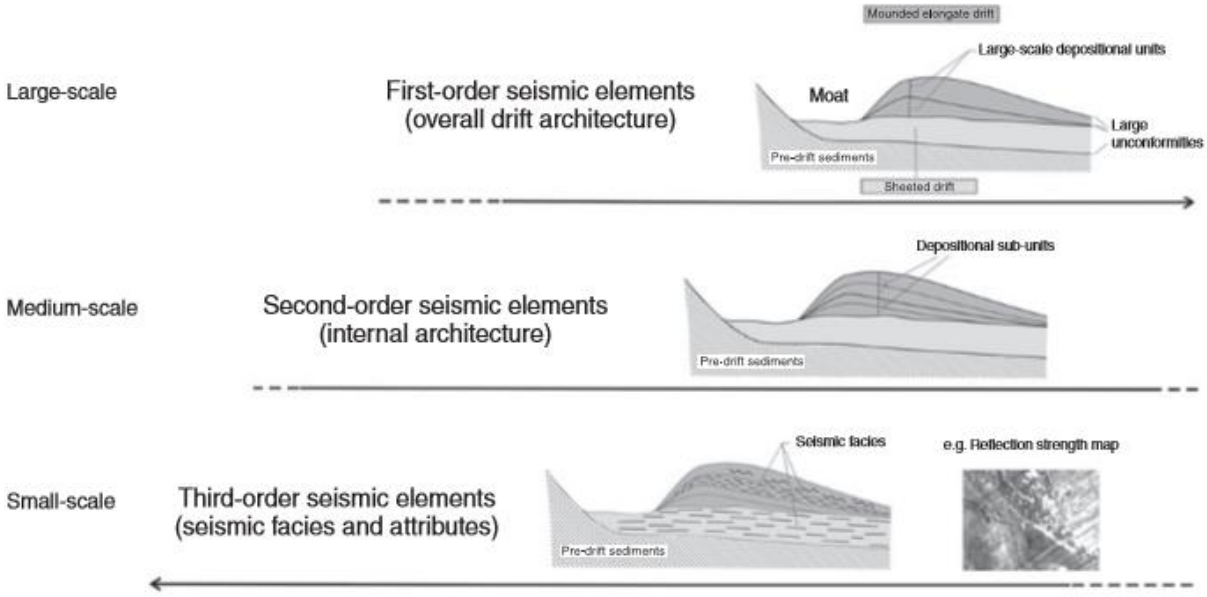

Figure 3.2.2: *An overview of the three orders of seismic elements, each seismic element shows seismic characteristic of contourite deposits. The figure is added from Nielsen et al. (2008).*

Large-scale, the first order of seismic elements

Identifying the overall architecture of the deposited contourite drifts, i.e. their external geometry is based on the identification of the upper and lower boundaries of confining drift system, and the configuration of the larger internal seismic units (Nielsen et al., 2008). Drift systems can be grouped based on geometry into seven types (Rebesco and Stow, 2001):

(1) *Sheet drifts* characterized by a very low relief and a large lateral extent (abyssal sheet, slope plastered sheet, slop patch sheet),
(2) *Giant elongated drifts* characterized by moderate to high relief and a variable extent (detached, separated, elongate to irregular small-scale patch mound),
(3) *Channel-related drifts*; patch drifts within channels/moats, contourite fans at the channel exit, contourite channel-levee drifts),
(4) *Confined drifts* located within (actively subsiding) basins or troughs,
(5) *Mixed drift systems* with moderate relief and relatively small extent (local infill at the head of slump scars),
(6) *Infill drifts* (turbidite-contourite, debrite contourite, hemipelagite-contourite, glacigenic contourite systems), and
(7) *Fault-controlled drifts* developed in response to fault-generated basement relief and subsequent syn-depositional fault reactivation.

A major change in depositional style from a current-affected regime to a non-current affected regime, and vice versa may occur when contourite drifts were deposited. These changes may result in regional unconformitites with can be identified as high amplitude reflection both at the base and within the drift (Rebesco and Stow, 2001; Nielsen et al., 2008). Internally, reflection often show a low-angle downlap onto the basal unconformity (Sangree and Widmier, 1977; Nielsen et al., 2008). A whole drift has often a uniform pattern of continuous, low- to medium-amplitude internal reflection (Nielsen et al., 2008). The shape of these first-order units tends to follow the overall geometry of the drift, often extensive and sub-parallel of moderate to low amplitude with gradual changes reflecting temporally and laterally stable conditions, and these can indicate the temporary character of the changes in the depositional regime (Rebesco and Stow, 2001; Nielsen et al., 2008).

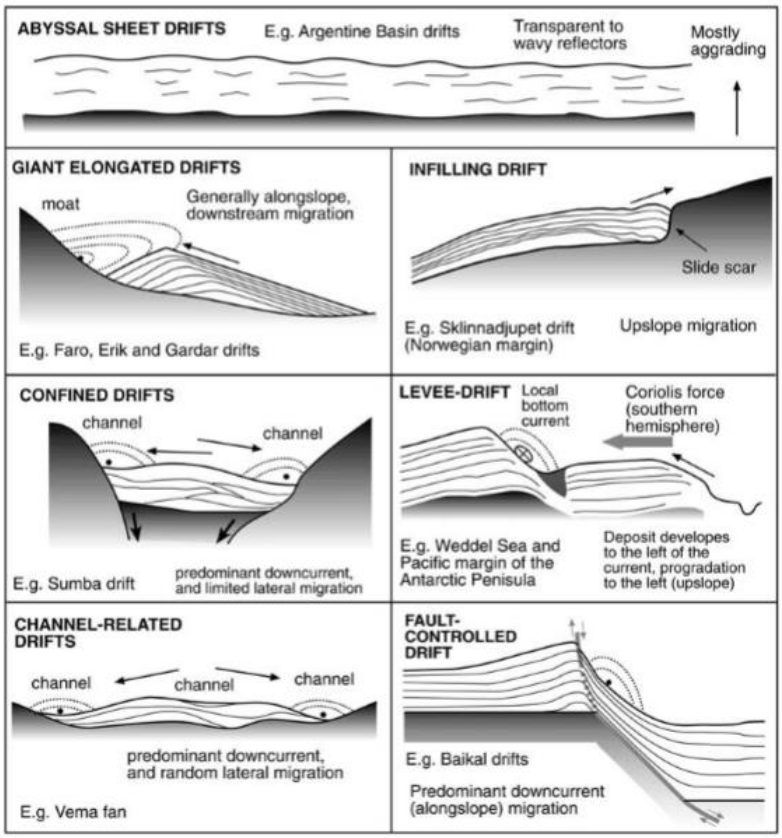

Figure 3.2.3*: The seven different types of contourite drifts is showing their large-scale geometry. Black arrows indicate migration trend and inferred axis of bottom-current flow is shown with dashed curves. Illustration is added from Rebesco and Stow (2001).*

Medium-scale, the second order of seismic elements

Based on the internal drift architecture, that is the internal character of the large-scale units, commonly composed of sub-units including the following reflection pattern; (1) broadly lenticular, upward-convex seismic units, (2) progradational stacking of units showing migration in a down-current direction or an aggrading stacking pattern, (3) downlapping and sigmoidal progradational reflection patterns are typical, though onlapping reflectors may commonly occur along steep slopes (toplapping might occur in connection to internal erosional unconformities), (4) the lateral migration direction is influenced by the Coriolis force, providing the right morphological context, current direction and latitude of deposition (Rebesco and Stow, 2001; Nielsen et al., 2008). The second-order seismic sub-units results from smaller fluctuations causing variations in sediment characteristics like composition, homogeneity, compaction, bedding, and bioturbation (Nielsen et al., 2008).

Small-scale, third order seismic elements

Small-scale, third order seismic elements cannot alone be used as a diagnostic tool, but may be useful in combination with the geometry of the seismic units and by correlation with core information (Nielsen et al., 2008). The seismic facies configurations normally found in contourite drifts are; (1) Continuous, (sub) parallel reflection configurations; (2) Wavy reflection configurations; and (3) structureless or non- reflection configurations.

Seismic attributes can be used to map current-induced bedforms, such as sediment waves, ripples, erosional furrows, moats, and channels which can be related to different current regimes and sediment types. Seismic facies analysis is useful in interpretation of variations in the contourite depositional environment (Nielsen et al., 2008).

3.2.3 Seismic attributes

An attribute is essentially a product of a basic seismic measurement. The basic formation is time, amplitude, frequency and attenuation and these form the basis of attribute classification (Fig 3.2.4) (Brown, 1999). A widely used generalization is that time-derived attributes present structural information, while amplitude-derived attributes present stratigraphic and reservoir information. Frequency are not well used but may give additional useful reservoir and stratigraphic information. Post-stack attributes can be extracted from one horizon as in Figure 3.2.4 (Brown, 1999).

Attributes are calculated and extracted from the data volume, following automatic spatial tracking. These data will provide time values for a horizon at the crest of a reflection with an accuracy of about a quarter of millisecond (Brown, 1999). **Dip** or dip magnitude is another time-derived horizon attribute focusing on structural details. The true dip of local plane is the attribute dip, the direction of that dip is the azimuth, **or dip azimuth** which is used in a similar way to dip (Brown, 1999). **Chaos** is measuring of the "lack of organization" in the dip and azimuth estimation method. It can be used to identify faults and discontinuities and for seismic classification of chaotic texture, and Chaos can be associated with local geologic features, which are affected by gas migration pathways, salt body intrusion, channel infill, etc. (Schlumberger, 2015). **Coherence**, continuity, semblance and covariance are all similar. The aim of these attributes is to convert a volume of continuity (the normal reflection) into a

volume of discontinuity (faults or other boundaries). These attributes run within the time window and use a variety of mathematical approaches similar to correlation. These attributes require an interpreted horizon as their input producing a volume where a discontinuity from a fault will be represented by a continuity (Brown, 1999).

Reflection amplitude extracted over one horizon produces a display normally called a horizon slice. **RMS, Root-mean-square** amplitude is more effective than absolute amplitude because of the high amplitudes are boosted by the squaring and divided it by the number of samples within a specific time window (Brown, 1999; Schlumberger, 2015). The RMS attribute is a good indicator of acoustic contrasts, which could indicate a change in lithology or the presence of hydrocarbons.

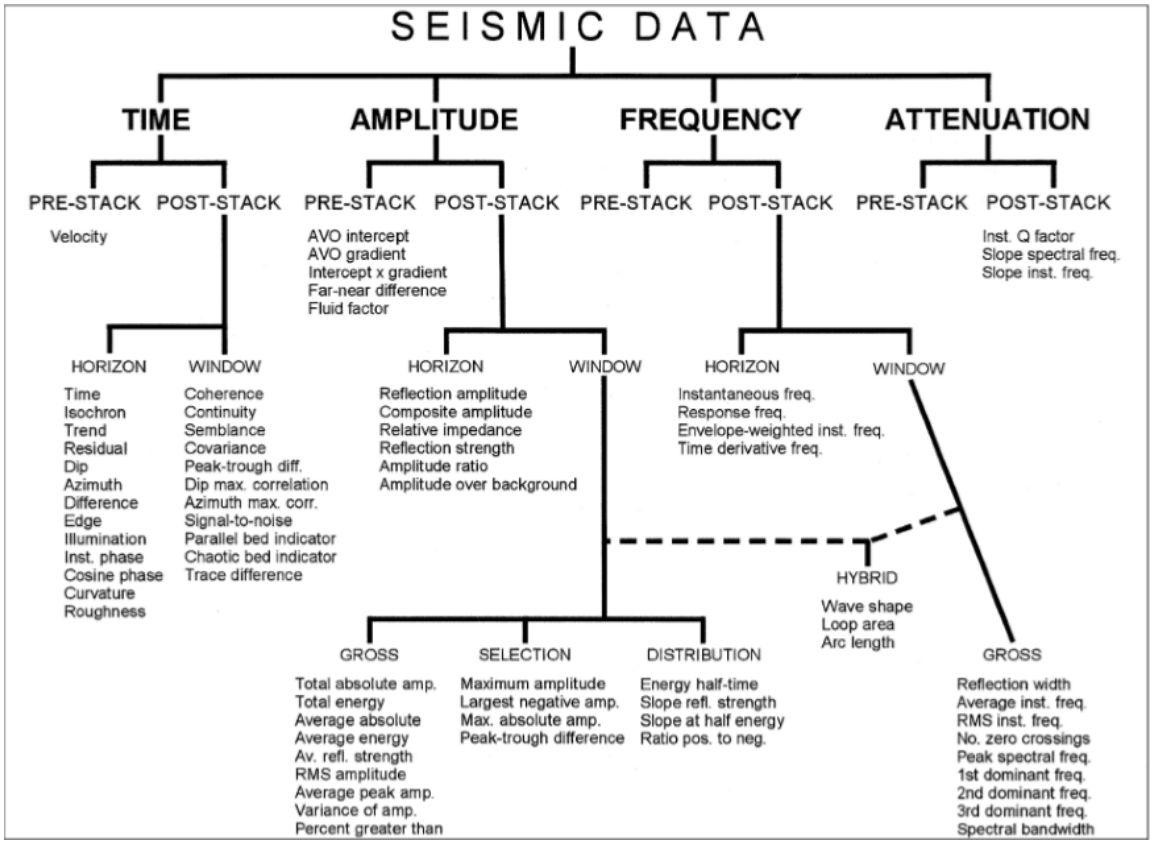

Figure 3.2.4*: A diagram showing seismic attributes, which are derived from the basic seismic information of time, amplitude, frequency and attenuation. The investigated window can be a constant time interval, as from one horizon or the interval between two horizons. The Figure was added from Brown (1999).*

3.3 Well logs

This is one well in the study area and these logs contains measured physical data. Some part of the well data covers our seismic. This well comprises three logs; Gamma ray, P-Sonic, Density (Table 3.3). The function and typically using of these logs will be mainly described base on the book "The Geological Interpretation of Well Logs" by Rider and Kennedy (2011). The position of well is located at 66°47'1.79" N and 4°33'34.85" E (NPD, 2017). The seismic data is covered by the well is indicated in Fig 3.3.1, the point on the line present the well top and surfaces, associated with information data of the three log types that is present in Fig 3.3.2.

Log type	Abbreviation	Value range and unit
Gamma ray	GR	0-100 gAPI
Density	DEN	1-3 g/cm^3
P-sonic	DTC_11	50-230 us/ft

Table 3.3: *An overview of log type, the abbreviation, value range and unit used in the well section window for these three logs.*

Three well-tops are located in the interpreted seismic section that marked the starting of a Formation (Fig 3.3.1), and can be given by different colors of surfaces to present the beginning of the Naust, Kai, and Brygge Formations, as shown in the window section (Fig 3.3.2). The well data have been used convert from two-way travel time to depth in meters and to obtain lithological information. In the well section window, the well top shows their relative position can be given both in two-way travel time (TWT) and depth in meters by using check-shot calibration, shown in Fig 3.3.2.

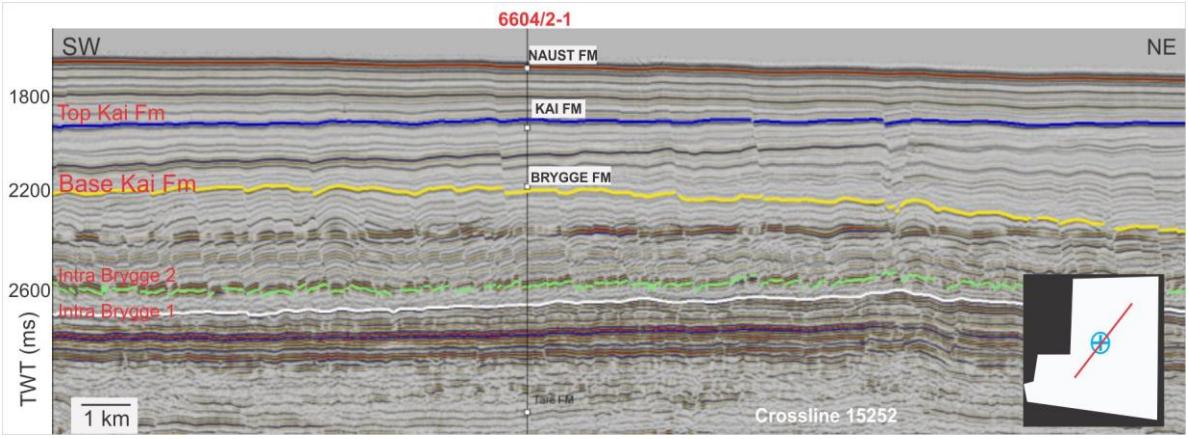

***Figure 3.3.1**: A NE-SW oriented seismic section* within 3D-survey BG12M02, and *relates to well 6604/2-1 is used in this study. The top of Formation is marked as a point on the well 6604/2-1 line.*

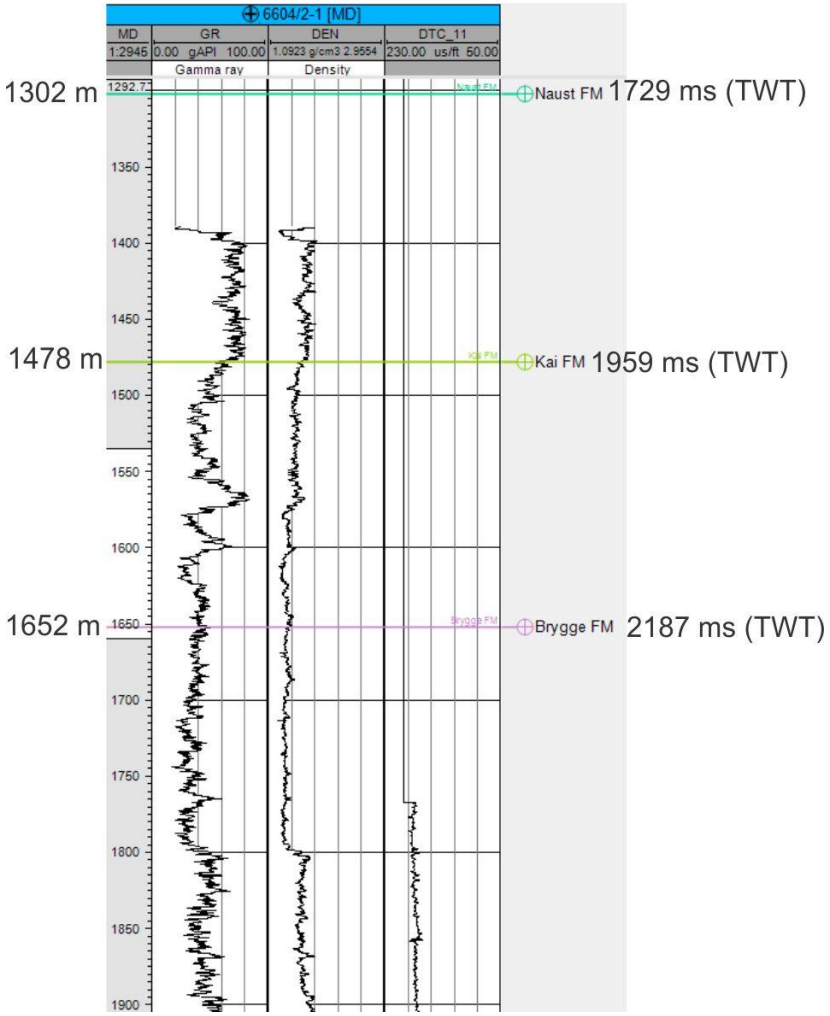

***Figure 3.3.2:** A well section window with all three log used in this study. The position of well tops is indicated according to NPD (2017). The P-sonic well logs (DTC_11) is flatten upward from the Brygge Formation. The value range and unit for each logs us summarized in table 3.2. **MD** in the first column is the depth domain that correspond to the start of the Naust, Kai and Brygge Formations, given in meter (m).*

3.3.1 Gamma Ray Log

The gamma ray logs give the detail of a formation's gamma radioactivity from naturally uranium, thorium and potassium (Fig 3.3.3). The simply log give a total count rate, which cannot separate these three individual elements. Most rocks comprise indication of gamma-emitting elements and radioactive in several degrees; igneous and metamorphic rocks more than sedimentary rocks. Between the sediments, shales have the highest gamma activity and this is the reason the gamma ray log is called "the shale log", but in generally not all shales are radioactive and not all that is radioactive is automatically shale.

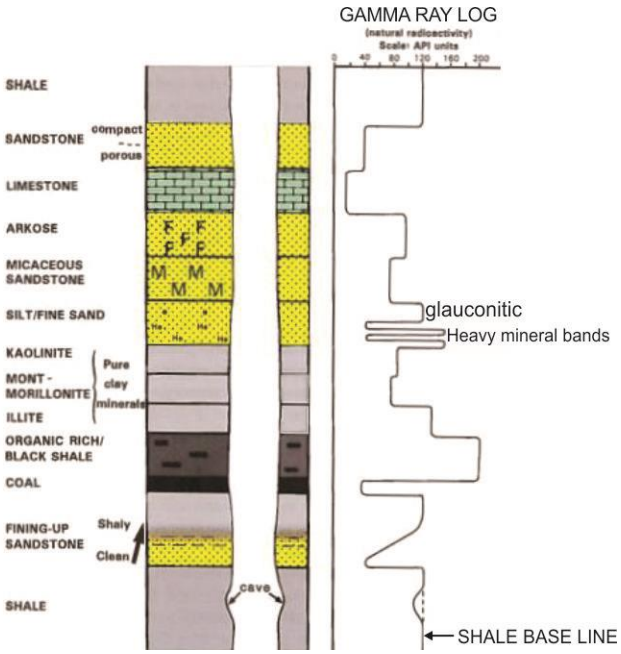

***Figure 3.3.3**: The gamma ray log and some typical responses. The gamma ray log shows natural radioactivity. F= feldspar, M = mica, * = glauconite, He = heavy minerals. The figure is modified after Rider and Kennedy (2011).*

The gamma ray log is the most important used as a shale indicator. Base on the quality of data, the gamma ray log can be used to identify lithology to propose facies and sequences, to identify stratigraphic surface and stratigraphically correlate (Rider and Kennedy, 2011). It can also indicate dominant clay mineral types, give indication of depositional environment, localize source rocks and major sequences stratigraphic surfaces (Rider and Kennedy, 2011)

Simple wireline gamma ray log. The energies of gamma ray is present in form of electromagnetic radiation, and are normally given in kilo or Mega electron volts (keV or MeV) which is commonly used in nuclear physic. While the accepted unit for radioactivity loggings is the API (American Petroleum Institute) unit and is defined in a reference pit of the

University of Houston, Texas. An API unit is 1/200 of the difference between the two radioactivities, as the low and the high values. The API units will be used as a calibrate tool and scale in the gamma ray log is usually designed to an average shale and reads at 100API units (Rider and Kennedy, 2011). Logging While Drilling (LWD) gamma ray log is used to calibrate with the API gamma ray pit, thus a typical shale will be read 100API units. Both of the LWD gamma ray and the wireline tool is a simple type, then the measurements can be presented the same way as a curve (Rider and Kennedy, 2011).

The gamma ray log is a good indicator of shales and will be the first indicator of lithology. The high API values is often related to increasing percentage of shale. However, the radioactivity of some typical lithologies other than shale should be considered. Therefore, any lithology indicated by the simple gamma ray log must be confirmed by using another logs, it could be several unexpected results (Rider and Kennedy, 2011)

Sandstones are usually show low API values in the gamma ray logs because there have quartz as the principal component of the coarse-grained detrital rocks and show no-radioactivity. However, these detrital mineral are radioactive, such as feldspars, micas comprise potassium, heavy minerals comprise thorium and lithic fragments comprise shales. These all cause that sandstones with high to moderate API values in the gamma ray logs. Marine sand comprises often glauconite and if the concentrations are high, then there will show high API values (Rider and Kennedy, 2011).

3.3.2 Sonic Log

The sonic log gives a measurement of the acoustic characteristics of a formation and present in interval transit time (Δt) or formation's slowness. The time for a transmit sound wave travel a known distance through the formation can be measured, as a sonic log was shown in figure 3.3.4. Sonic logs are used as an assistance to seismic investigations because these can be basically used to connect a well to the seismic, then we can find an accurate depth conversion, interval velocity, to calculate velocity profile, and produce an acoustic impedance log. The sonic log are importantly to help in seismic processing and attribute analysis. The compressional sonic log (p-sonic log) can be used to identify lithology, indicate source rocks, normal compaction and overpressure, and is regularly used in correlation (Rider and Kennedy, 2011).

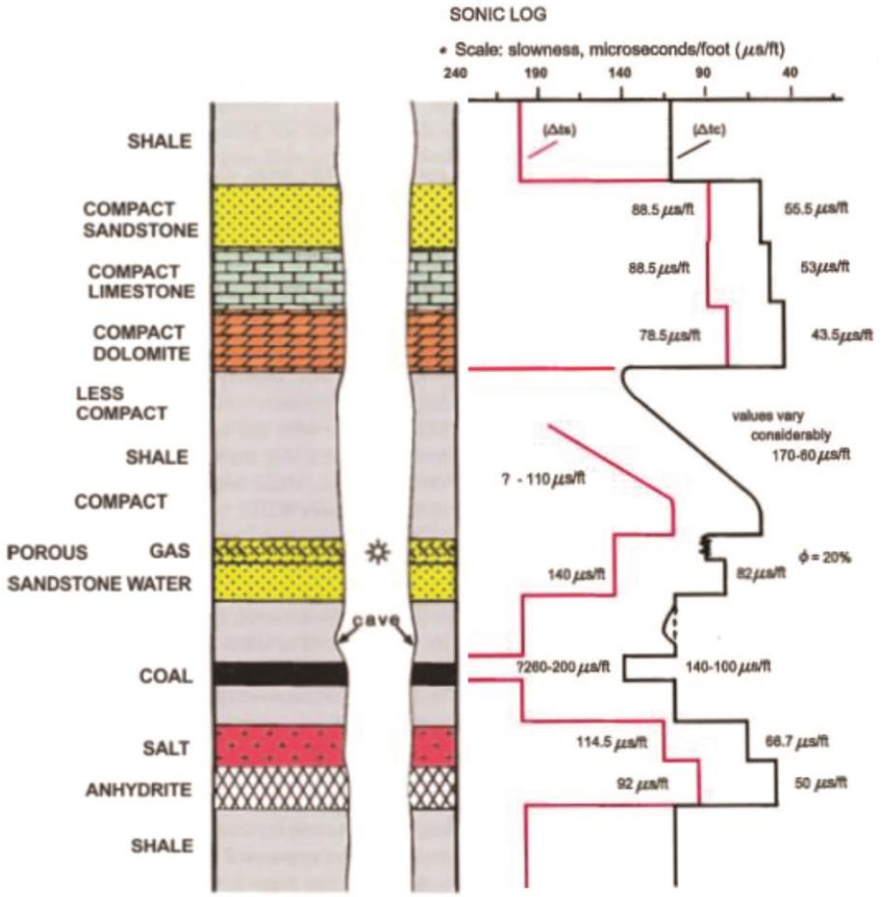

Figure 3.3.4: *The sonic log shows a formation's ability to transmit sound waves, which is expressed as slowness or Interval Transit Time, Δt. *(1x10^6) / Δt = sonic velocity ft/sec. Δtc = compressional slowness; Δts = shear slowness. The figure is added from Rider and Kennedy (2011).*

3.3.3 Density Log

The density log is a record of the formation's bulk density (Fig 3.3.5), which includes the solid matrix (as the minerals forming in the rocks) and the fluid within the pore spaces. The relationship between density and porosity is strictly true. In comparison to another logs, the density log has great vertical resolution. The density tool is designed to measure densities between 2 to 3 g/cm^3 with the accuracy of modern tools is ±0.01 g/cm^{3,} and this corresponds to the accuracy of ±0.5 pu (porosity units) in a typical porosity calculation. Together with sonic log, it can produce the acoustic impedance log, which is used to model seismic responses. The density log is a useful lithology indicator because it can identify specific minerals, and help to evaluate source rock organic matter content, and may use to identify overpressure. It is normally combined with the neutron log (Rider and Kennedy, 2011).

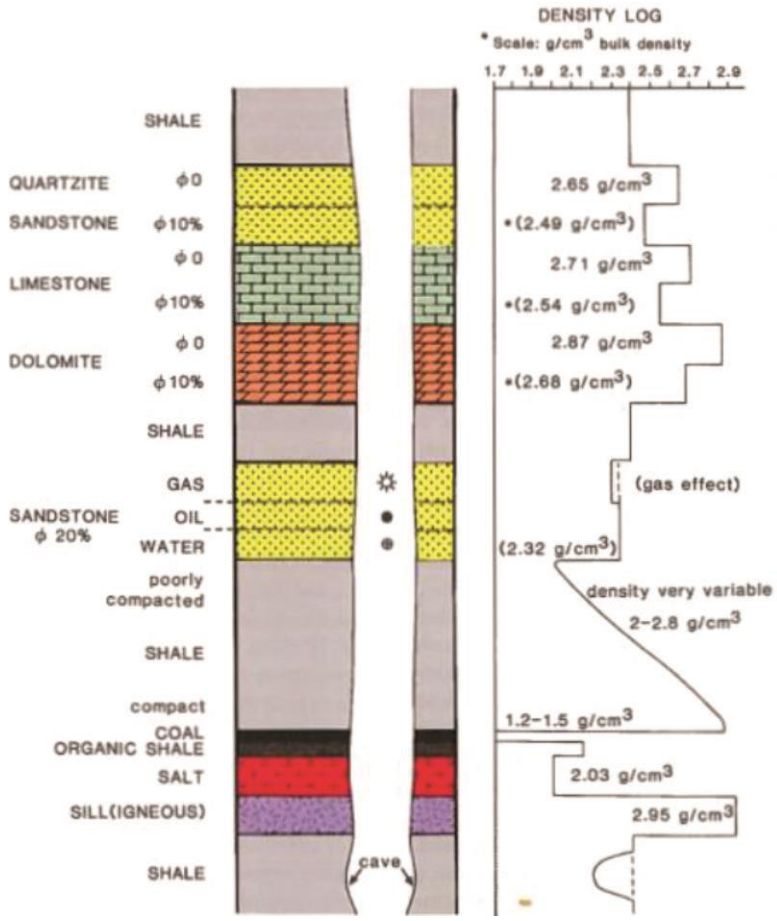

Figure 3.3.5: *The density log and some typical responses. The density log is record of a formation's bulk density. The figure is modified after Rider and Kennedy (2011).*

All density tools develop 'gamma-gamma' scattering to measure density. The tool both releases and detects gamma rays, then the density will be count at a detector depends on the density between it and the releaser. Detector counts are converted directly to bulk density in g/cm^3, which is normally plotted on a linear scale. The density difference in composition and texture, may have densities ranging, therefore the density log alone is commonly a poor indicator for lithology. It should to combine with the neutron log it will become probably the best qualitative indicator of general lithology (Rider and Kennedy, 2011).

Shale compaction contains a series of changing in texture and composition, resulting in decreasing in porosity and corresponding increase in density. As shallow, uncompacted clays have density around 2.0 g/cm^3 and then rises to 2.6 g/cm^3 with gradually increasing depth. The best view of compaction changes could be seen in the density log at a compressed vertical scale, as mechanical compaction is dominant in the near sub-surface at low temperature, while chemical compaction dominant below about 2 km and at the higher

temperatures. Shale density is often an indication of age, as older shales are denser than younger and lesser compacted shales. While shale porosity generally decreases as the older it gets (Rider and Kennedy, 2011).

In sandstone, the variation of bulk density is often associated with porosity changes, but it is not always correct if there are changes in grain density. As orthoquartzite (pure sand) have a grain density of 2.65 g/cm^3 but in reality sands are normally mixed with feldspars (2.52-2.74 g/cm^3) micas (2.82-2.99 g/cm^3), lignite fragments (0.5-1.8 g/cm^3) and rock fragments. Heavy minerals (3.0-4.19 g/cm^3) may also be component (Rider and Kennedy, 2011).

3.4 Software

3.4.1 Petrel

In this study the seismic interpretation and visualization program *Petrel 2015* software from Schlumberger has been used. Petrel is developed and built by Schlumberger and is used to interpret the 3D seismic data. Horizons have been interpreted by using 2D auto tracking and guided auto tracking. All seismic depth below the sea-surface are given in negative values in two-way time (TWT), in millisecond (ms). All the interpreted horizons will be further used to produce;

- Seismic stratigraphic analysis (see chapter 3.2).
- Isochore maps are contour maps that display variation in time between two seismic reflectors.
- Isopach maps displaying thickness variation of a formation, which can be used to identify the geometry of the formation.
- Seismic attribute (Schlumberger, 2015) :
    - RMS attribute calculated from the square root of the sum squared amplitude divided by the number of samples within the specific window used (default: 9 samples). This can display areas of high reflectivity with the aim of identifying hydrocarbon indicator and/or other features of high amplitude in the study area.
    - Variance attribute with dip-guidance is useful for accentuation structures like faults. Variance is used to isolate edges from the input data set, it means discontinuities in the horizontal continuity of amplitude.
    - Chaos attribute in signal pattern can be affected by gas migration, salt body intrusion, and for seismic classification of chaotic texture. Scaled from 0-1.

3.4.2 Corel Draw

The *CorelDraw X6* program has been used to modify and display most of the figures derived from Petrel.

4 RESULT

This chapter presents observations from the 3D-seismic survey BG12M02.3D and the exploration well 6604/2-1, and includes the description and interpretation of the Kai Formation and the uppermost part of the Brygge Formation. The interpretation will be based on several paleo-surfaces, thickness maps and volume attributes. This involves the morphology of buried surfaces and thickness variation of the Kai Formation and the upper part of the Brygge Formation. Internal seismic sub-units will also be described and interpreted in order to improve more detailed understanding of the paleo-environment during deposition.

4.1 Seismic stratigraphy and age estimation and lithology of the Brygge and Kai Formations

4.1.1 Age estimation

The seismic stratigraphy of the Kai Formation was correlated with previous work including Blakstad (2016), Rise et al. (2010) and Eidvin et al. (2014) while the upper Brygge Formation was correlated to studies from Eidvin et al. (2007; 2014). In addition, the established seismic stratigraphy was correlated to well 6604/2-1. Contrasting age estimates for the Kai and the upper Brygge formations have been identified in previous studies. Based on biostratigraphy and seismic correlation in the Norwegian Sea, south of Lofoten, Eidvin et al. (2007) interpreted the Kai Formation to be deposited during the late Miocene and early Pliocene, while results from the Gjallar Ridge in Vøring Basin implied a middle Miocene age of the Kai Formation (Eidvin et al., 2014). Løseth and Henriksen (2005) suggest a late middle to late Miocene age for the Kai Formation. In this study the most recent age estimate is used, i.e. the age estimate of Eidvin et al. (2014).

4.1.2 Lithology

The Brygge Formation comprises mainly clay on the present-day shelf, and is ooze-dominated in the distal, deeper marine of the Vøring Basin (Eidvin et al., 2014). These ooze sediments are characterized by small-scale polygonal faulting, caused by compaction and water expulsion (Eidvin et al., 2014). The Brygge Formation was deposited mainly from early Eocene to early Miocene time (Eidvin et al., 2007) (Fig 4.1.1).

The Kai Formation is overall clayey on the continental slope (Eidvin et al., 2014) while the basinal part as well as the Vøring Basin is in general mud-dominated (Laberg et al., 2005a; Stoker et al. 2005a) and infilled by fine-grained siliceous oozes, interpreted to have been deposited in a deep-sea environment (Laberg et al., 2005a; Stoker et al. 2005; Eidvin et al., 2007, 2014; Rise el al., 2010) (Fig. 4.1.1).

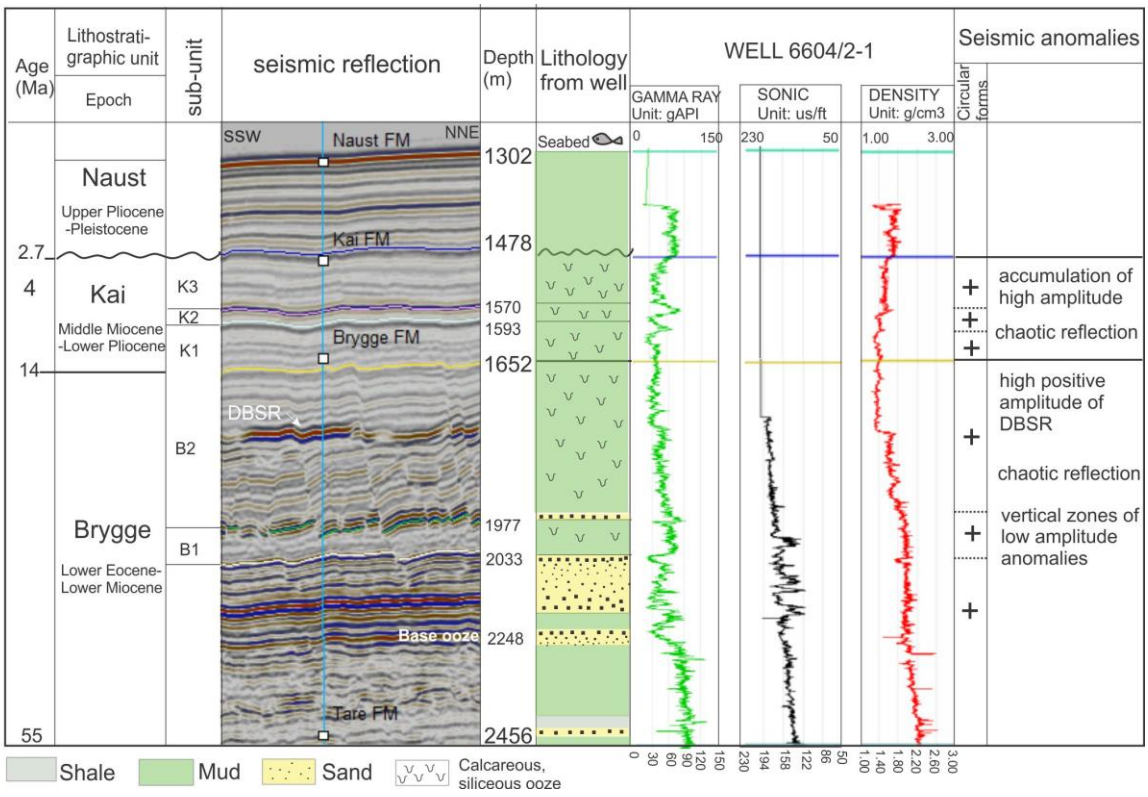

Figure 4.1.1: *Seismic section with the line of well 6604/2-1 presented by gamma ray, sonic and density logs in relationship to lithology from well and lithostratigraphy in the study area.*

Seismic overviewSurvey BG12M02.3D is subdivided into seismic sub-units based on both seismic reflection configuration and the results from well logs. The interpreted seismic sub-units from the 3D seismic data was correlated with earlier studies of the Kai formation from regional 2D seismic lines (Blakstad, 2016). An overview of the interpreted seismic reflections is shown in figures 4.1.2-4.1.5. The lines show mainly moderate to low amplitude, discontinuous and a parallel reflection configuration in the lower part of the seismic section, while these reflections are more continuous and parallel with moderate-low amplitude towards the upper part (Figs 4.1.3-4.1.5). All seismic sections were present as two-way travel time (TWT), in milliseconds (ms) in negative values due to depth below the sea-surface.

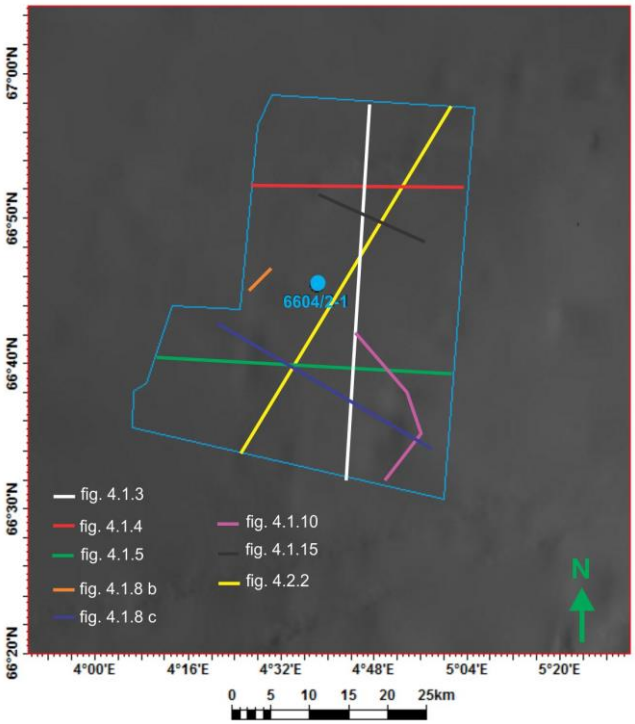

Figure 4.1.2: *Location of seismic lines shown in the result chapter. The blue circle is the position of well 6604/2-1 used in this thesis*

Six seismic horizons were identified, dividing the studied interval into five sub-units, each of which differs from the over- and underlying sub-units with respect to both seismic reflection configuration and geometry. However, in the lower part of the studied interval the seismic signature is disturbed that makes the interpretation difficult. Therefore, a volume attribute was created to improve the interpretation in this interval.

Seismic anomalies, characterized by a high positive amplitude has also been identified. The high positive amplitude reflection within the Brygge Formation in the Vøring Basin occurs at various depths. These are not parallel with the seafloor reflection (Brekke, 2000), but are rather (generally) concordant to the underlying stratigraphy (Figs 4.1.3-4.1.5). This reflection is interpreted as a digenetic reflector or diagenetic bottom-simulating reflection (DBSR) caused by the Opal A to Opal CT conversion (Neagu et al., 2010) (Fig. 4.1.3). The DBSR disturbs the reflection pattern in some parts of the Brygge Formation and is cross-cut by numerous polygonal faults, but as the DBSR is not the focus of this study it will not be further discussed.

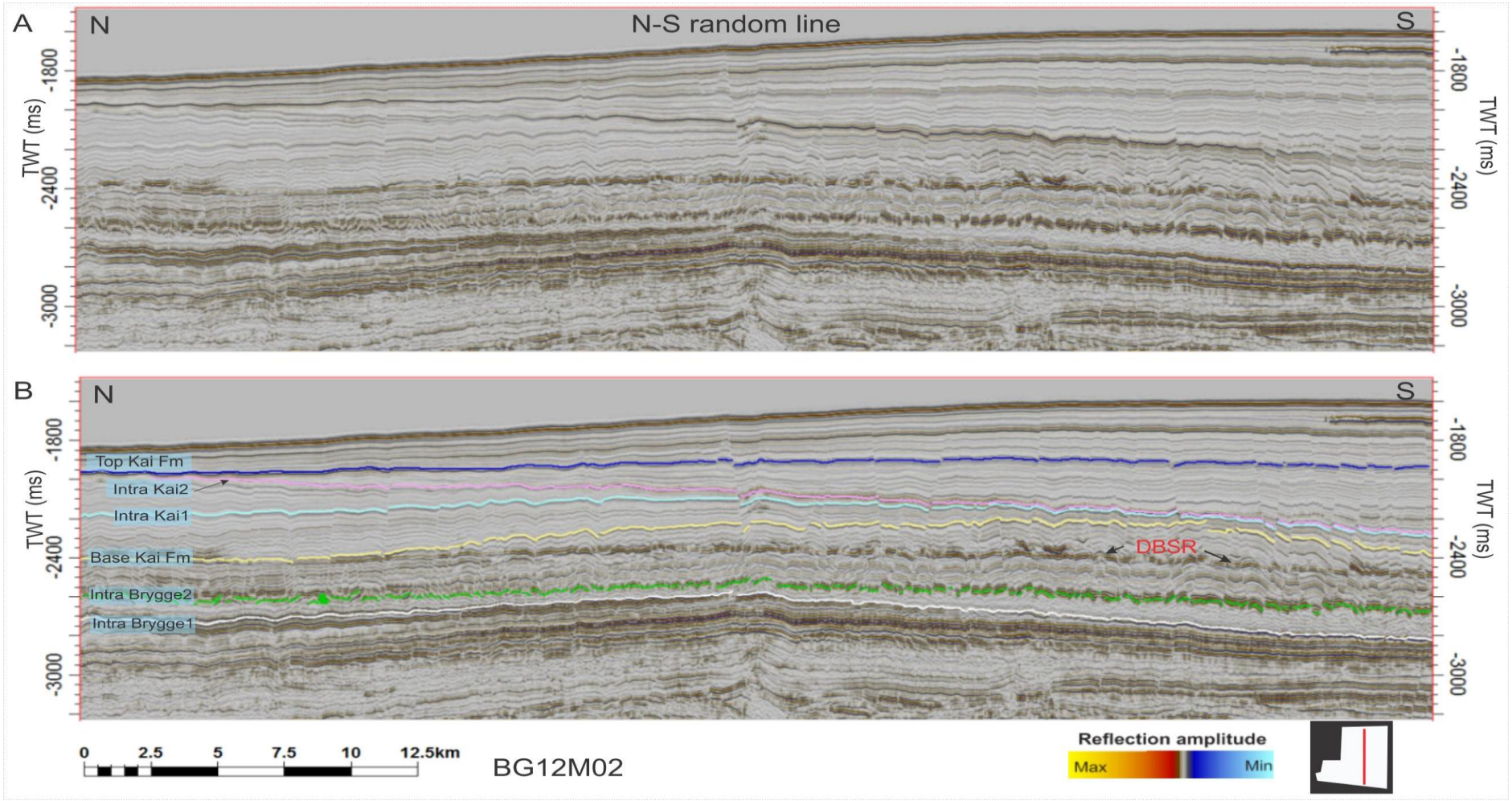

Figure 4.1.3: *A N-S oriented seismic section within 3D-survey BG12M02. (A) the seismic section without interpretation. (B) the interpreted seismic horizons along this section. Notice the high-amplitude reflection located between the underlying intra Brygge 2 and overlying base of the Kai Formation reflector interpreted as a diagenetic reflection or diagenetic bottom-simulating reflection, DBSR. The location of the seismic section is shown in the lower right corner.*

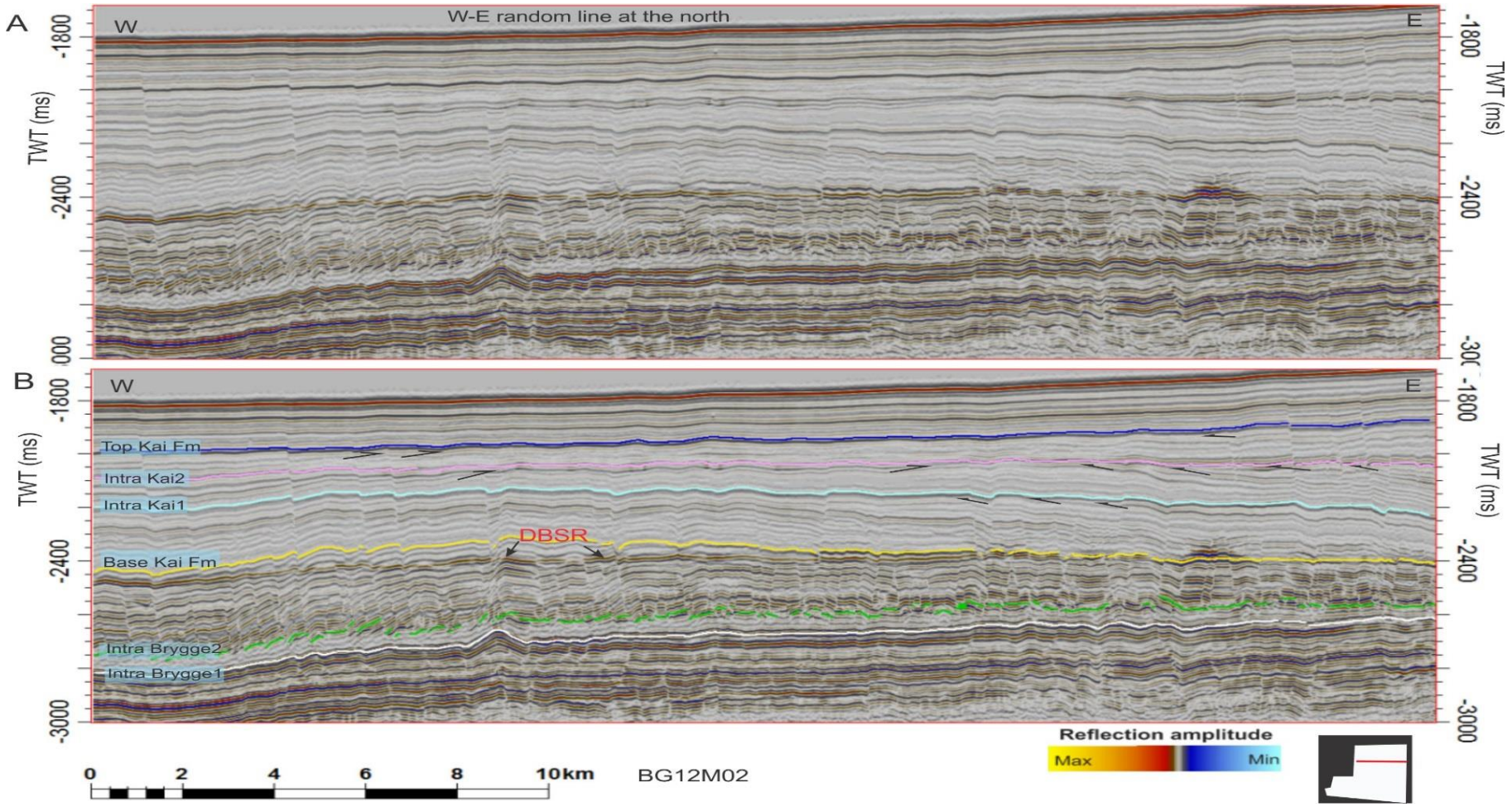

Figure 4.1.4: *A E-W oriented seismic section in the northern part of 3D-survey BG12M02. (A) the seismic section without interpretation. (B) the interpreted seismic horizons along this section. The black arrows indicate seismic reflection truncation of the underlying reflectors. The location of the seismic section is shown in the right corner of seismic section B.*

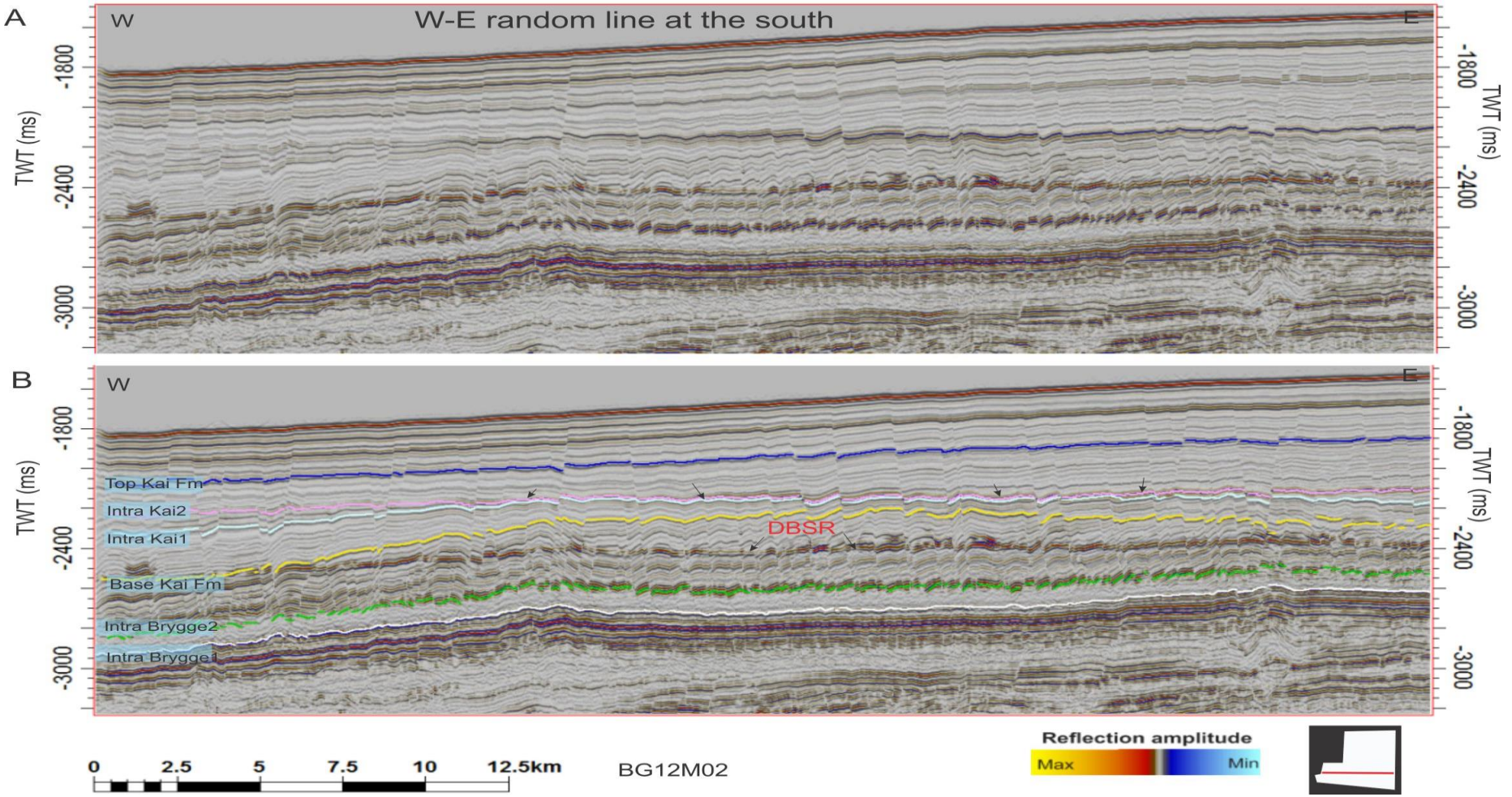

Figure 4.1.5: *A E-W oriented seismic section in the southern part of 3D-survey BG12M02. (A) the seismic section without interpretation. (B) the interpreted seismic horizons along this section. The black arrows indicate an interference of two reflectors. The location of the seismic section is shown in the right corner of seismic section B.*

4.1.3 Seismic reflections and paleo-surfaces

The Intra Brygge 1 (IB1) is the deepest interpreted surface of this thesis. The IB1 reflection is a continuous, positive, high-amplitude reflection. The surface varies in depth from -2750 ms in the north to -2825 ms (TWT) in the south (Fig. 4.1.3), with a dome in the middle part of the study area at -2600 ms (Figs 4.1.3, 4.1.6). From east to west, the IB1 reflection is dipping downward from -2600 to -2850 ms in the north (Figs 4.1.4, 4.1.6) and deeper, to -2950 ms in the south (Figs 4.1.5, 4.1.6).

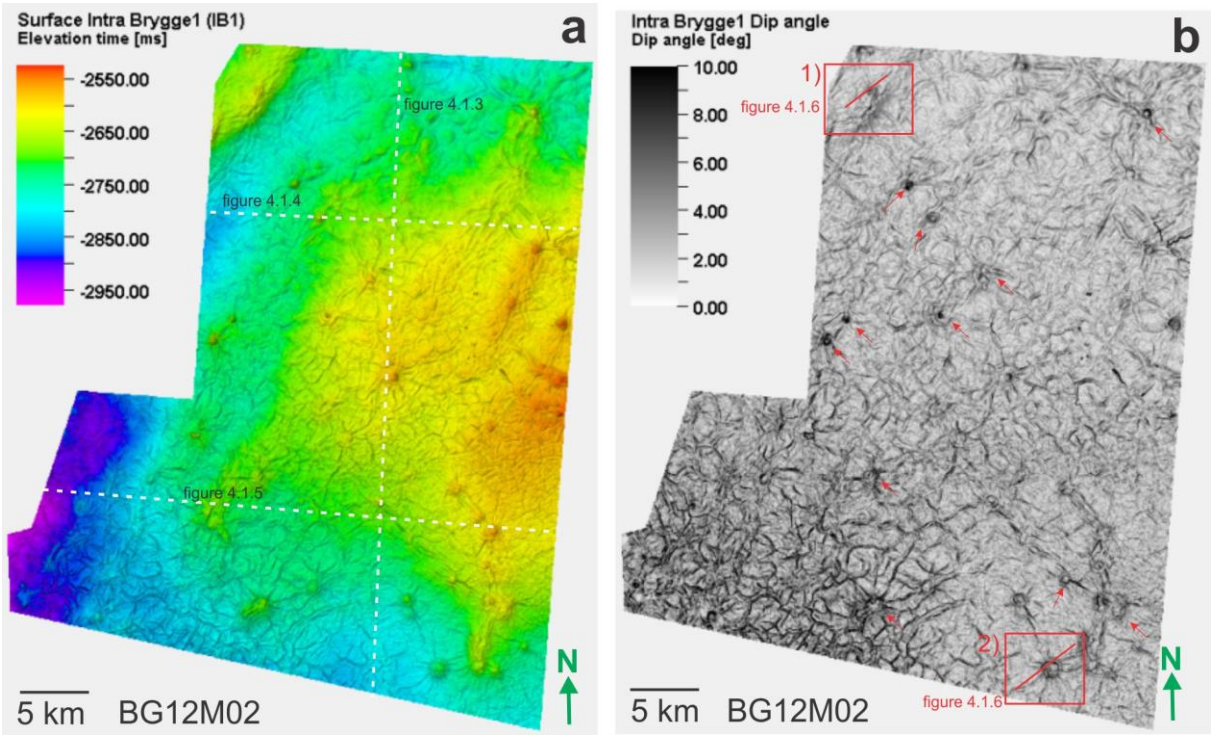

Figure 4.1.6: *The seismic horizon intra Brygge1 (IB1) of the upper Brygge Formation. A) Isochrone map of intra Brygge 1 showing depth and morphology of the paleo-surface (ms: millisecond TWT), vertical exaggeration 7.5. B) Dip angle map of the intra Brygge 1 surface.*

Irregular lines, some with random orientation, others forming a polygonal pattern have been observed all over the IB1 surface, most visible on the dip angle map. They are most frequent in the southwestern, deepest part of the survey (Fig. 4.1.6 b). These features were interpreted as part of a *polygonal fault system*.

The IB1 dip angle map also reveals several circular forms with or without a radial fault pattern (two examples are shown in figure 4.1.7). The circular forms with a radial fault pattern are most frequent and occurs in various parts of the study area. However, a few of them do not include a radial fault pattern, as shown in the northwestern part of this study. The height a

few meters to tens meters, and width around 700 - 1400 meter of these circular forms are presented in figure 4.1.7.

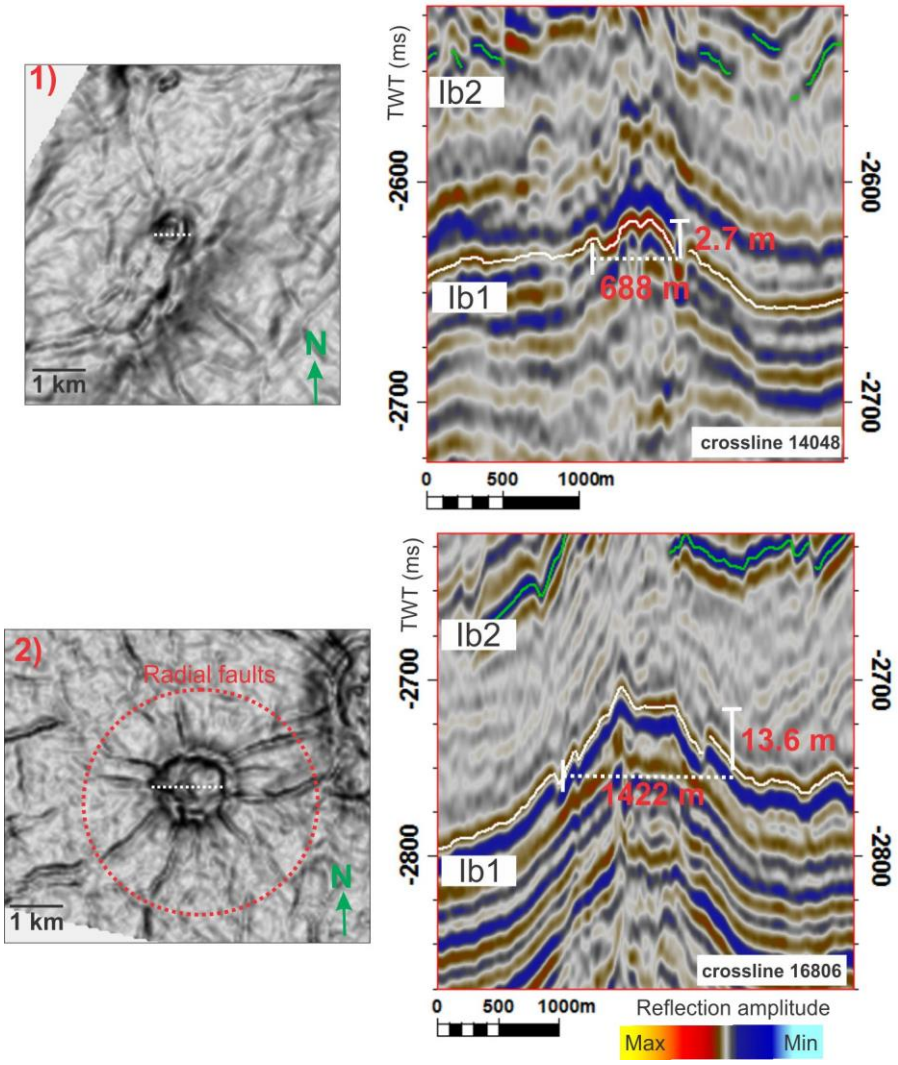

Figure 4.1.7: *Dip angle map of the intra Brygge 1 surface illustrating a radial fault pattern around the circular forms in 1) and 2). The white dotted line is a diameter of their circular forms, corresponding to the width in seismic sections on the right-hand side. The circular forms have been measured in height and width of their features.* ***Ib1****: Intra Brygge 1 reflection,* ***Ib2****: Intra Brygge 2 reflection.*

The circular forms corresponds to an upward bending part of the reflection. Both above and below these circular features the reflections are disturbed and/or masked up into the Kai Formation where high-amplitude anomalies are seen in several stratigraphic levels (Fig. 4.1.8 b).

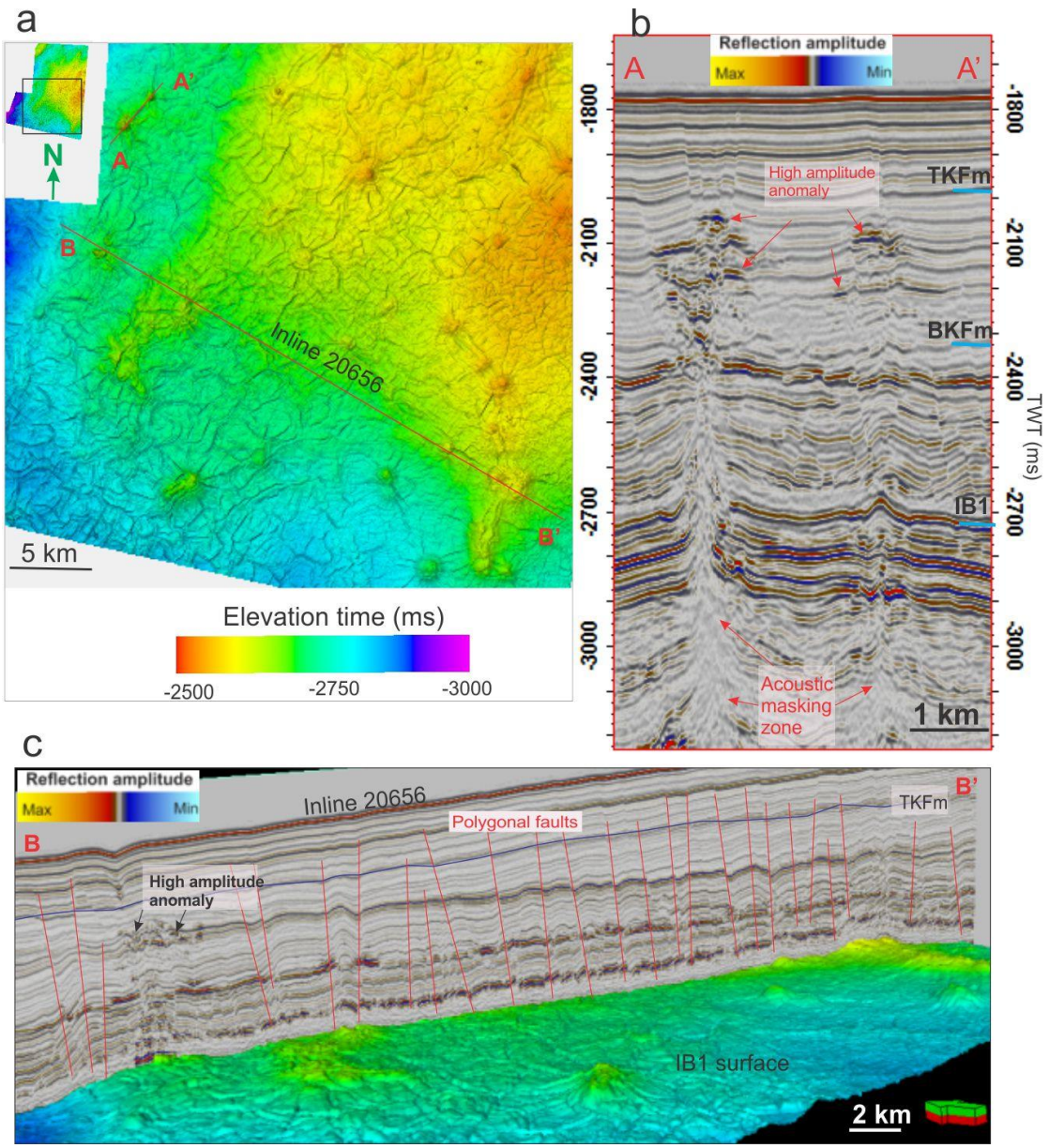

***Figure 4.1.8**: Different displays of Intra Brygge 1(IB1). (a) Detail view of southern part of IB1. Location of b and c indicated. (b) Seismic section shows accumulation of high amplitude anomalies and acoustic masking zone between the underlying IB1 surface to the top of the Kai Formation. (c) 3D window display combination between a seismic inline 20656 and IB1 surface to present high amplitude anomaly, polygonal faults (vertical red lines) and distribution of small circular features on IB1 surface.*

The Intra Brygge 2 (IB2) reflection marks the base of sub-unit B2 and subdivides the uppermost part of the Brygge Formation into sub-units B1 and B2. The reflection is discontinuous with high amplitude. The reflection is generally dipping westwards, and is found between -2550 ms to -2800 ms in the northern parts, and -2500 ms to -2850 ms in the southern parts of the studied area (Figs 4.1.4 and 4.1.5). The horizon varies in depth from -2600 ms in the north to -2700 ms in the south (Fig. 4.1.3).

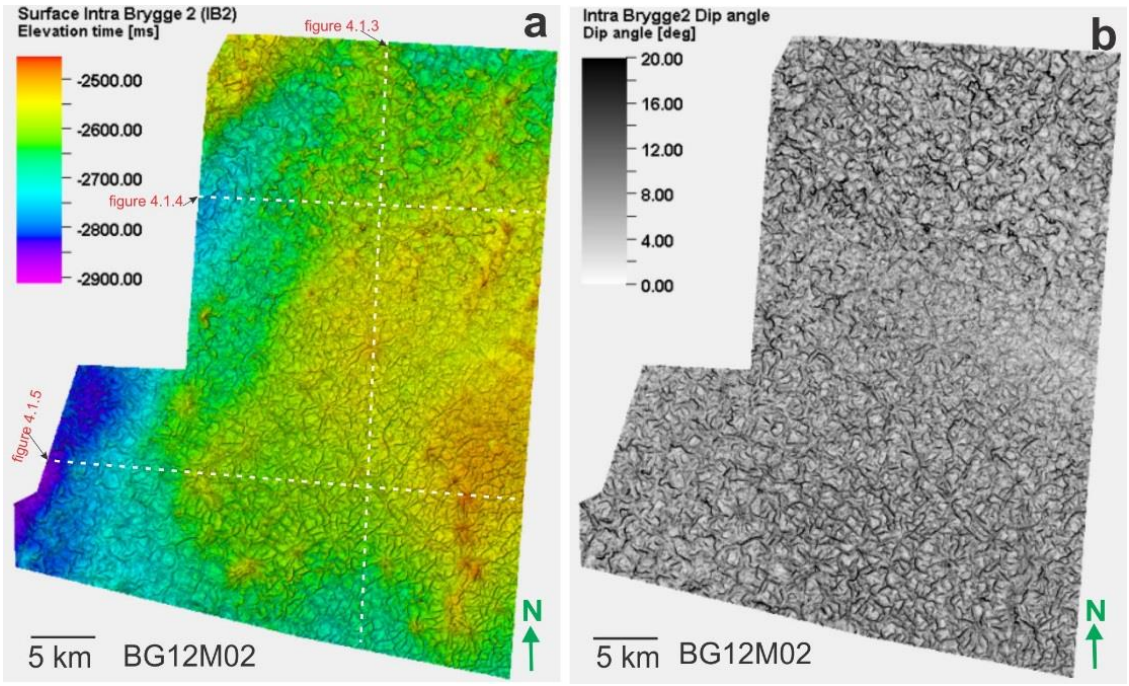

***Figure 4.1.9**: The seismic horizon intra Brygge1 (IB2) of the uppermost of Brygge Formation. **a)** Isochrone map of intra Brygge 2 showing depth and morphology of the paleo-surface (ms: millisecond TWT), vertical exaggeration 7.5 and three seismic lines are displayed in Figs 4.1.3, 4.1.4 and 4.1.5. **b)** Dip angle map of the intra Brygge 2 surface.*

The IB2 surface (Fig. 4.1.9) shows many similarities to the IB1 surface, with a dome form in the southeastern part, and a SSW-NNE oriented elongated depression. On the IB2 surface the small circular forms could also still be observed. In addition, polygonal faults have also been identified, and these are more pronounced at this level compared to the IB1 surface (Fig. 4.1.9 b). The polygonal faults will be further presented and described below using volume attribute to display these features in 3D-view (chapter 4.4).

The circular forms link to similar forms on both the over- and underlying strata, as seen by using a combination of seismic composite lines and several time-slices (Fig. 4.1.10 B, C-1 to C-7). Below the IB2 surface, seismic reflection are observed to bend upwards towards the axis of the forms between C-4 to C-7. The reflections have been disturbed by highly chaotic reflections around the forms below the IB2 surface (Fig. 4.1.10 B, C). This pattern, that may be related to fluid migration from deeper stratigraphic level will be further presented and described using volume attribute plots.

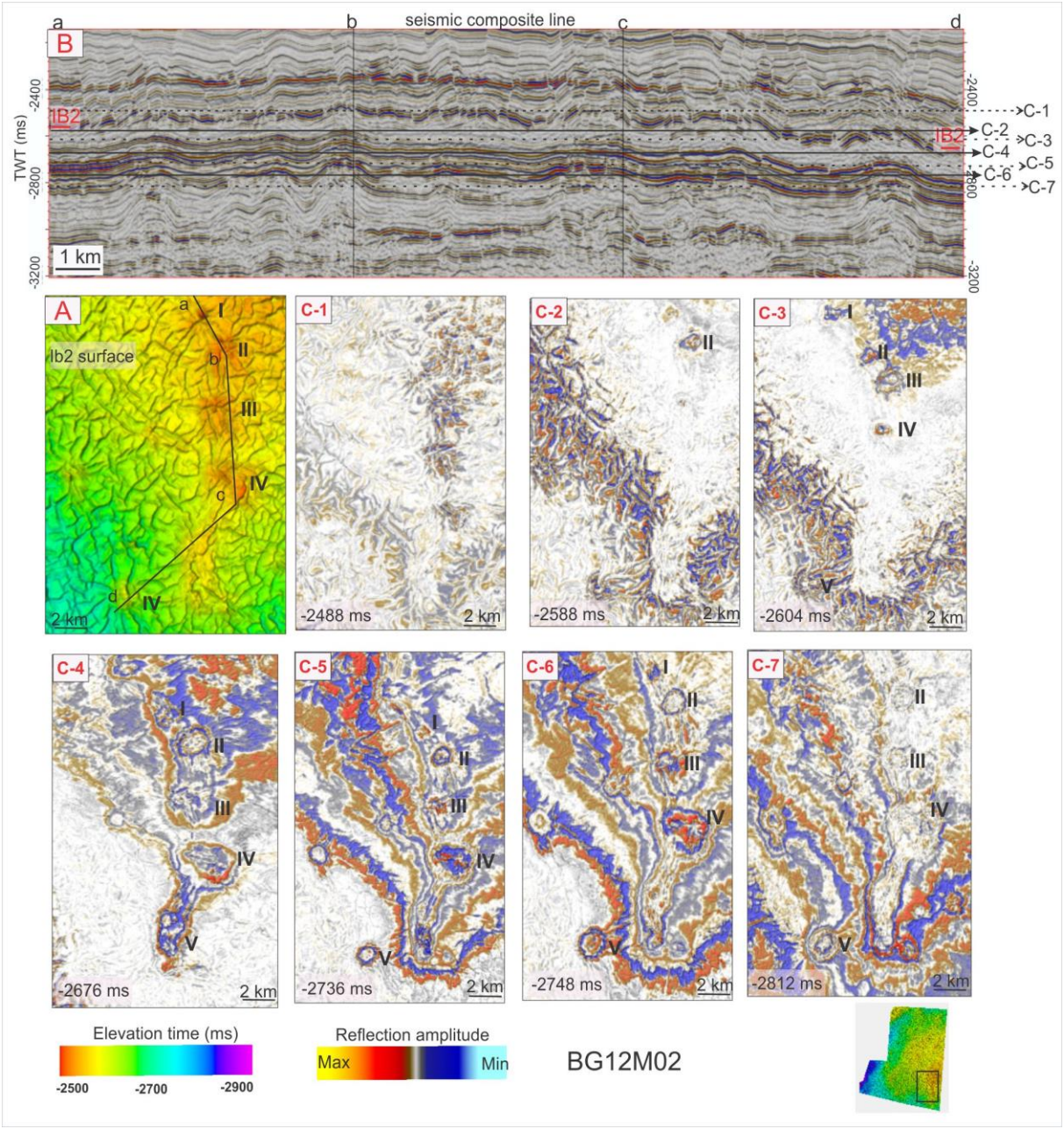

Figure 4.1.10: *The circular forms on IB2 surface, which are developed and restricted to the interval below.* ***A)*** *Seismic composite lines across the circular forms on IB2 surface and located at the southeast of this survey.* ***B)*** *Seismic section shows up-bending and chaotic reflection associated with these circular forms.* ***C)*** *Several horizon time-slices, C-1 to C-7 displaying the development of these circular forms (marked with I-V) in different stratigraphic level.*

The Base Kai Formation (BKFm) reflection separates the Kai and the Brygge Formations. The BKFm reflection is interpreted along a discontinuous, negative, high-amplitude reflection which is highly affected by polygonal faults. The most disrupted part of the reflection occurs in the northeastern part of this survey. The reflection is also interrupted by the DBSR which further complicates the mapping of the BKFm horizon (Fig 4.1.11). The horizon is located at

-2400 ms depth in the north and south, with a dome structure in the central part of the study area (Figs.4.1.3 and 4.1.11). In the southernmost part of the study area, the reflection is dipping westward, cross-cut by the DBSR, and varies in depth between -2200 ms to -2550 ms (Figs. 4.1.5 and 4.1.11). The plan form pattern of polygonal faults has been observed all over the BKFm surface, and these are most frequent with a high dip angle in the southern part (Fig 4.1.11 b).

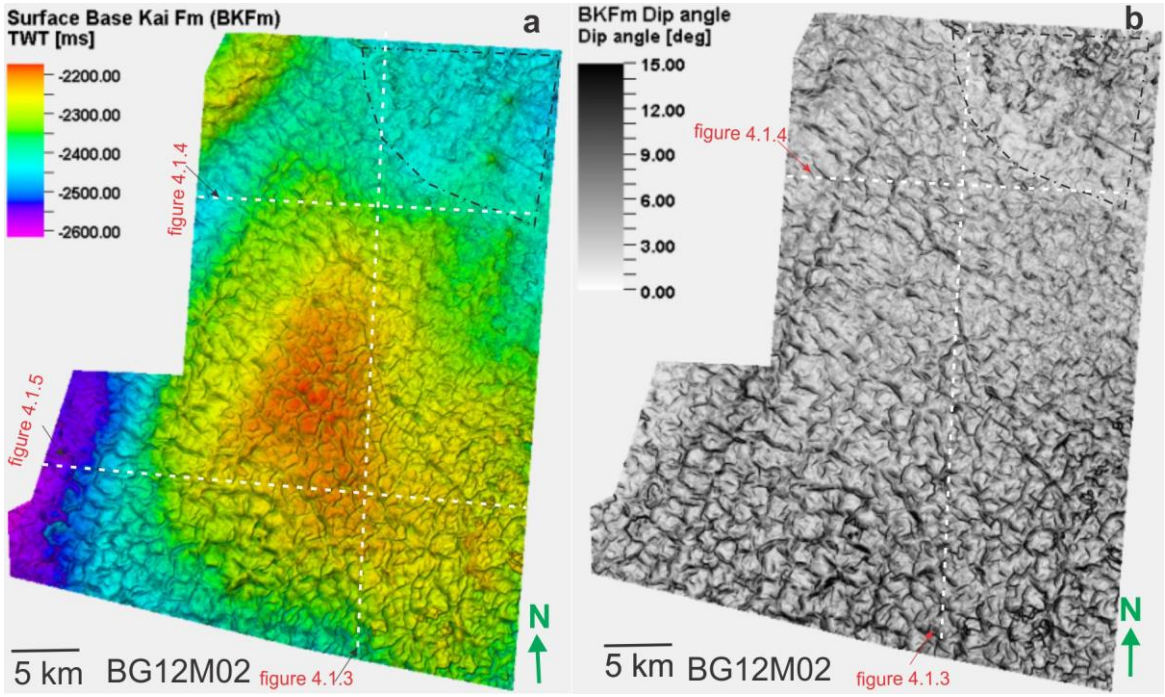

Figure 4.1.11*: The seismic horizon of the base of the Kai Formation.* ***a)*** *Isochrone map of the base of the Kai Formation showing depth and morphology of the paleo-surface (ms: millisecond TWT), vertical exaggeration 7.5 and three seismic lines are displayed in Figs 4.1.3, 4.1.4 and 4.1.5.* ***b)*** *Dip angle map of the base of the Kai Formation surface. Notice that the area with dotted line present uncertainly interpreted surface, result in poorly seismic reflection and interrupted reflections by DBSR.*

The Intra Kai 1 (IK1) reflection a continuous, positive, medium-amplitude reflection, having a slightly wavy to parallel reflection configuration, parallel with both the over- and underlying reflections. The horizon is interpreted to be an erosional surface, as it truncates underlying strata (Fig. 4.1.3), the horizon is located at -2200 ms depth in the north, and -2300 ms in the south, with a dome structure in the central part of the study (Fig 4.1.12). Viewed from west to east, the horizon has a nearly constant depth at c. -2250 ms, and is parallel to the base of the Kai Formation (BKFm) reflection (Fig 4.1.3). In the southern part of the study

area the reflection is highly interrupted by polygonal faults (Fig 4.1.12 b), resulting in discontinuous reflection (Fig. 4.1.5).

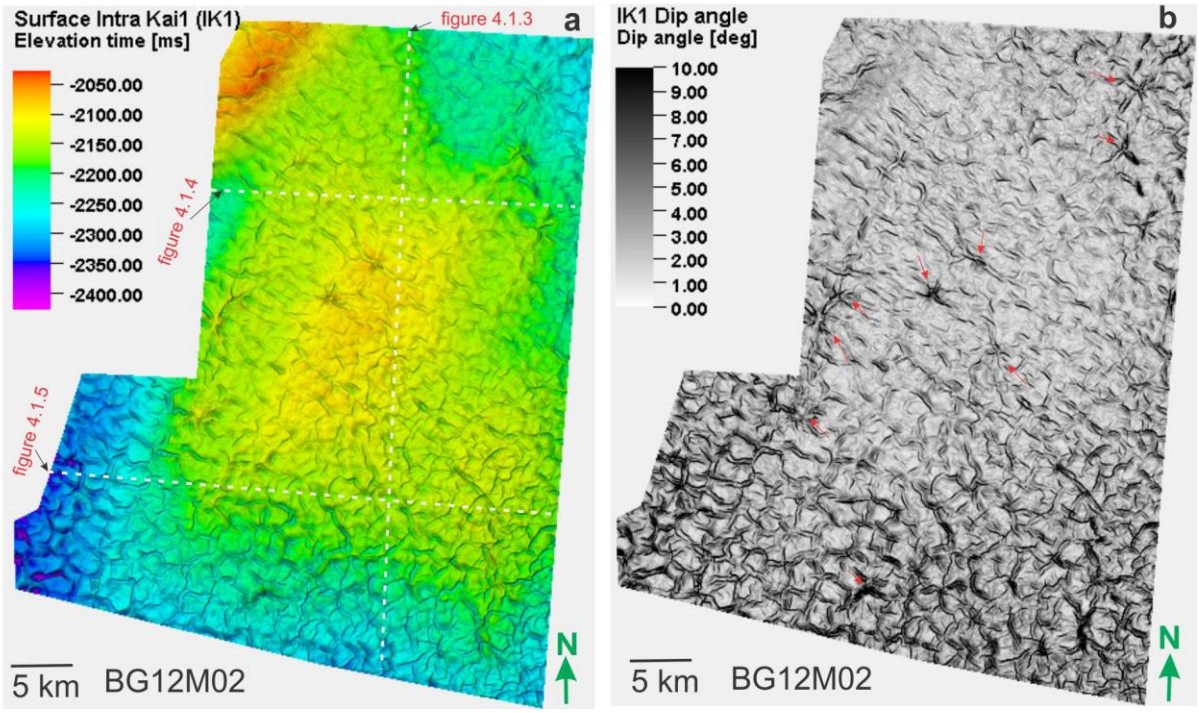

Figure 4.1.12: *The seismic horizon of intra Kai 1 (IK1).* ***a)*** *Isochrone map of intra Kai 1 showing depth and morphology of the paleo-surface (ms: millisecond TWT), vertical exaggeration 7.5 and three seismic lines are displayed in Figs 4.1.3, 4.1.4 and 4.1.5.* ***b)*** *Dip angle map of intra Kai 1 surface. Polygonal fault pattern are marked with red arrows.*

A polygonal fault pattern around the circular forms is observed (Fig. 4.1.12 b). These circular forms probably relate to similar forms a deeper stratigraphic level as they are located at about the same geographic position (Fig. 4.1.6).

The Intra Kai 2 (IK2) is a continuous, negative, high-amplitude reflection. The horizon truncates underlying reflections and is thus representing an erosional surface (Fig 4.1.4). The reflection is generally dipping southwards (Fig 4.1.13), and from the middle part the reflection appear to interfere with the underlying IK1 reflection (Fig 4.1.3), this is particularly evident in the southern part (Fig. 4.1.5). The horizon varies in depth between -2000 ms to -2300 ms. In the northern part of the study area the reflection is disturbed by DBSR reflection that make mapping of the IK2 horizon difficult and somewhat uncertain.

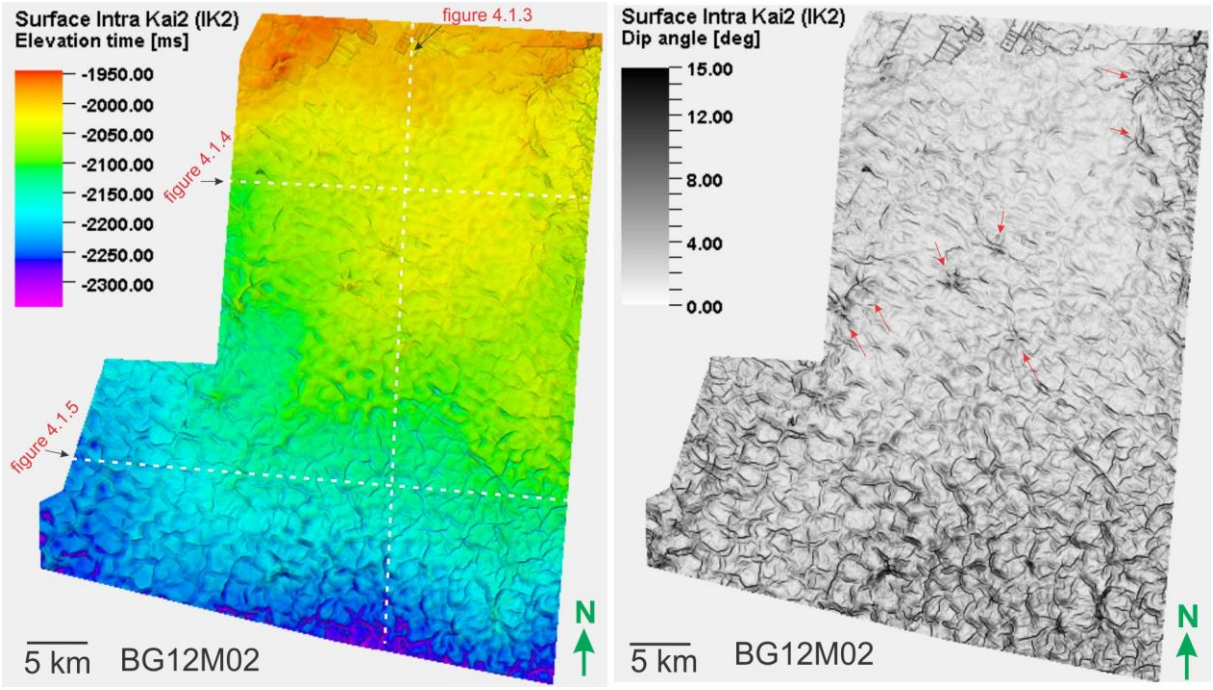

Figure 4.1.13: *The seismic horizon of intra Kai 2 (IK2).* ***a)*** *Isochrone map of intra Kai 2 showing depth and morphology of the paleo-surface (ms: millisecond TWT), vertical exaggeration 7.5 and three seismic lines are displayed in Figs 4.1.3, 4.1.4 and 4.1.5.* ***b)*** *Dip angle map of intra Kai 2 surface. Some of the polygonal faults are marked with red arrows.*

The circular forms can still be observed on the IK2 surface (Fig. 4.1.13b), which could be associated with circular forms of the IK1 surface in order to the same geographic position (Figs 4.1.6, 4.1.12).

The Top Kai Formation (TKFm) is following a continuous, positive and high-amplitude reflection. The underlying reflections are truncated by this reflection, and in the northern part it truncates the underlying intra K2 reflection (Fig.4.1.3). The horizon is dipping westwards (Figs 4.1.4, 4.1.5 and 4.1.14) while it has a nearly constant depth at approximately -1950 ms in N-S orientation (Fig 4.1.3). The deepest part of the top surface is located in the southwestern part of this survey, with depth of around -2150 ms (Fig 4.1.14 a). The frequency of polygonal faults at this depth is increasing southwest-ward (Fig 4.1.14 b).

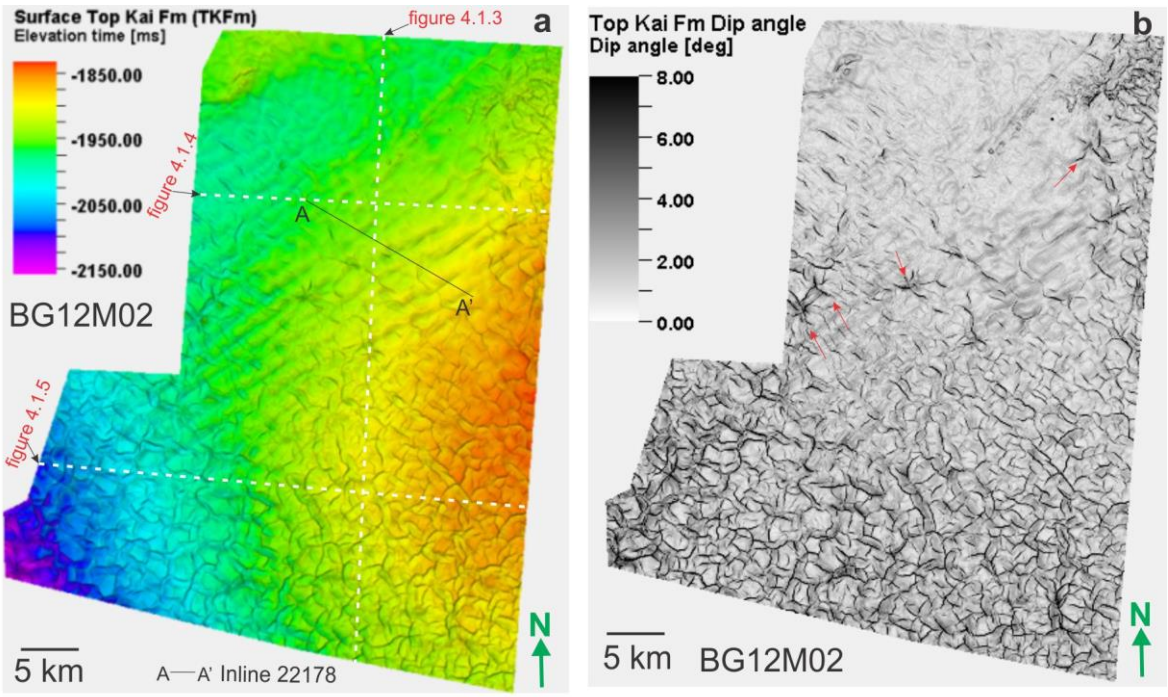

Figure 4.1.14: *The seismic horizon of the top Kai Formation (TKFm). a) Isochrone map of TKFm showing depth and morphology of the paleo-surface (ms: millisecond TWT), vertical exaggeration 7.5 and three seismic lines are displayed in Figs 4.1.3, 4.1.4 and 4.1.5., a seismic line used to further described and interpretation. b) Dip angle map of TKFm surface.*

In the middle part of the TKFm surface, positive elongate features with NE-SW orientation is observed in the middle part of the survey (Fig 4.1.14 a, Fig. 4.1.15). The elongated, wavy features have a height of nearly ten meters and a width of over one thousand meters. Their forms are parallel to slightly sinuous in planform (Fig 4.1.15 a), and developed to be larger form eastward (Fig. 4.1.15 b). These wave-shaped features is interpreted as a series of migrating sediment waves moving across this surface (Mitchum et al., 1977), and this wavy reflection configuration is probably formed by ocean currents. Alternatively, these are elongated erosional features, termed furrows by Stow et al. (2009). This will be further discussed below.

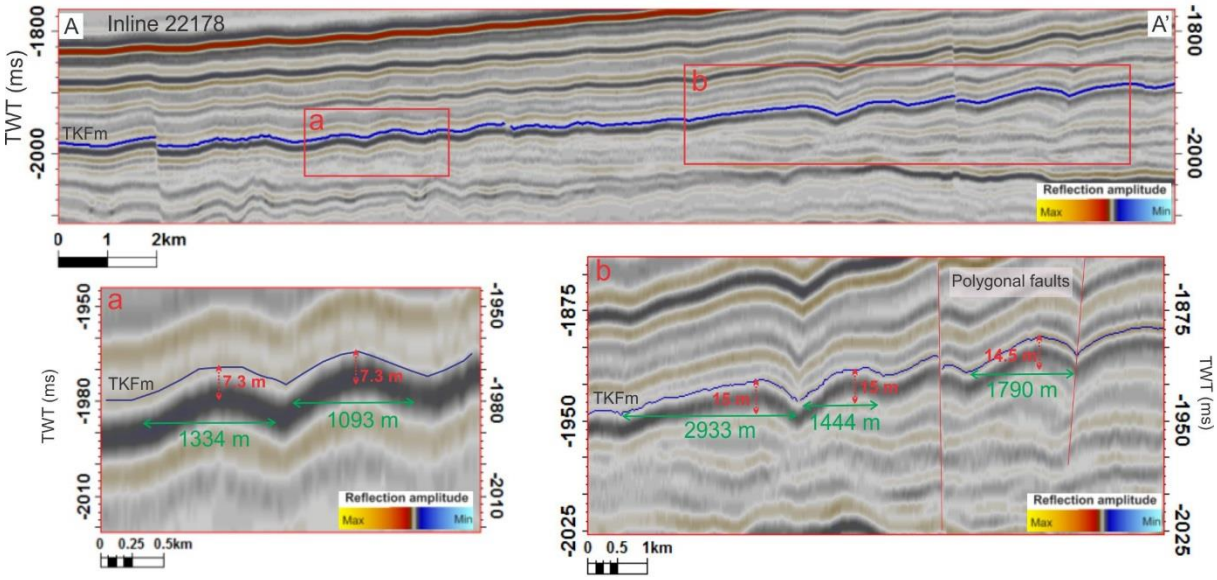

Figure 4.1.15: *Seismic section from inline 22178 across elongate features on the TKFm surface in Fig. 4.1.14 a showing a) and b) the high and width measurement method for these elongate features.*

4.2 Seismic facies and isopach maps

Isopach maps were created to identify and describe the geometry of the Kai Formation and the upper part of the Brygge Formation. Thickness maps for the sub- units will be given as two-way travel time (TWT), in milliseconds (ms). The upper part of the Brygge Formation comprise two subunits, B1 (lowest) and B2 while the Kai Formation comprise three main sub-units, K1 (oldest), K2 and K3. The thickness map of the Kai Formation was also created to display the sediment distribution of the whole Formation in the study area.

Sub-unit B1 is delimited by the underlying IB1 surface and the overlying IB2 surface (Figs 4.2.1, 4.2.2). The internal seismic signature is characterised by discontinuous, low amplitude, sub-parallel to wavy reflections. The thinnest part (40 ms) is found in the central, eastern part of the survey, whilst the greatest thickness (up to 150 ms), is observed in the northern and the southern part of the study area (Fig 4.2.1 a).

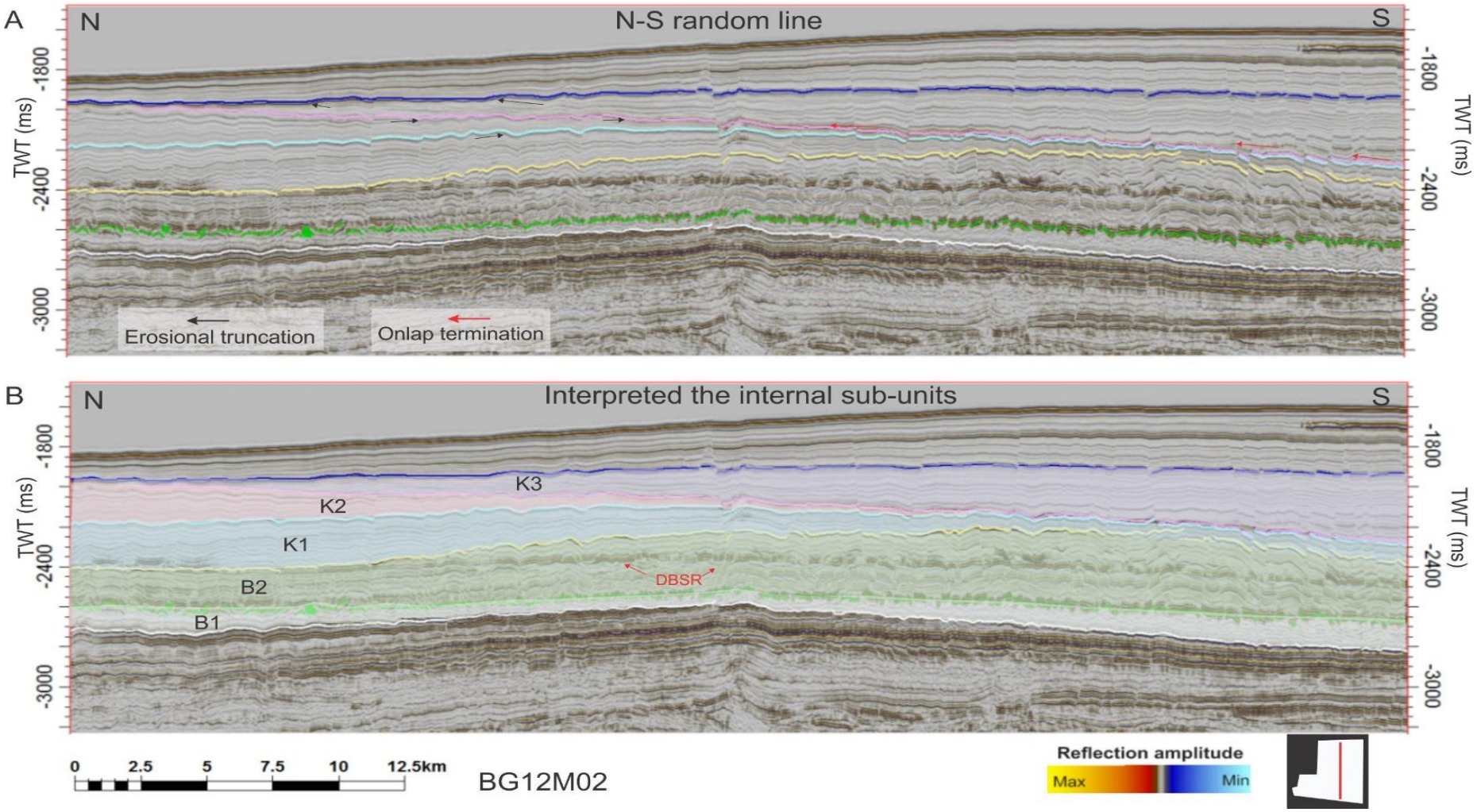

Figure 4.2.1: *A N-S oriented seismic section within 3D-survey BG12M02.* ***A)*** *the seismic section without interpretation.* ***B)*** *the interpreted seismic of the internal sub-units; B1, B2, K1, K2 and K3 show the different sub-units from oldest to youngest. The location of the seismic section is shown in the right corner of seismic section.*

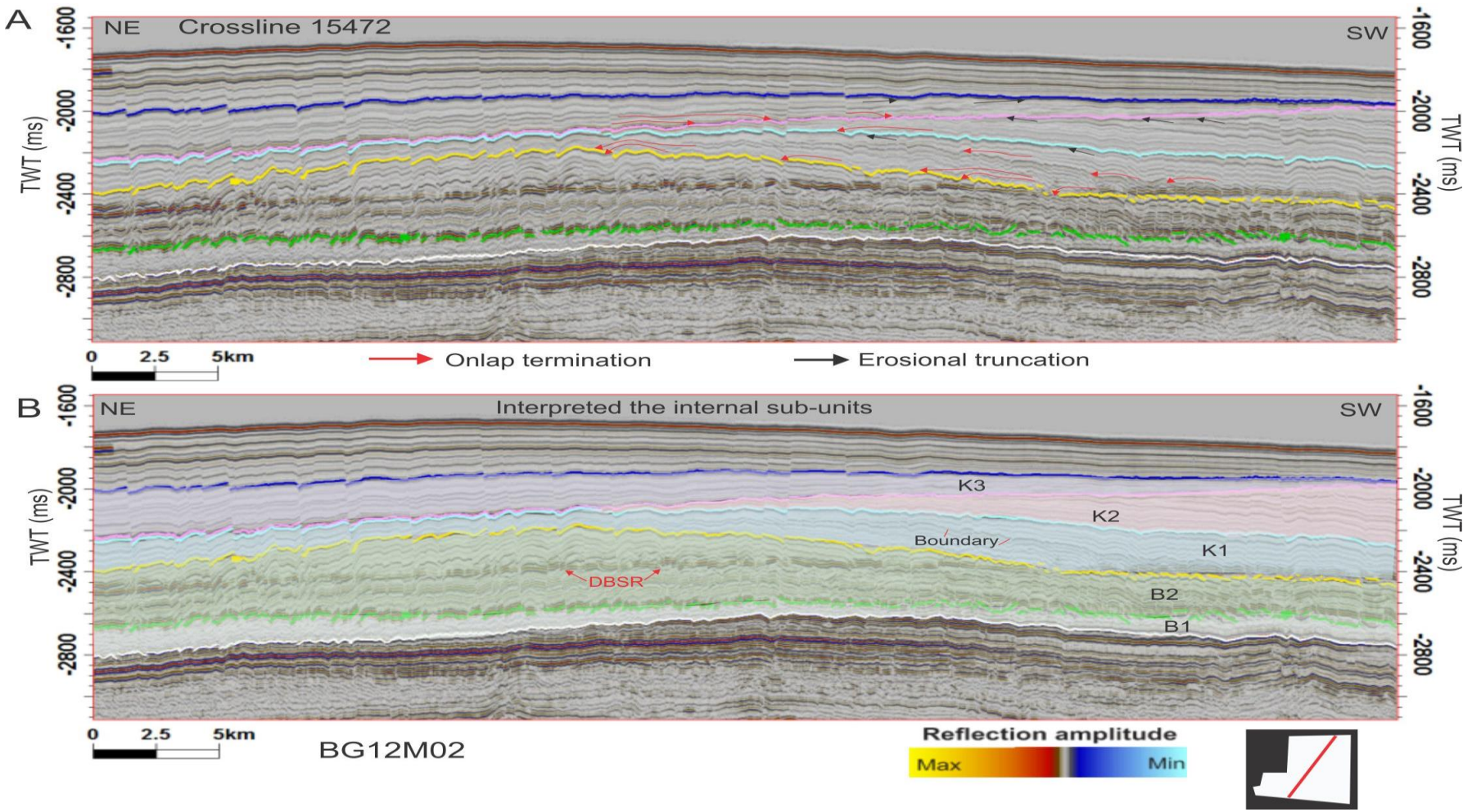

Figure 4.2.2: *A NE-SW oriented seismic section within 3D-survey BG12M02. (A) the seismic section without interpretation. (B) the interpreted seismic of the internal sub-units; B1, B2, K1, K2 and K3 show the different sub-units from oldest to youngest. The location of the seismic section is shown in the right corner of seismic section B.*

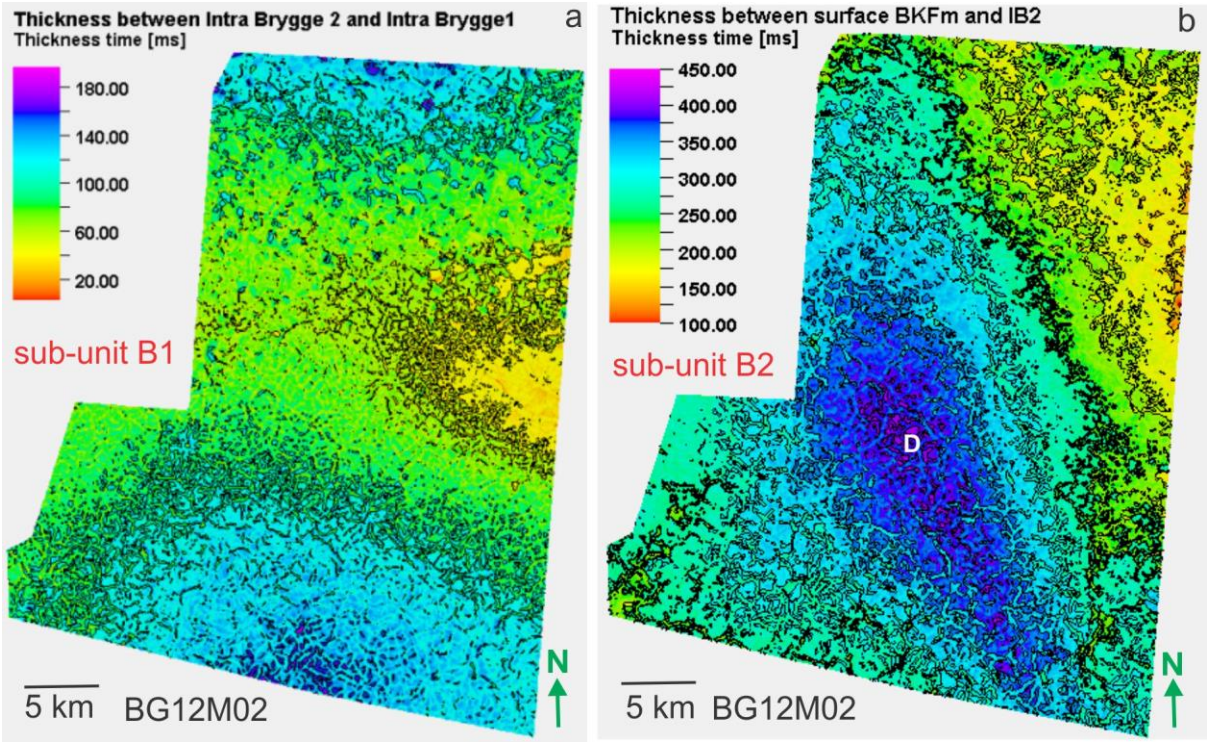

Figure 4.2.3: *Isopach map of subunits B1and B2.* ***a)*** *the time thickness map of the subunit B1 is created from the interpreted IB1 and IB2 surface.* ***b)*** *the time thickness map of the subunit B2 is created from the interpreted IB2 and BKFm surface,* ***D****: deposenter. The colour indicates two-way travel time thickness in millisecond, ms.*

Sub-unit B2 is the uppermost sub-unit of the Brygge Formation. Low to medium amplitude, parallel to sub-parallel, and discontinuous reflections dominates within this subunit. The top boundary is an erosional surface (the BKFm surface) that separates the Paleogene strata from the younger Miocene strata. This boundary correspond to the base Kai unconformity; BKU (Laberg et al., 2005b; Stoker et al., 2005).

The internal reflection configuration within sub-unit B2 is interrupted by polygonal faults and the DBSR reflector, which makes the interpretation of the sub-unit somewhat uncertain. The sub-unit has an internal seismic reflection onlap onto the base of intra Brygge 2 surface, and reflection could not be identified at the top boundary due to polygonal faults and the DBSR reflector (Fig. 4.2.2). The sediment thickness gradually increases from approximately 150 ms in the northeast towards southwest, where a dome-shaped accumulation with thickness up to 450 ms occur (Figs 4.2.2, 4.2.3 b). Away from the depocentre, there is a reduction in thickness towards the south and southwest, where a lens-shaped form is present (Figs 4.1.5, 4.2.2, and 4.2.3b).

The intern seismic reflection, which has a characteristic of onlap termination observed in the southwestern part area, could be indicated as contourite drift deposition (Fig 4.2.2). According to Laberg et al. (2005a, 2005b), ocean currents controlled the sediment erosion and deposition on the northern, inner part of the Vøring Plateau during the Oligocene. The internal seismic reflection configuration show an upslope progradational pattern, at the lower slope, depocenter was generated, as effected by contourite drift deposition from alongslope flowing currents (Laberg et al., 2005b).

Sub-unit B2 is heavily influenced by polygonal faults, and the frequency of the polygonal faults seem to decrease upwards. The diagenetic bottom-simulating reflection (DBSR) caused by the Opal A to Opal CT conversion (Neagu et al., 2010) is particularly well developed within this sub-unit (Figs 4.2.2, 4.2.3).

Sub-unit K1 is bounded by the base of the Kai Formation surface and the overlying intra K1 surface. Low to medium amplitude, parallel to sub-parallel reflections characterize the internal reflection configuration. This sub-unit can be divided into two parts by an internal reflection, which separates low amplitude reflections above from medium amplitude internal reflections below (Fig. 4.2.2). At the northern part of this survey, the internal reflections in the lower part of the subunit onlap onto the base of BKFm surface, and are concordant to the top boundary, while in the upper part the internal seismic reflection is dipping downward and has been eroded by the overlying IK1 surface (Figs 4.2.2, 4.2.3). This sub-unit partly form *a mound structure*. The thinnest part is located in the southwest, with a thickness of only 50 ms, and the sediments are widely deposited from this area outward to reach a thickness up to 275 ms, confined to the northern and southwestern part of this survey (Fig. 4.2.4 a).

According to Hjelstuen et al. (2004a, 2005) and Laberg et al. (2005a), the sediments in the Vøring Basin have been influenced by ocean currents during the Miocene. In the early Miocene, uplift of anticline structures in this area occurred, as a result currents were affected by some of these features including the Helland-Hansen Arch. (Hjelstuen et al., 2004a, 2005).

Sub-unit K2 is generally characterized by the same internal seismic reflection pattern as the underlying sub-unit K1, with low to medium amplitude, parallel to sub-parallel reflections. The reflection termination at the base of this sub-unit is located outside of the study area,

while the internal reflections are dipping downwards with the same trend as within sub-unit K1 (Fig. 4.2.2). The reflections is cut by the overlying IK3 reflection at the top of the sub-unit K2, interpreted as an erosional truncation (Figs 4.2.1, 4.2.2). Sub-unit K2 increases in thickness towards the northeast where it reach its greatest thickness of up to 300 ms (Fig. 4.2.4 b). The subunit is thinning out southwards and is thinnest in the southern part of this survey (Figs 4.2.2, 4.2.4 b). The age of deposition was interpreted by Eidvin et al. (2014) to be late Miocene to early Pliocene.

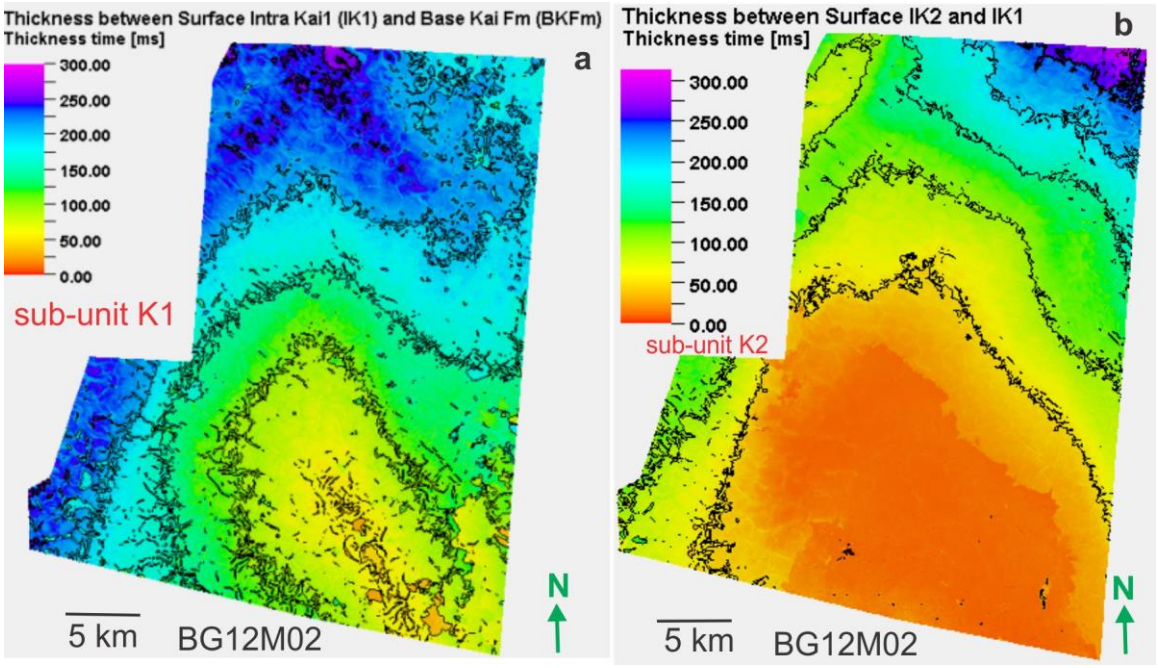

Figure 4.2.4**:** *Isopach map of sub-unit K1and K2.* ***a)*** *the time thickness map of sub-unit K1 is created from the interpreted BKFm and IK1 surface.* ***b)*** *the time thickness map of sub-unit K2 is created from the interpreted IK1 and IK2 surface. The colour indicates two-way travel time thickness in millisecond, ms.*

Sub-unit K3 has low to medium amplitude reflections which are parallel to sub-parallel, with slightly wavy configuration. The thickness of subunit K3 is limited by the underlying intra Kai 2 and the overlying of TKFm surfaces (Figs 4.1.3, 4.2.2). Sub-unit K3 is divided into two parts; in the lower part, a few onlap termination at the base of intra K2 surface in the south area could be observed (Fig. 4.2.2), this may indicate the sediment deposition migrated upslope. In the upper part, the internal seismic reflection configuration is gently divergent to the south and southwest, but its termination towards the basal boundary could not be determined from this survey. However, the reflection at the top of the sub-unit K3 is truncated

by the top of the Kai Formation surface, i.e. the Base Naust Unconformity; BNU (Laberg et al., 2005b; Stoker et al., 2005). The sediment thickness is lowest in the northwest while it gradually increases in thickness towards the southeast, and a depocentre is seen at the southwestern part of this survey, with a thickness of approximately 300 ms. (Fig. 4.2.5 a).

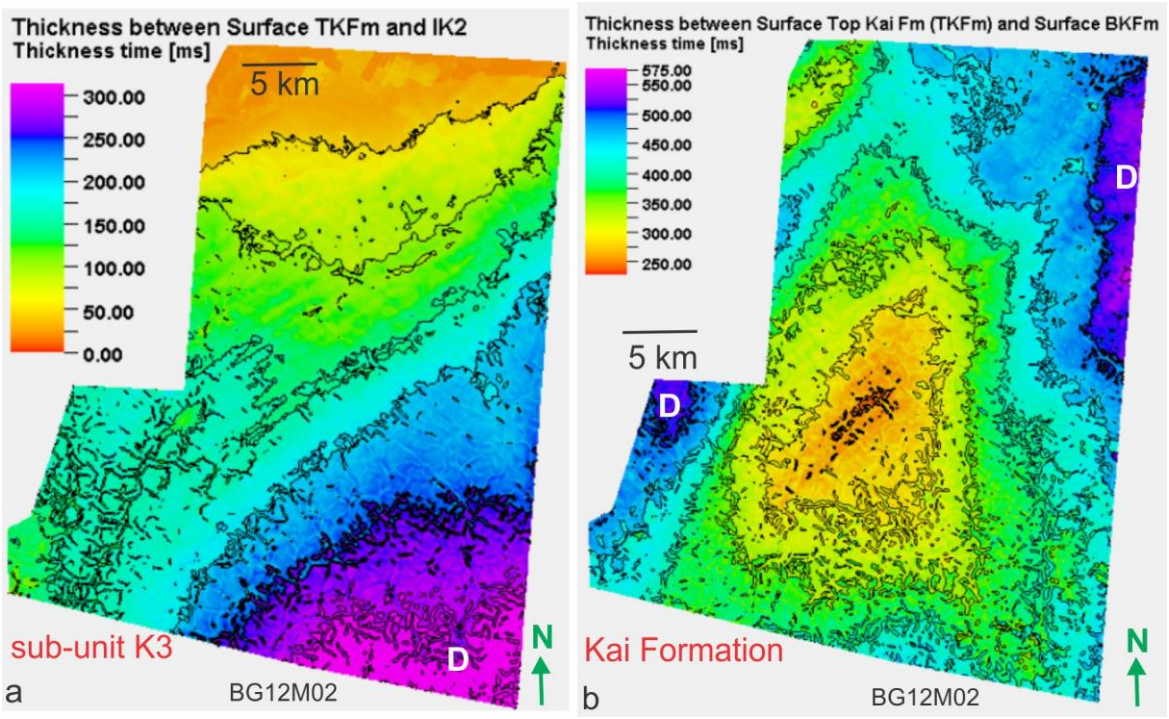

Figure 4.2.5: *Isopach maps of subunits K3 and Kai Formation.* ***a)*** *the time thickness map of the subunit K3 is created by the interpreted surfaces between IK2 and TKFm.* ***b)*** *the time thickness map of the Kai Formation is created by the interpreted surfaces between BKFm and TKFm,* ***D:*** *depocentre. The colour indicates two-way travel time thickness in millisecond, ms.*

The Kai Formation is located between the unconformities of the underlying Brygge Formation and overlying Naust Formation. Total sediment thickness is varying between 250 to 575 ms, where the thinnest part is located in the centre of this survey, and its thickness regularly increase outward from the centre (Fig. 4.2.5 b). The depocentres are located at the northeastern and southwestern edges of this survey, with thickness up to 575 ms. The sediments deposited within the Kai Formation is dated to middle Miocene to early Pliocene (Eidvin et al., 2014).

4.3 Lithology interpreted from logs

Below the lithology of all the sub-units will be addressed using a combination of well data from well 6604/2-1 and the seismic data available. The well data comprise three main logs; the gamma ray log (GR), the density log (DEN), and the P-sonic log (DTC_11). A composite seismic line shows the location of the well and the seismic signature of the studied interval (Fig 3.3.1). Description and interpretation of lithology will be described using well log characteristics as *gamma ray shape*, and *baselines* (Rider and Kennedy, 2011). The well logs are correlated to the interpreted sub-unit shorizons from this thesis and well tops from NPD (2017). In this chapter the lithology of the deeper strata, below sub-unit B1 (Tare and Tang Formations) will be also described and interpreted, as these results will be further used for seismic anomaly interpretation in the next chapter (chapter 4.4.4).

Baselines are defined by a constant vertically value, as shown in the Gamma-ray log. The Kai and the Brygge formations have a high average value of 100 API, this value is indicating shale, and is termed "*shale line",* while the low baseline value at 20 API is indicating sand, and is termed *"sand line".* The Tare and the Tang formations have a shale line at 120 API and sand line at 40 API (Figs 4.3.1, 4.3.2). The baseline values are different between these formations because the shale within each formation has a different composition and texture (Rider & Kennedy, 2011).

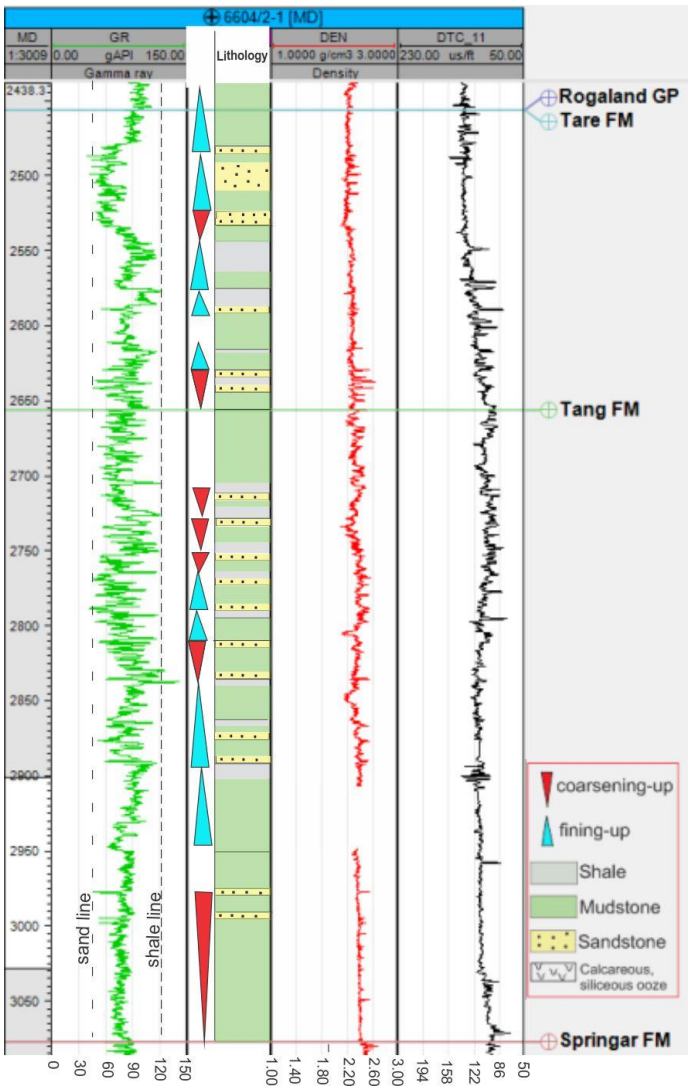

Figure 4.3.1: *The gamma-ray (GR), density (DEN), and sonic logs (DTC_11) of well 6604/2-1. The interpreted lithology of the Tare and Tang Formations is also indicated. The horizontal lines locates the top of each formation. MD: depth in meter.*

The top of the Tang Formation is located at 2656 m depth. Based on biostratigraphical data it was moved 213 m shallower from 2869 m (NPD, 2016). From the base of the Tang Formation (top of the Springar Formation) upwards (to c. 3000 m depth), the gamma ray value is varying from 75 to 90 API indicating mudstone. Some spikes of low gamma ray value down to 40 API, together with density log average values of 2.6 g/cm^3 may indicate thin levels of sandstone (Fig 4.3.1). From 2900 m upwards high gamma ray values up to 120 API may indicate shale (Fig 4.3.1). The sonic log shows low values ranging from 80 to 120 us/ft with an increasing value upward within this formation. The density log has an average value

of 2.2 g/cm^3, and intervals of higher values, as to 2.6 g/cm^3 is interpreted to indicate sandstone, corresponding to low gamma ray values (Fig 4.3.1).

From 2950 to 2840 m depth, two bell-shaped intervals are identified, with the gamma ray value is increasing upward, are indicated fining-upwards successions with an increasing clay content. Several spikes of low slowness in the sonic log are observed, except for these there is a regular increase in velocity downward, interpreted to be a result of normal compaction in shale. At the upper part of the Tang Formation, the gamma ray is ranging from 90 to 100 API, indicating mudstone.

The Tare Formation has its formation top at 2456 m depth. The lower part of this formation has a varying gamma ray value, which indicates shale, mud and sand interbedded. From ~2641 m depth and upwards, the gamma ray value increases gradually from 48 to 110 API, interpreted to represent a coarsening-up succession, with an indication of sandstone at the base (Fig. 4.3.1). These indications of sand is correlated to increasing values of the density log from 2.2 to 2.5 g/cm^3. The sonic log shows an increasing slowness from the base of the Tare Formation and upward (Fig. 4.3.1).

From 2625-2556 m depth, increasing gamma ray values are seen, forming a bell-shaped log pattern, indicating a fining-upward succession. This probably corresponds to an increasing clay content (Fig. 4.3.1). Several spikes of low slowness could be observed and is interpreted to be due to varying shale compaction. Above, the gamma ray value shows regularly decreasing trend again, down to 30 API. Here the density log shows values ranging between 2.2-2.4 g/cm^3, and the sonic log varies from 130 us/ft to 80-90 us/ft. This is interpreted to reflect sandstone. At the top of formation, the gamma ray value is slightly stable, around 80-90 API, interpreted to reflect mudstone.

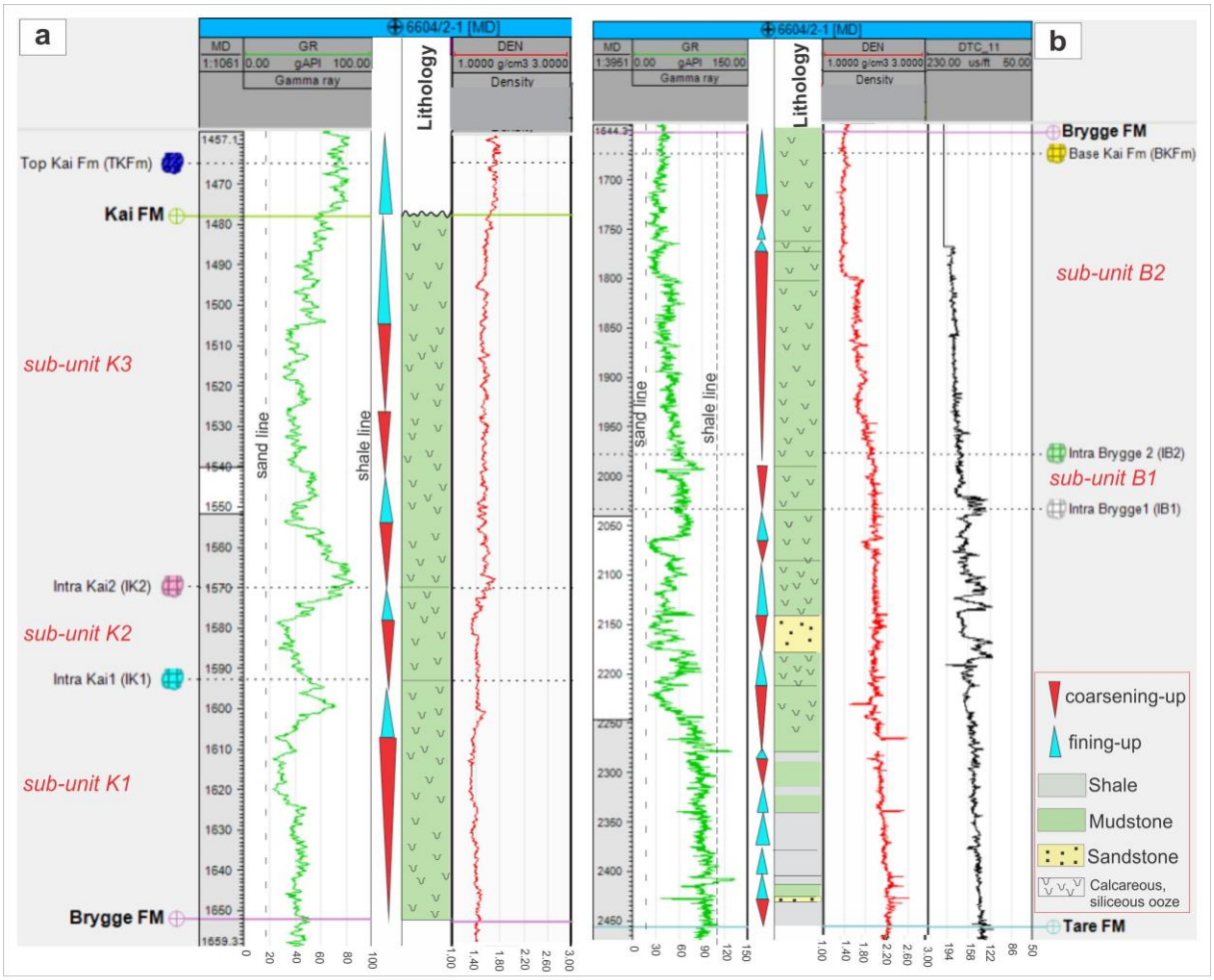

Figure 4.3.2: *The well 6604/2-1 gamma-ray (GR), density (DEN), and sonic logs (DTC_11) and the interpreted lithology in: a) the Kai Formation, and 2) the Brygge Formation. The formation tops are indicated by horizontal lines. The dotted lines indicate the depth if the interpreted surfaces in this thesis.* ***MD****: depth in meter.*

The top of the Brygge Formation located at a depth of 1652 m. The formation is divided into three sections. The lowest section is located between the top Tare Formation and the intra Brygge 1 paleo-surface, the middle section is the sub-unit B1, and the upper section is the sub-unit B2 (Fig. 4.3.2 b).

The lowest section is showing gamma ray values of about 90 API. A spike of low gamma ray values, ~40 API is observed at a depth of 2427 m, corresponding to an increasing bulk density value up to 2.60 g/cm^3, and the sonic log shows average slowness values of around 140 us/ft, indicating sand within this section. In this interval the gamma ray log is showing gradually lower values upwards, this trend correspond to a funnel shape log pattern, representing a coarsening-up interval. Above, the gamma ray value increases upwards, forming a bell shaped

log pattern, indicated fining-upward due to an increasing clay content. Between 2170 m and 2130 m depth, the gamma ray is 20 API, with high slowness values, which is an indication of sandstone in this interval. From this position upwards the gamma lay value is gradually decreasing in this borehole, to reach a minimum value into 21 API, at depth 2075 m. with the bulk density decreasing to 1.75 g/cm^3, slowness value was changing, interpreted as mudstone with high porosity, may a result of siliceous/calcareous ooze. (Fig. 4.3.2 b).

Sub-unit B1 is located at a depth between 2038 and 1977 m (Fig. 4.3.2 b). The gamma ray value is here between 50 - 60 API. An interval of decreasing gamma ray value to 25 API could be observed between 1996 - 1993 m depth, this low value is associated with silt. Then the log value shows a spike of ~60 API that indicate increasing clay content. The density log in this sub-unit shows average value of 2.0 g/cm^3. The sonic log in the lower part of this sub-unit is showing a slowness value varying between 125-160 us/ft before it becomes more stable upwards with an average value of 180 us/ft, interpreted as mudstone (Fig. 4.3.2 b).

Sub-unit B2 is located between 1977 - 1652 m depth. The gamma ray value is gradually decreasing from 70 to 40 API, forming a funnel shape log pattern, which is indicative of a coarsening-up interval with increasing sand content. Above the gamma ray value turn down to a maximum value of 60 API, indicating mudstone (Fig. 4.3.2 b). Further up the gamma ray value is decreasing again to reach a minimum value of 17 ATP. From this depth and upwards to the base of the Kai Formation the gamma ray log is showing a bell-shaped pattern, where the gamma ray value increases regularly upwards. This is interpreted to indicate increasing clay content. The density log is showing a degreasing bulk density, from 1.8 g/cm^3 down to 1.3 g/cm^3, and then it is stable into the overlying Kai Formation. The sonic log show high values, ranging from 175-185 us/ft throughout the unit. Sonic log data has not been available from the upper part of sub-unit B2 and upwards, interpreted mudstone with high oozes sediments (Fig. 4.3.2 b).

The Kai Formation top is located at a depth of c. 1478 m. This formation is divided into three parts, corresponding to the sub-units K1, K2 and K3 (Fig. 4.3.2 a). In this study, the interpreted top of the Kai Formation surface (TKFm) is located at depth 1465 m, this is 13 m over the top depth of the Kai Formation as identified by NPD (2017).

Sub-unit K1, located in the lower part of this unit, is showing gamma ray values ranging from 40-45 API. From a depth of ~1623 m, the gamma ray values decreases regularly upward to 25 API, and present stable values within a 20 m interval, a funnel-shaped gamma ray log pattern observed, indicating a coarsening-up succession. The density log shows values of 1.3 g/cm^3, approximately the same value as within the uppermost part of the Brygge Formation, interpreted as mudstone with high oozes. At the intra K2 surface, the density value increase to 1.43 g/cm^3 corresponding to an increasing gamma ray value from the minimum value up to 80 API, is probably reflect to mudstone (Fig. 4.3.2 a).

Sub-unit K2 shows a thickness of around 30 m. In this interval a funnel-shaped gamma-ray log pattern is observed, with a decreasing value from 60 to 30 API. The density log is showing values ranging from 1.3 to 1.5 g/cm^3. This is indicated a change in lithology, and this unit is interpreted to consist of mudstone (Fig. 4.3.2 a).

Sub-unit K3 is located between 1478 to 1570 m depth. The lower part of this sub-unit is showing upward decreasing gamma ray values from 80 to 30 API, interpreted to result from a coarsening-up succession. From a depth between 1540-1515 m the gamma ray curve varies between 30-50 API, probably representing mudstone and claystone. From a depth 1505 m and upward, the gamma ray values increases to the top of the Kai Formation, with the density log ranging from 1.44 to 1.53 g/cm^3 , indicating mudstone with high concentrations of ooze (Fig. 4.3.2 a).

4.4 Seismic anomalies

The seismic anomalies observed in the study area occur within zones that are interpreted to present accumulation of fluids, associated with fluid migration from different levels in the subsurface. In order to identify areas of fluid migration not clearly visible from seismic profiles (i.e. areas that not include high amplitude seismic anomalies), a set of advanced seismic volume attributes have been analysed, and they are optimized in order to try to detect fluid migration pathways. The type of seismic attributes that were extracted include Chaos, Variance, and Ant-tracking attributes. A Chaos cube is used for identifying gas and fluid migration, and has variance values ranging between 0 and 1. The area with high variance values in the Chaos cube represent locations that are interpreted to represent gas and fluid migration. The Variance attribute is used to identify faults, and this attribute display values between 0 and 1, where high values indicate strong lateral amplitude discontinuity, referred to as fault zones. The Ant tracking attribute is used to improve the interpretation of major faults, with a range of values between 1 and -1. High values indicate major faults.

4.4.1 Relationship between seismic anomalies and the fault structures

The seismic anomalies identified seems to be related to both major faults in deeper strata and polygonal fault system in the Brygge and Kai formations. This relationship was improved by using variance attribute plots. At approximately -3088 ms depth, close to the base of the Brygge Formation, polygonal faults start (Fig 4.4.1). The polygonal faults are seen to be marked by steeply dipping fault plains from the intra Brygge 1 reflection upwards into the base of the Kai Formation surface (Fig 4.4.1). The most intense faulting is observed at the upper part of the Brygge Formation, the intensity decrease upward into the overlying Kai Formation (Figs 4.4.1, 4.4.3, 4.4.4, 4.4.5). A few faults can be followed into the Naust Formation and probably to the present-day seabed (Figs 4.4.1, 4.4.3, 4.4.9). Bright spots were observed along the faults (Figs 4.4.1, 4.4.2).

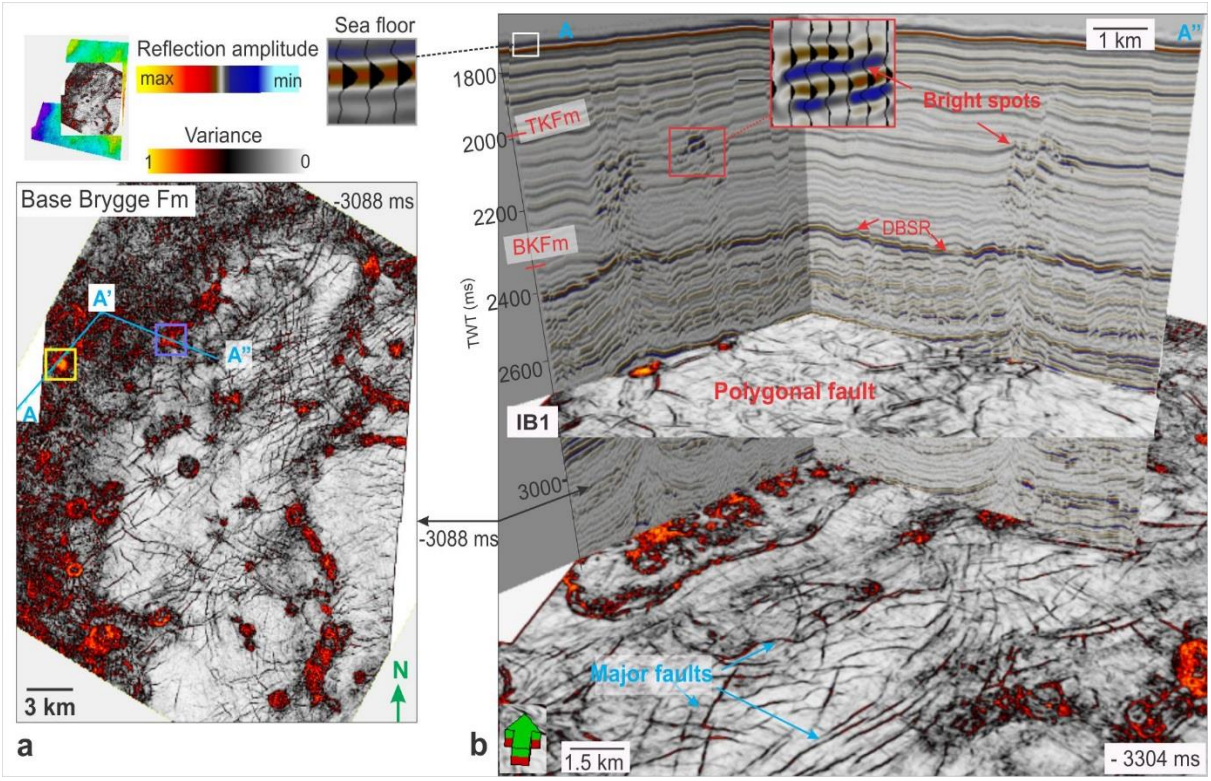

Figure 4.4.1: *3D displays a relationship between seismic anomalies to fault structures.* ***a)*** *a variance horizon at -3088 ms (TWT) separated from b), as located at the base of the Brygge Formation, shows a major fault structure and fault zones with high variance in red color, a blue seismic line will be further interpreted in b.* ***b)*** *a combination between a seismic section and two timeslices from variance attribute show a connection between deep-faults and polygonal fault system that located in the same geological fault zones. Acoustic masking located under the fault zones and several accumulations of bright spots in the Kai formation are observed.*

High amplitude anomalies, both positive and negative amplitude reflections, have also been detected using an RMS amplitude map (Fig 4.4.2 a). The bright spots are characterized by high negative amplitude anomalies, a polarity reversal, therefore they could be more precisely identified using a minimum-value seismic amplitude attribute map, that will display only the strongest negative amplitude values (Fig 4.4.2 a, c). Within the Kai Formation, the bright spots accumulations are clearly seen in relationship to deep fault structures (Fig 4.4.2).

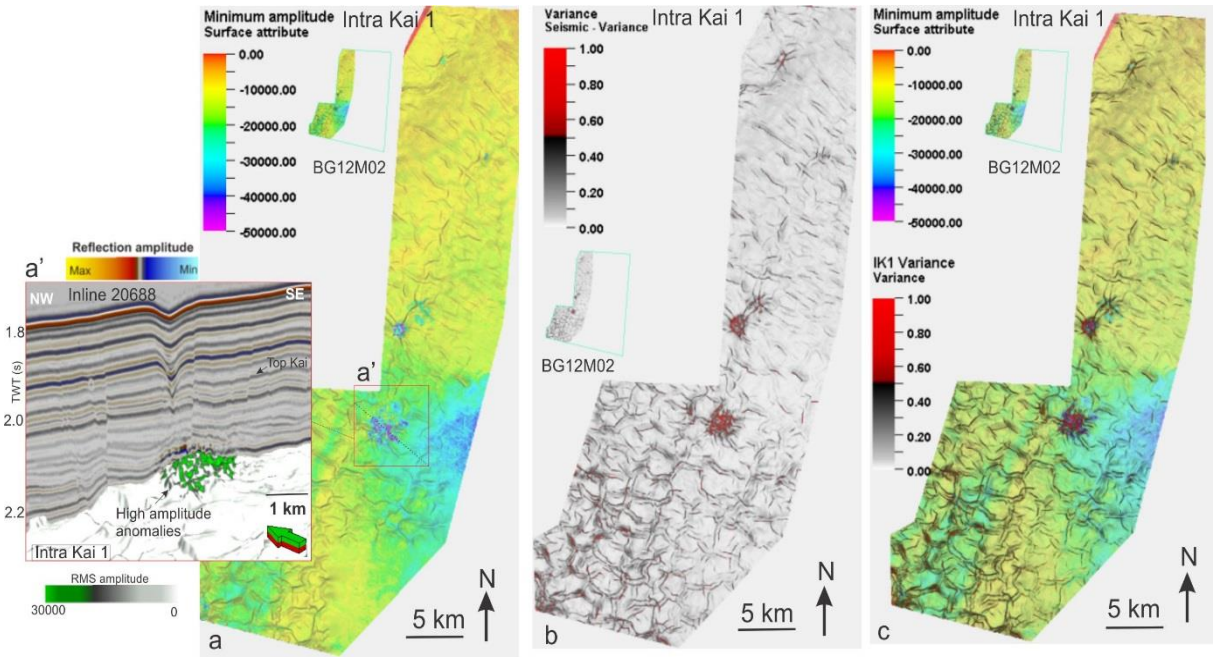

Figure 4.4.2: *The accumulation of bright spots show in* ***a)*** *Minimum amplitude map will be then more specific selected only high negative amplitude of bright spots, as located in the red rectangle. These were referred to high amplitude anomalies (green color) in RMS amplitude map.* ***b)*** *Variance attribute of Intra Kai 1 surface shows fault zones with red color.* ***c)*** *the minimum amplitude map in a) is overlain by the variance horizon from b).*

The relationship between seismic anomalies and fault structures could also be seen using the Ant-tracking volume attribute (Fig 4.4.3). The Ant-tracking attribute extracts mainly regional/major faults from small faults or/and fractures. The high value of ant-tracking is related to deep-faults as identified from the base of the Brygge Formation and downwards (Fig 4.4.3). Some of deep-faults penetrate upward into the Kai and Naust Formations, while some of them die out below the intra Brygge 1 reflection. A high density of low Ant-tracking values are located between the intra Brygge 1 (IB1) and the base of the Kai Formation reflections (BKFm), interpreted to relate to the polygonal faults (Fig 4.4.3.a).

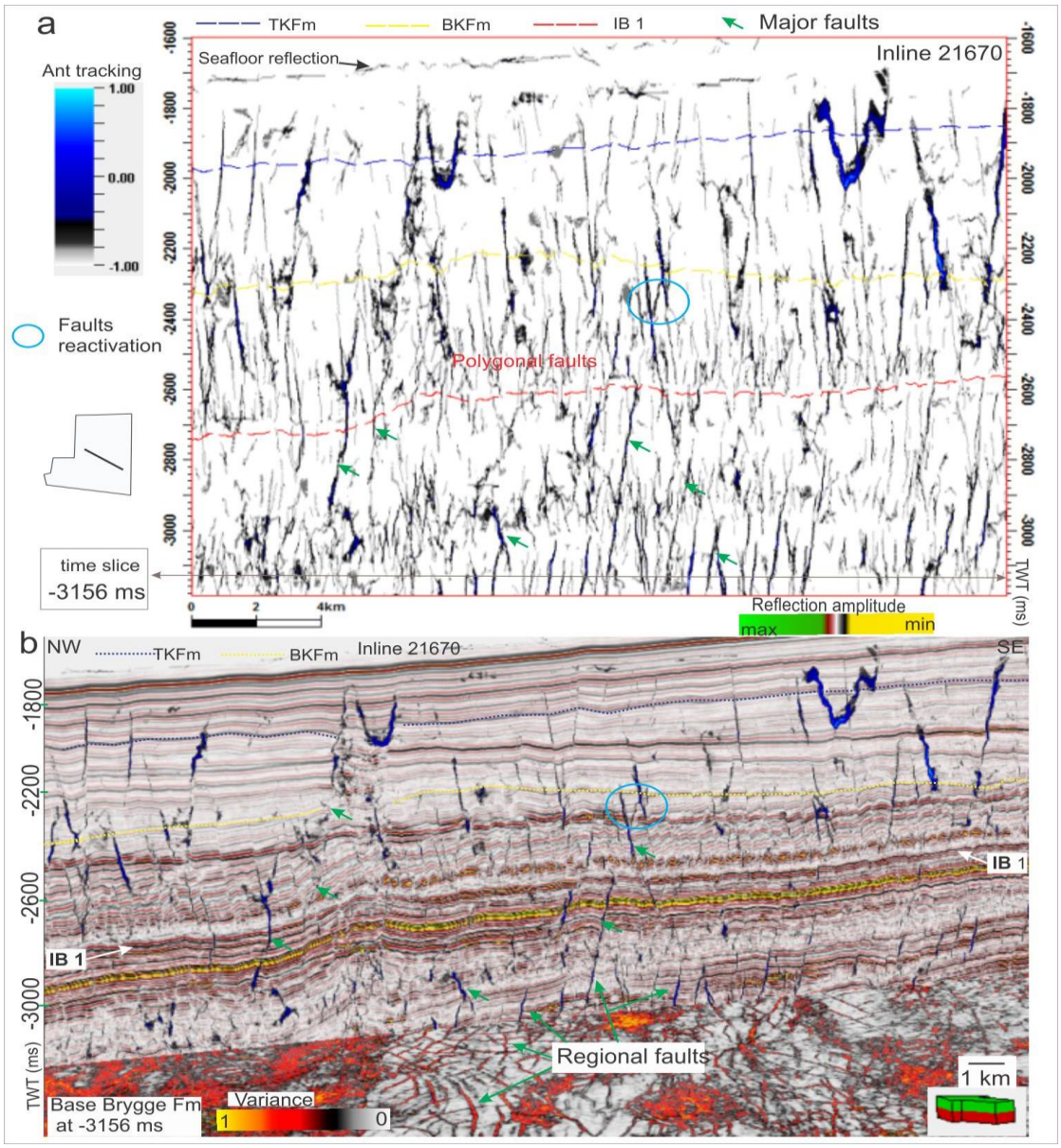

Figure 4.4.3*: Ant-tracking attribute showing enhanced major/regional faults.* ***a)*** *Ant tracking from inline 21670 showing the character of major fault, represented in the high value with blue color, black color is predicted polygonal fault system.* ***b)*** *A seismic section with overlay of ant-tracking, as shown on the similarity vertical section in a), combined with a variance map of the base of the Brygge formation. Notice that the green arrows point to major faults.*

4.4.1 Circular forms and faults

Circular forms were observed on several of the paleo-surfaces, and the variance volume attribute show that these are located in the same geographical area as fault zones (Figs 4.4.4, 4.4.5). These faults are observed in the deeper part of the stratigraphy, from approximately the base of the Brygge Formation (Top Tare Formation) and downwards (Fig 4.4.4). Some fault zones can also be followed upward to shallower horizons, including the top of the Kai Formation (Fig 4.4.5). The deep-fault structures that were observed at the top of the Tare Formation are more pronounced in the deeper part of the strata (Fig 4.4.4 d, e, f). Variance attribute reveals a variation of diameter of the fault zones in different stratigraphy levels, which were represent by circular or sub-circular shaped and size. Some of the fault zones in the south-eastern and north-eastern part of the study area are more clearly seen associated with larger circular-shaped features at the top of the Tare Formation (Fig 4.4.4 d), but these decrease in diameter from intra Brygge 1 to the top of the Brygge Formation horizon (Fig 4.4.4 a, b, c).

The fault zones in the western part of the study area (Fig 4.4.5) has a similarly trend to the previous interpreted area (Fig 4.4.4). The diameter of polygonal fault is decreasing upwards to a depth of -2400 ms (close to the base of the Kai Formation surface) as shown in detail on Fig 4.4.5; 4. The diameter of the polygonal faults then increase to reach the largest values at a depth between -2288 ms to -2187 ms (Fig 4.4.5; 2, 3), i.e. close to the intra Kai 2 and intra Kai 1 surfaces, respectively. The density of faults is decreasing upwards to the top of the Kai Formation (Fig 4.4.5; 1).

The well-developed polygonal fault system was observed from the intra Brygge 1 horizon and upwards (Figs 4.4.4 c, 4.4.5). The polygonal faults are observed to have highest intensity at the intra Brygge 2 level (Fig 4.4.4 b), and then decrease in intensity to the top of the Brygge Formation (Fig 4.4.4 a) and through to the base of the overlying Kai Formation (Fig 4.4.5). This could indicate that the development of polygonal faults were mainly restricted to the upper Brygge Formation affecting, with low displacement, the lower part of the Kai Formation.

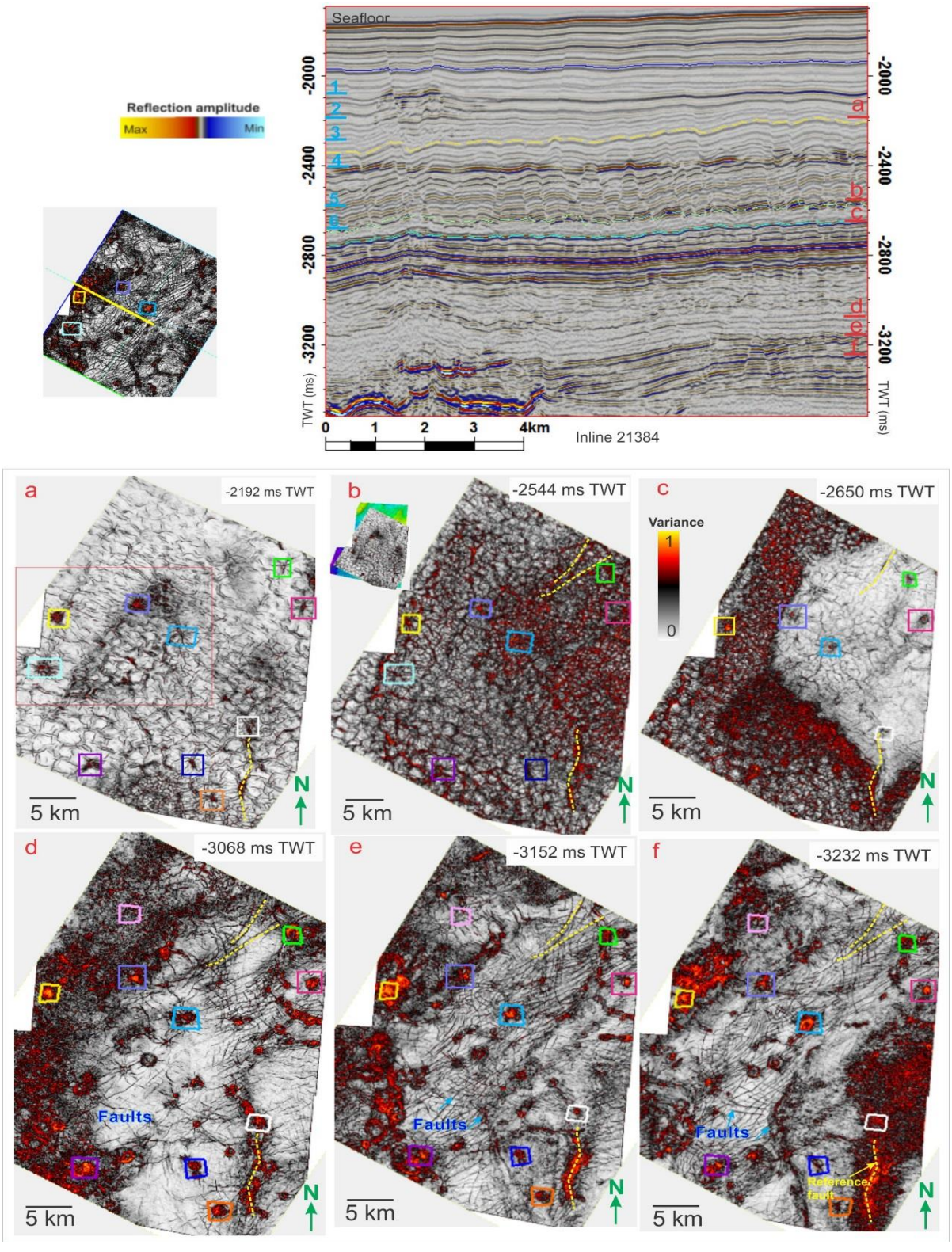

***Figure 4.4.4**: : Seismic profile showing the location of Variance attribute time slices (a-f in the seismic profile).The red zones are interpreted to be circular features (marked by rectangles with several colors) corresponding to fault zones. **a)-c)** show circular features and a polygonal fault system, which are located close to the top of the Brygge Formation, intra Brygge 2 and intra Brygge 1 paleo-surfaces, respectively. **d)-f)** show circular features and deep fault structures occurring between the top of the Tare and Tang Formations. Notice that the yellow dash lines present a reference deep-fault, which appeared at several stratigraphic levels and will also be shown in figure 4.4.8. The red rectangle in a) will also be shown in figure 4.4.5 with a marked blue color 1-6 in the seismic profile.*

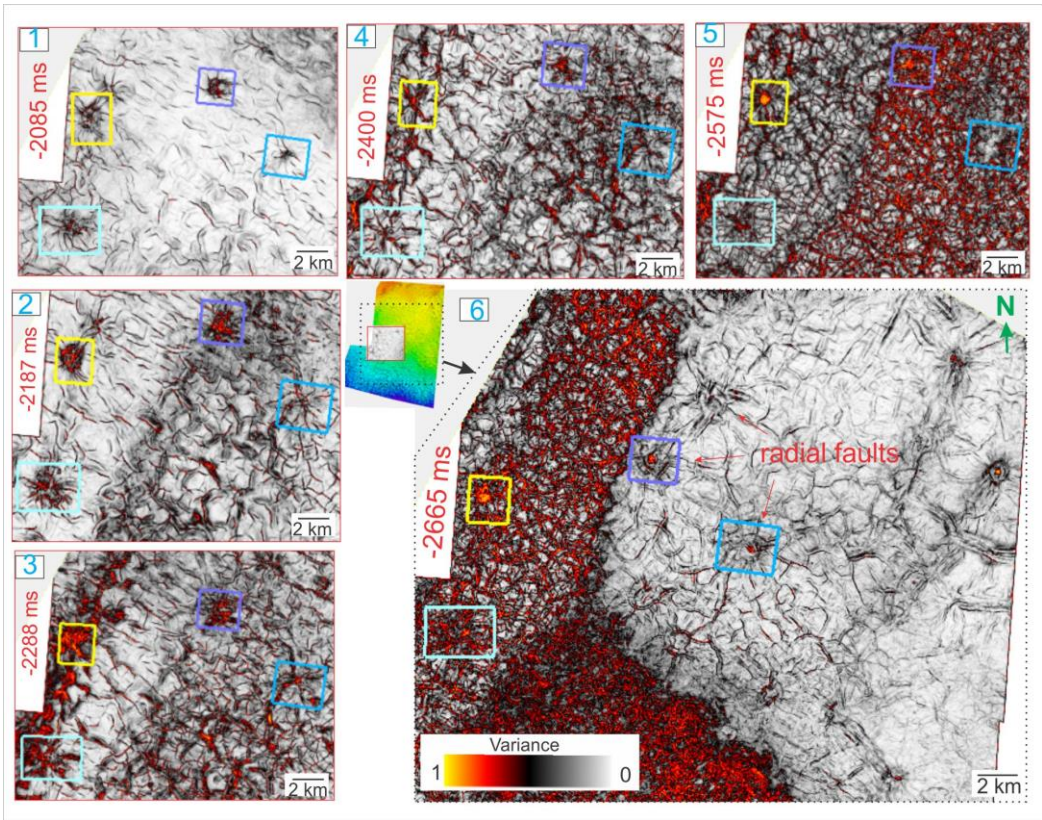

Figure 4.4.5: *Variance cube with several horizon slices from the Kai Formation (1-3) and the upper Brygge Formation (4-6). The red color corresponds to the high density of fault zones. Coloured rectangles highlight located in the western part of the study area.*

4.4.2 Distribution and dimension of circular forms

The circular forms were clearly seen on the intra Brygge 1 surface where they could be observed as positive relief circular forms (Figs 4.1.6, 4.1.8, 4.4.7). In this study, around 30 circular forms have been mapped and analysed, and three different types of circular forms have been identified based on their height and width and the presence or absence of high-amplitude anomalies around these forms.

The distribution of the three types of circular forms is shown in figure 4.4.6. The type 1 form is located mainly in the south-eastern part of this study area, while types 2 and 3 forms are mostly found in the middle and the northern part (Fig 4.4.6).

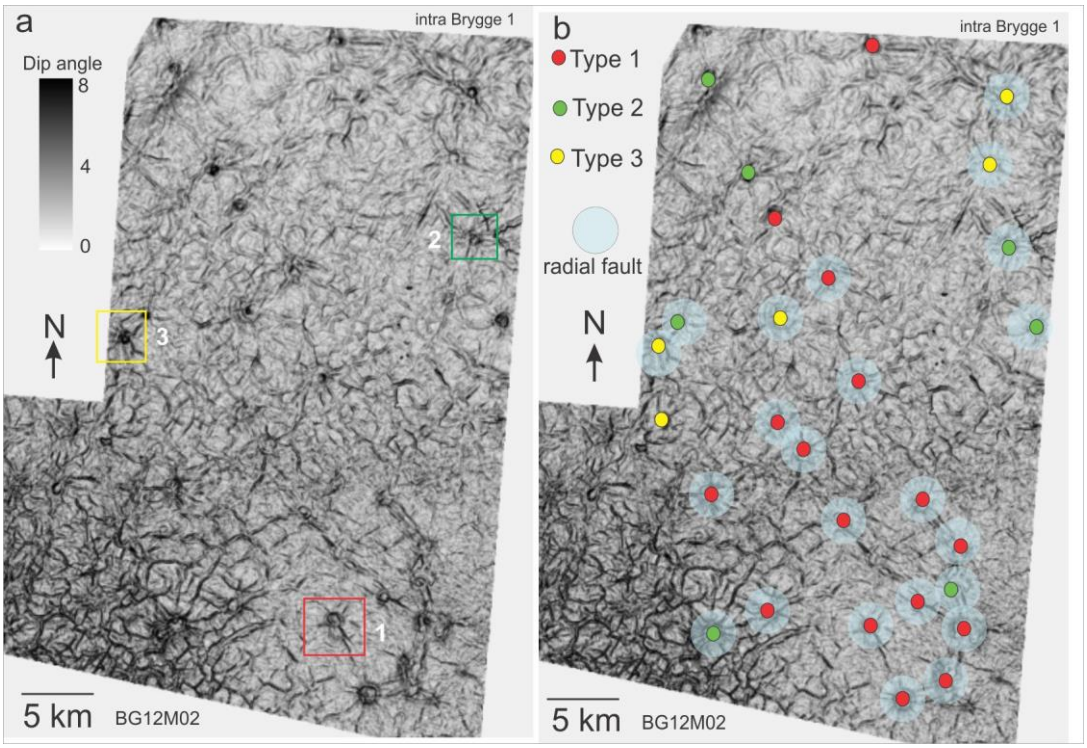

Figure 4.4.6: *Dip angle map of the intra Brygge 1 surface showing the three types of circular forms identified in this study in a) and their lateral distribution in b). Notice that the polygonal faults have a high density in the southern area, where type 1 with radial fault pattern dominates.*

Type 1 circular forms are mainly located in the south-eastern part of this study area (Fig 4.4.6 b) and typically range from 1200 to 2000 meters in width and 40-50 meters in height. There are mostly observed in the interval between -2750 ms to -2900 ms (twt) depth (Fig. 4.4.7 a), where discontinuous, parallel high-amplitude reflections characterize the seismic facies. Below this interval, a volume of chaotic reflection pattern and low amplitude anomalies could be observed at depth between -3100 and -3400 ms (twt). These reflections are truncated by narrow, sub-vertical zones of distorted low amplitude reflections, here termed acoustic pipes (Fig 4.4.7 a). Above the intra Brygge 1 reflection, several truncated reflections are observed. They are truncated by polygonal faults and penetrate the Kai Formation (Fig 4.4.4 a). The distribution of type 1 circular form is dense in the southern part of this study, probably associated with the location of the faults (Fig 4.4.6). The density of type 1 is interpreted to be related to deeper faults at the top of the Tang Formation as they are located above them (Figs 4.4.4).

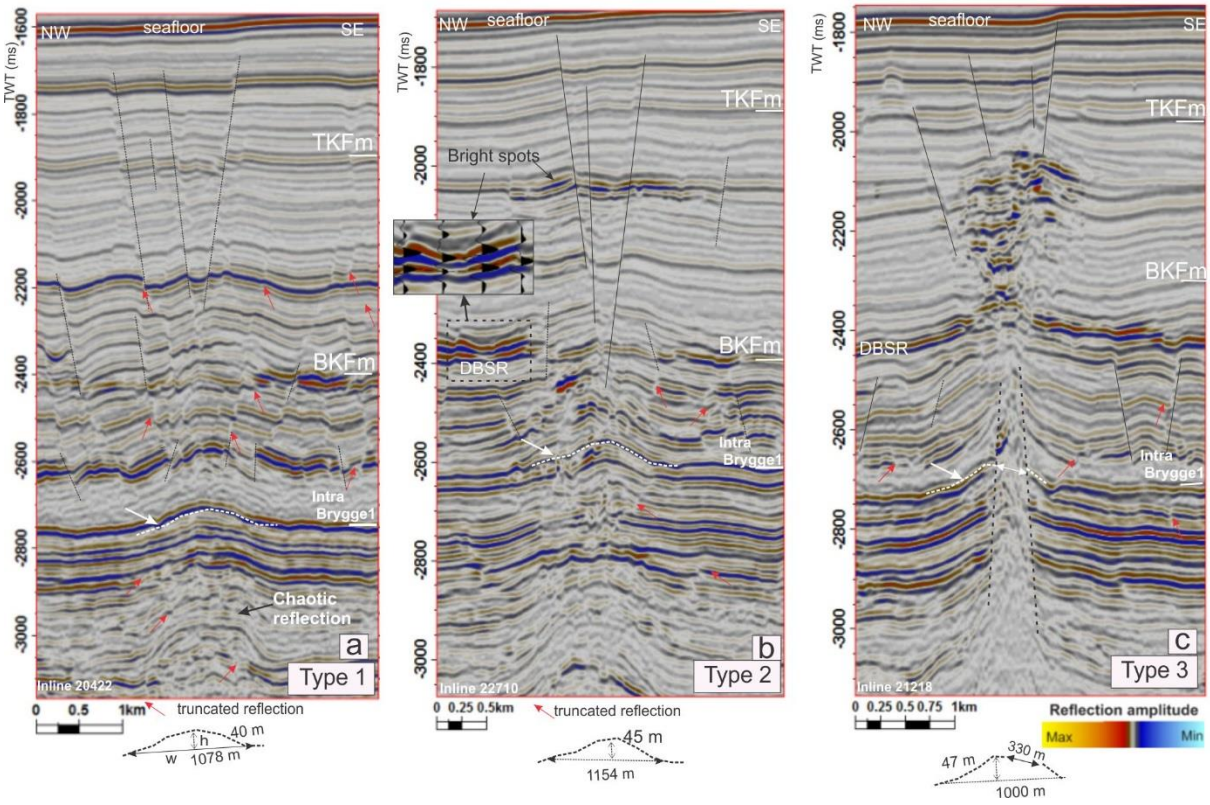

Figure 4.4.7*: Seismic section of three types of circular forms showing height and width measurement. a) type 1 are confined at the intra Brygge 1 reflection with underlying amplitude anomalies. b) type 2 are located at the intra Brygge 1 reflection, and these area truncated by narrow, sub-vertical zones of low amplitude anomalies. High amplitude anomalies are observed for this type. c) type 3 is restricted to the interval below the intra Brygge 1 reflection.*

Type 2 circular forms are smaller than type 1, they typically range from ~1000 to 1200 meters in width and ~45-60 m in height. This pattern is truncated by narrow, sub-vertical zones of low amplitude anomalies and a chaotic reflection pattern. The high amplitude anomalies, or bright spots represent a negative change in acoustic impedance (Figs 4.4.7 b). The bright spots are found in the upper part of the acoustic pipes, where some of them are found to have migrated laterally in the strata, as observed within the interval between intra Brygge 1 and the top of the Kai Formation (Fig 4.4.7 b). Some of high amplitude anomalies could also be observed over the DBSR reflection (Fig 4.4.7 b). The type 2 circular forms is located near to the type 1 circular forms (Fig 4.4.6), and seem to be related to the deep faults at the top of the Tang Formation (Figs 4.4.4).

Type 3 circular forms are smaller than the types 1 and 2 circular forms. They range from 800 to 900 meters in width and have a height of 40-50 m, and they are in general located in the vicinity of the type 2 circular forms. The height of the top of the up-bending reflection could not be measured precisely, because of the cross-cutting of the reflections by a vertical zone of low amplitude reflection, here termed an acoustic pipe (Fig 4.4.7 c). The acoustic pipes seems to have an origin from deep strata. The diameter of the pipe varies. Measured at the top of circular form reflection, it has a width of approximately 300-350 m, and it is decreasing in diameter upwards into the Kai Formation. Inside the acoustic pipes there are low amplitude anomalies that becomes more diffuse with depth (Fig 4.4.7). An accumulation of bright spots is generally observed at the flanks, and above the acoustic pipes. A chaotic reflection pattern is observed both inside and at the top of acoustic pipes (Fig 4.4.7 c). The acoustic pipe terminates under the top of the Kai Formation surface, where a cluster of bright spots and chaotic reflection pattern is observed (Fig 4.4.7 c).

The distribution of type 3 circular forms is similar to the type 2 circular forms, that they are observed at or near faults (Fig 4.4.6), and are overlying deep fault structures, as observed at the top of the Tang Formation (Figs 4.4.4).

Chaos volume attribute with high variance, referred to chaos textures, and gas migration pathway, which mainly were heavily presented as following along the fault plane from the upper Brygge Formation up towards the Naust Formation in the southwestern part of the study area (Fig. 4.4.8). The type 2 circular form with accumulation of bright spots at near the top of the Kai Formation was observed (Fig. 4.4.8).

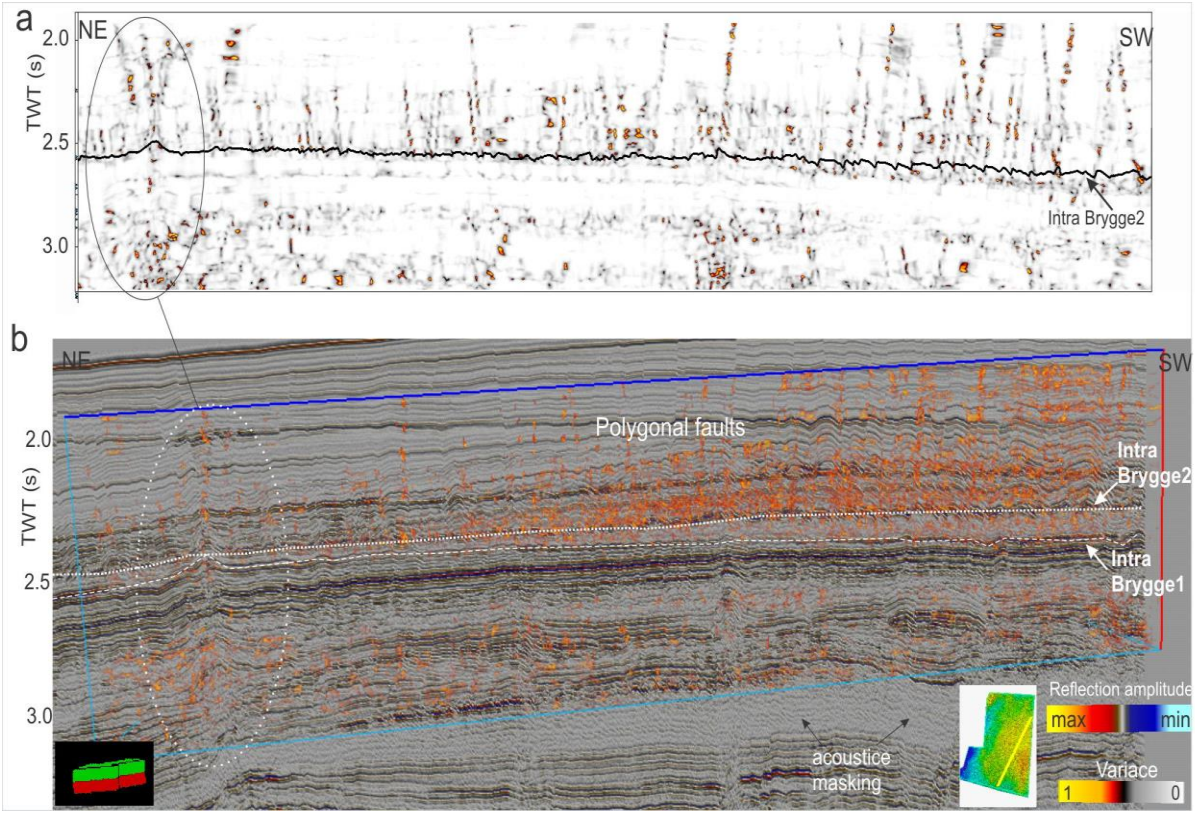

Figure 4.4.8: *Chaos attribute displayed discontinuities, chaotic textures as indication of gas migration.* ***a)*** *A vertical section of chaos attribute show faults structures in black color and probably indicators of gas and fluid in warm color, this vertical section will be also displayed in b).* ***b)*** *A seismic section is overlain by the vertical section of chaos attribute in a). Warm color in variance present gas and fluid migration pathway by means of acoustic pipes and polygonal faults. The oval lines indicate the area, where is associated with a migration pathway.*

4.4.3 Relation of the interval of seismic anomalies to the lithology

In the study area, the Tare and Tang formations consist claystone and shale, interbeded with sandstone (Fig 4.3.1). They are overlain by the lower Eocene to lower Miocene Brygge Formation, which comprise mainly calcareous and siliceous oozes (Fig 4.4.9). At a depth of about 2248 m in the Brygge Formation, the base of the interval including a chaotic reflection pattern, dim amplitude anomalies, and acoustic pipes occur (Fig 4.4.9). Acoustic pipes that are observed in sub-unit B1 appear to spit into several discontinuity vertical zone within the interval of sub-unit B2, as in this part consist mudstone with dominated oozes. These acoustic pipes terminate at the DBSR reflection. The interval above the DBSR reflection and to the top of the Kai Formation consists mainly of mudstone, which is dominated by calcareous and siliceous oozes, polygonal fault systems is well-developed in this stratigraphic interval (Fig 4.4.9).

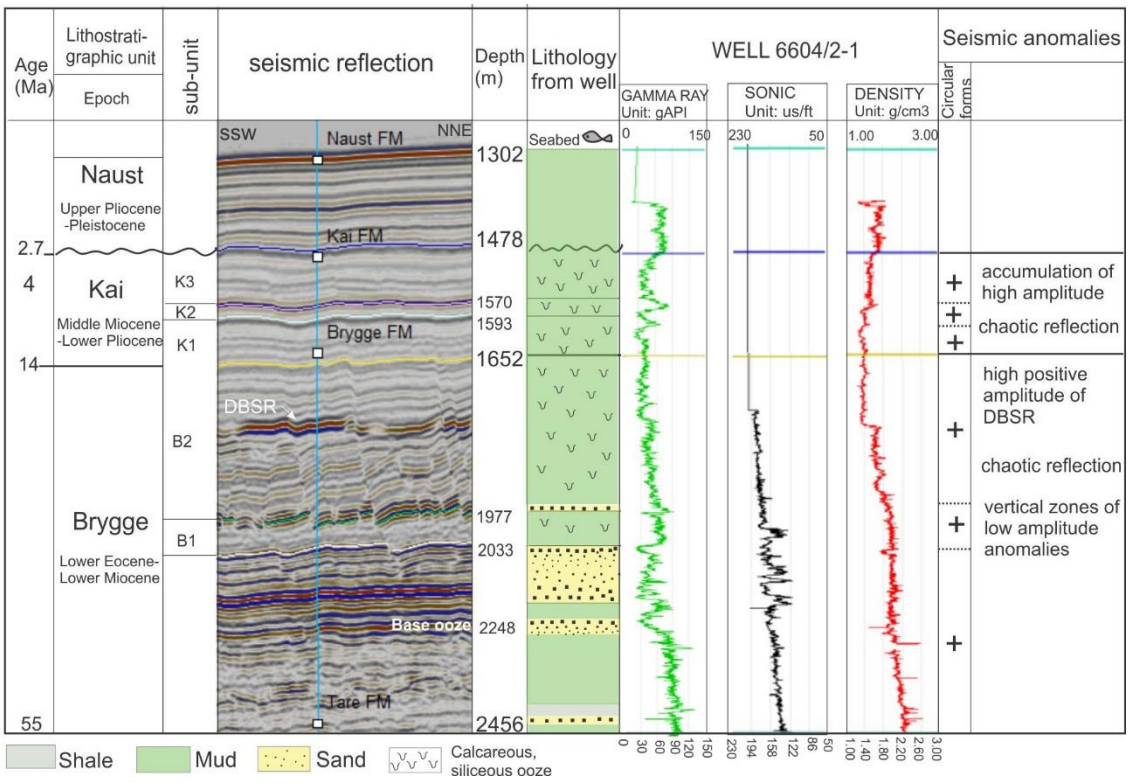

Figure 4.4.9*: Seismic section with the line of well 6604/2-1 presented by gamma ray, sonic and density logs in relationship to lithology from well and lithostratigraphy in this study area (added from the figure 4.1.1).*

4.4.4 Relation to other, under- and overlying types of seismic anomalies

Below acoustic pipes (Fig 4.4.10 a), the interval between -2800 ms to -2900 ms comprise a local down-bending, discontinuous, low amplitude seismic reflections, indicating reflection "push down" at this depth (Fig 4.4.10 a, c). Bright spots, potential indicators of gas accumulations are observed at the top of the push down and distributed in several stratigraphic levels (Fig 4.4.10 a). At proximately -2200 ms, a cluster with a size around 2 km width can be observed, having amplitude anomalies and chaotic reflections, locate above the underlying acoustic pipes. This pattern could be related to hydrocarbon gas and/or fluid migration.

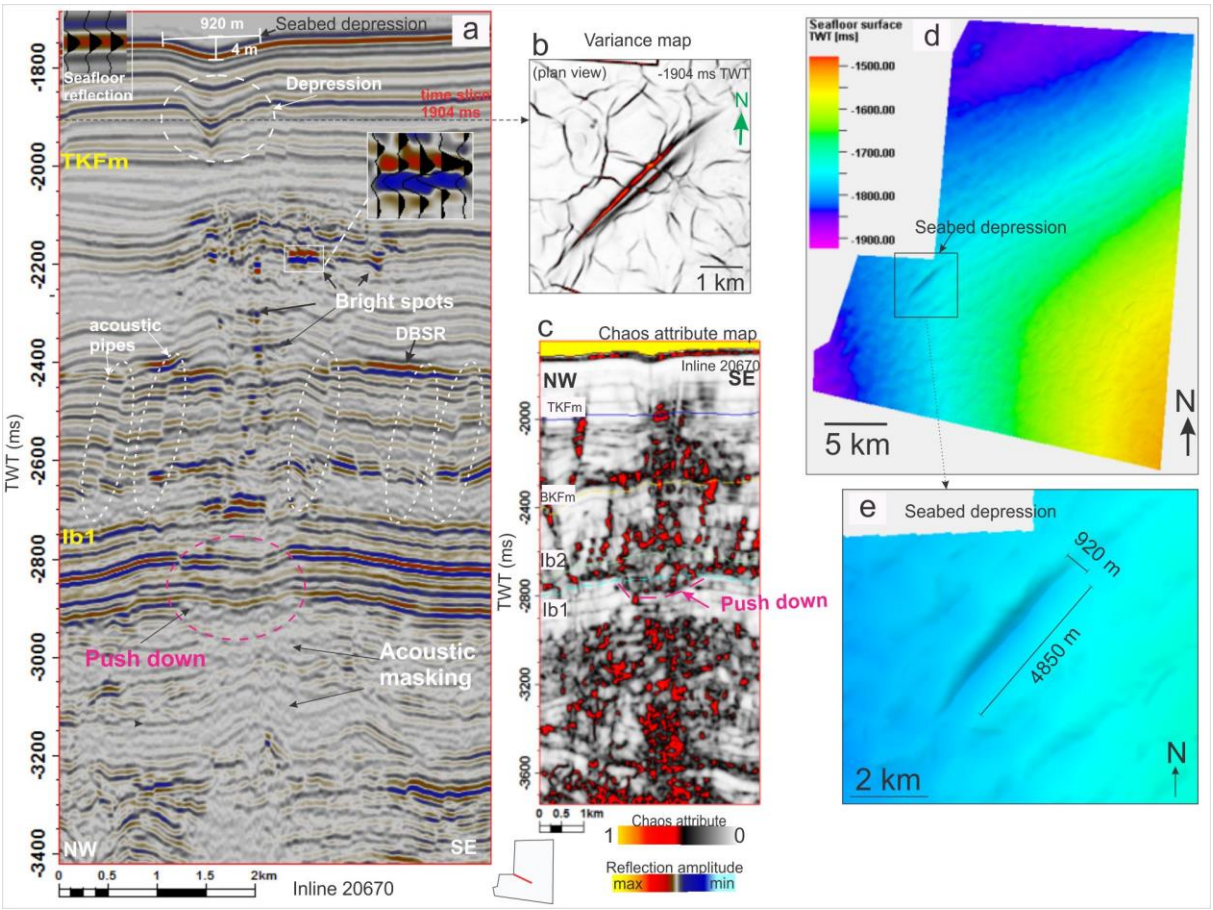

Figure 4.4.10: *show an interpretation of migration pathway.* ***a)*** *seismic profile showing a vertical zone of acoustic mashing, which is associated with acoustic pipes, bright spots, push down of the underlying strata, a cluster of high amplitude anomalies in the subsurface, a local depression and seabed-depression.* ***b)*** *Local depression feature in a time slice of variance attribute.* ***c)*** *A vertical section from chaos attribute, as the same area in the seismic section in a) show high variance represent seismic anomalies and their vertical movement.* ***d)*** *Isochrone map of the seafloor surface showing depth and morphology (ms: millisecond TWT), vertical exaggeration 7.5.* ***e)*** *A rectangle from d) present a seabed depression feature with a dimension in width and length.*

4.4.4.1 Seabed depression

Above the top of the Kai Formation reflection, at a depth of about -2000 ms, down-bending seismic reflections are occurring, forming a depression zone (Fig 4.4.10 a). An elongated feature forming a depression could be seen on the seismic section and a time slice of the variance attribute at -1904 ms (Fig 4.4.10 a, b). This zone have also affected the seafloor reflection, resulting in a seabed depression (Fig 4.4.10 a, d, e). The observed seabed depression is 4850 meters in length, 920 m in width, and c. 4 m deep (Fig 4.4.10 a, e). A vertical push down of reflections is observed at a depth of -2800 ms, right below the seabed depression (Fig 4.4.10 c).

In summary, the different types of seismic features including push down, acoustic masking, acoustic pipes, bright spots, and seabed depressions indicate hydrocarbon gas and/or fluid migration.

4.4.4.2 Pockmarks

Below the top of the Kai Formation surface, depression features of circular or elliptical forms are observed (Fig 4.4.11 A). The dimension of the negative depression features are between 150-200 meter in width, and 5-10 m. in depth (Fig 4.4.11 A). These depressions are observed above polygonal faults and below the top of the Kai Formation surface, and they are covered by discontinuous, low amplitude reflection of dimmed character. These features are here interpreted as pockmarks because of their form and dimensions. Several pockmarks are observed, concentration around fault structures (Fig 4.4.11).

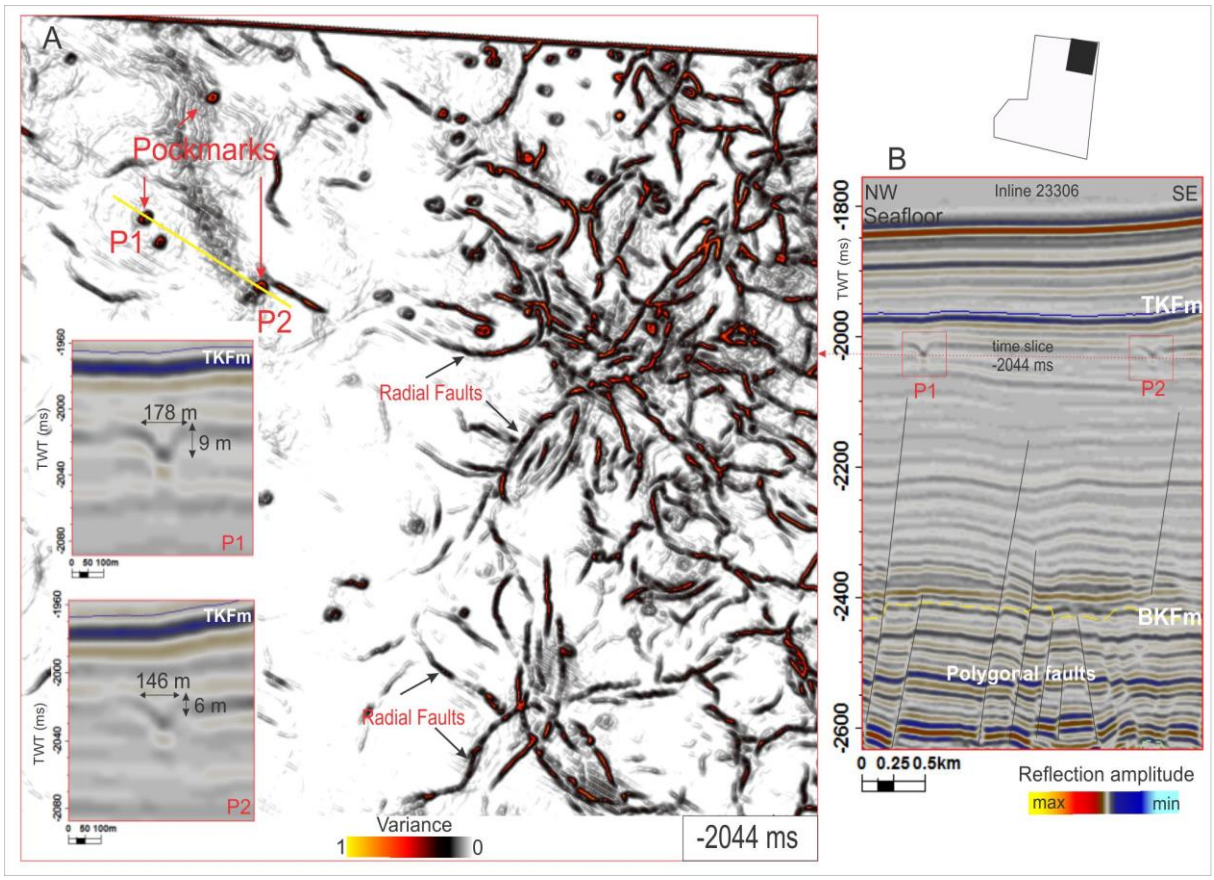

Figure 4.4.11: *A) A variance map of time slice -2044 ms TWT shows several depression features, interpreted as pockmarks, two seismic section with measurement method have shown in the left side of this map. A yellow seismic line will be interpreted in B. B) A seismic section shows two negative depression features, where are referred to A), a red line present a depth level that the time slice is displayed.*

5 DISCUSSION

In this chapter, the origin of the upper Brygge and Kai Formations will be discussed in relation to the paleo-environment during deposition. First, the geometry and internal seismic reflection facies and their origin as well as the morphology of buried surfaces will be discussed. The well data will be also discussed and associated with their lithology. Then the sedimentary environment will be discussed in relation to the development of the oceanic circulation. Finally, fluid and gas migration, associated with polygonal fault system and sediment remobilization will be presented and discussed including a suggested schematic model summarizing of current flow pattern and fluid migration.

5.1 Sedimentary environment

The sedimentary environment in the study area is related to the deposition of the upper Brygge and the Kai Formations can be classified as alongslopes sediment-drift accumulations, result of the interpreted indications of ocean bottom currents.

5.1.1 Alongslope process

In chapter 4.2, it was verified that the upper Brygge and the Kai Formation deposits are developed by alongslope processes, associated with erosion, transport, and/or deposition under the conditions of the ocean bottom currents. The seismic data shows an increasing thickness of contourite drift deposits upslope and a depocenter on the lower slope within the uppermost part of the Brygge Formation. Based on the seismic signature showing characteristic of contourites in medium-scale, the deposits was classified as mounded elongated contourite drifts. These massive deposits occur within the uppermost Brygge Formation.

The base Kai unconformity is located at the top of the Brygge Formation, separating lower Miocene from Paleogene strata. This could present the first indication of ocean bottom current circulation, possibly already during Oligocene time (Laberg et al., 2005 b, Stoker et al., 2005 b). The seismic data displays a sedimentation pattern characterized by alongslope deposit, the depocentre of each subunit is located on the lower part of the continental slope, and current-induced bedforms, such as sediment waves (Figs 4.1.14, 4.1.15, 5.1.2). This may be related to change in the ocean circulation pattern and sediment types, which have affected by

multiphase tectonic events during the Eocene and Miocene time, that control the seafloor morphology and submarine topography.

The opening of Faroe conduit

The exchange of deep-water between the Nordic Sea and the Atlantic Ocean was related to the opening of the Faroe conduit, deep-water flow across the GSR from the mid to late Miocene (Laberg et al., 2005 b; Stoker et al., 2005 a). This has an impact on sedimentation along the NW European margin. According to Stoker et al. (2005 b) the expansion of contourite sediment drifts in the north and south of the Greenland-Scotland Ridge is connected to the development of the Faroe conduit. Before the mid Miocene time, there was little or no deep-water exchange between the Nordic Seas and the North Atlantic. In addition, Paleogene and Neogene sediments (Brygge and Kai sediments) were deposited along the continental margin, and have characteristic of alongslope erosion and sedimentation since the late Eocene, it was not a result of a true deep-water connection, which was created across the Greenland-Scotland Ridge. This suggestion from Stoker et al. (2005a,b), that ocean circulation during the Oligocene was reflected to interbasinal circulation, was restricted to the Norwegian-Greenland Sea area and possibly linked to the northern North Atlantic was supported by Laberg et al. (2005a).

Local anticlinal highs

The study area is partly located at the Gjallar Ridge, in the western part of the Vøring Basin. The Gjallar Ridge is bounded to the west by the Vøring Escarpment, and to the southeast by the fault complexes, and anticlinal structure of the Helland-Hansen Arch. The Modgunn Arch is located in the south.

An early Tertiary reactivation phase of the major tectonic lineaments resulted in the formation of large domes and arches like the N-S oreinted Helland-Hansen Arch that is a result of reactivation of the Fles Fault Complex (Brekke 2000). The middle Miocene unconformity is defined on the top of the Helland-Hansen Arch surface. These local anticlinal highs probably played a central role in the flow of bottom currents and Miocene contourite deposition. Chand et al. (2011) suggested that the deposition of mounded contouritic sediments was affected by ocean currents, as sediments were deposited along the flanks of anticlines.

According to Laberg et al. (2005a) there are indications that the basement of anticlinal highs were eroded by an ocean circulation system affecting the Vøring Marginal High from Eocene time and onward. These tectonic events could have impacted the restricted ocean circulation pattern along the outer slope of Vøring Marginal High implying that the Eocene circulation could be mainly interbasinal.

5.1.2 Ocean circulation in the study area during the sediment deposition

In the study area, the sediments within upper Brygge Formation were divided in to two sub-units, B1 and B2. The Kai Formation was divided into 3 sub-units, K1-K3. The interpretation and discussion below will be based on seismic reflection pattern, -termination and their relation to ocean circulation. The sub-units differ both in sediment distribution and thickness through the study area. Two models of sediment deposition was suggested by illustration of seismic profiles in N-S and NE/SW orientation (Figs 5.1.1, 5.1.2), and an illustration was created to present the evolution of ocean circulation and current flow directions in the study area for each subunit, implied from the pattern of sediment distribution (Fig 5.1.3).

5.1.2.1 The upper of the Brygge Formation

Subunit B1

The interpreted lithology from the Gamma ray log indicate mudstone overlain by thin sandstone layers interbedded with mud. The sediments in B1 have a relative uniform thickness, this support the suggestion that B1 have been less affected by bottom currents. Also subunit B1 do not have any clearly evidence of contour-current-controlled sedimentation. B1 sediments may be deposited from suspension representing a more hemipelagic environment where the ocean currents had low velocity (Fig 5.1.1, 5.1.3 a).

Sediments might have come from a source areas to the west, the Vøring Marginal High which is located to the west of the study area, or ever further west. This is conformity by Brekke (2000) suggesting that the eastern flank of the Vøring Marginal High was a sediment source area, due to uplift during the latest Eocene to early Oligocene, as well as Laberg et al. (2005a) and Eidvin et al. (2007) suggested that the sandy mud found on the inner Vøring Marginal High was deposited due to tectonic subsidence of the outer part of Vøring Plateau, while the area located on the outerpart of the Vøring Marginal High influenced by high flow velocity of

ocean currents. This could assume that ocean currents in the study area had possibly low velocity during late Eocene, as support to low deposition of ocean current transported sediments. The sediments were possibly deposited by suspension.

From discussion above, a change amplitude from high to low, between the underlying part of the Brygge Formation and subunit B1 is interpreted to reflect a change in sediment lithology caused by tectonic events, due to regional uplift and subsidence, rather than affecting in the bottom current pattern.

Subunit B2

The western part of the study area shows the first evidence of bottom current activity. This is displayed by the seismic expression of the related sediment drift; the lenticular, upward-convex seismic signature of subunit B2, and a depocentre on the lower slope, located in the southern part of the study area. This subunit is interpreted as a mound structure in the uppermost of the Brygge Formation, implying that the uppermost Oligocene/lowest Miocene strata mainly is of contourite drift origin (Fig 5.1.1).

In relation to ocean circulation, this suggests that bottom currents with high velocity perhaps were flowing in the eastern part of the study area and towards north and northeast, flowing system in the Vigird Syncline area, whereas the western part of the study area may have had another bottom current pattern with a generally west and northwest along the high negative relief near the Vøring Escarpment (Figs 5.1.1, 5.1.3).

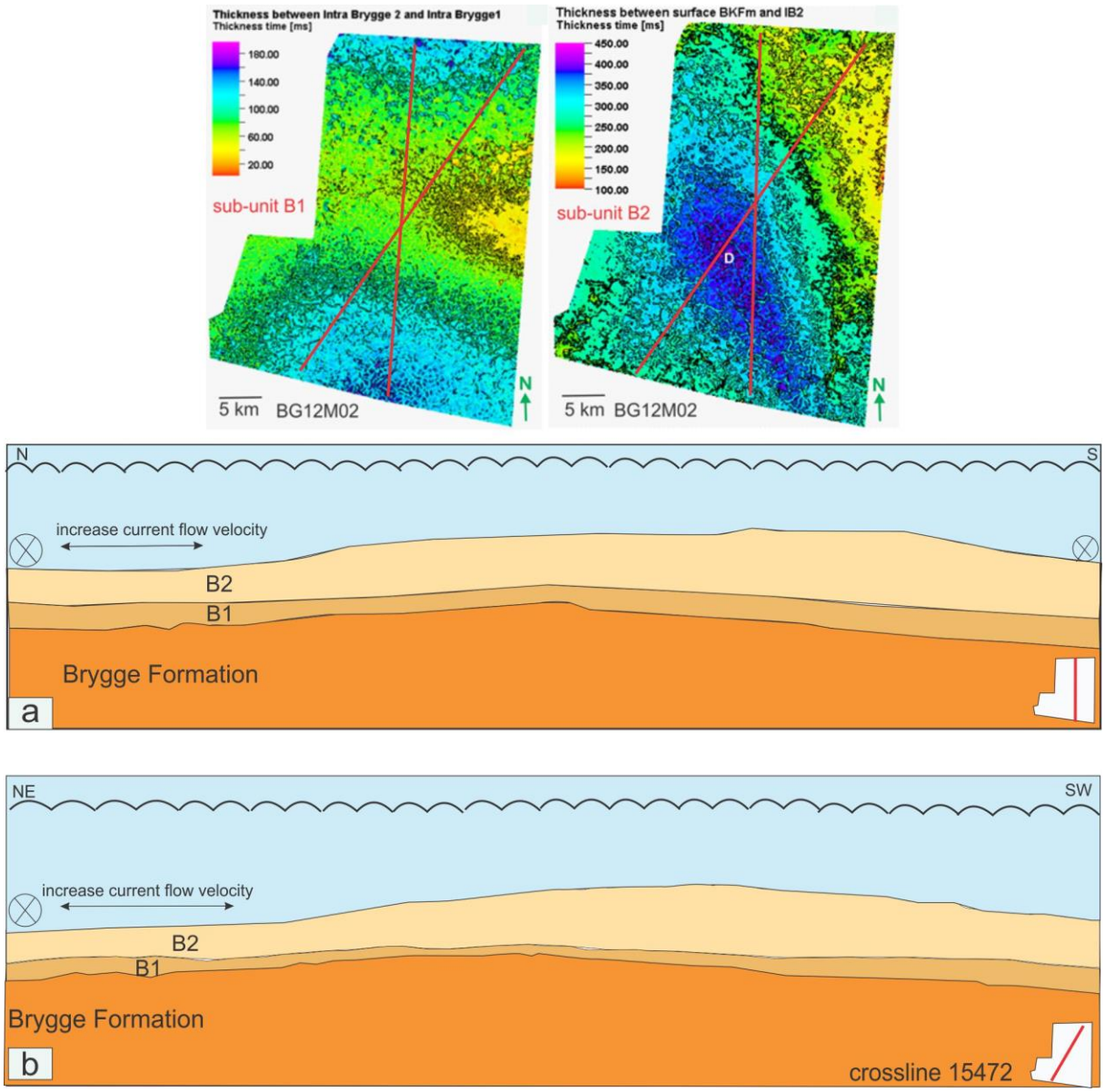

***Figure 5.1.1**: Thickness map of subunits B1 and B2 from upper Brygge Formation in the study area, with seismic composite lines. a and b) Geoseismic line with the distribution of upper Brygge Formation in a N-S and NE/SW orientation crossing the study area. Current flow direction is indicated.*

The sediments in the uppermost part of the Brygge Formation was supposed to have been deposited between early Eocene to early Miocene time. This is correspondence to Laberg et al. (2005b) who suggested that the first indications of bottom current circulation along the continental margin was found the in late Eocene time.

5.1.2.2 The Kai Formation (middle Miocene -lower Pliocene)

Subunit K1 generally follow the same seismic configuration pattern as the underlying subunit B2. The onlapping reflection termination, truncations of underlying strata in the southern area and, the mound structure in the northern area are interpreted to be the result of bottom currents (Fig 5.1.2). Subunit K1 might have been affected by the currents flowing in the same area as during deposition of subunit B2, along the negative relief to the western and northern side of the study area. An amplitude change was found in this subunit, which probably is associated with a change in the bottom current system. As K1 is thinning towards the south it is likely that the sedimentation rate is lower here, which imply higher rate of deposition from ocean currents in the northern part of the study area (Fig. 5.1.2).

Some parallel and dipping downward reflections located within the upperpart of subunit K1 observed. This may suggest a change in ocean current pattern, that sediments were deposited by low velocity flowing, as these were less effected by bottom currents. Sediment deposition in this part were alternatively deposited by suspension.

Subunit K2 is following the same structural pattern as the underlying sediments. It includes a few onlapping termination towards the southwestern part. Erosional truncation was clearly identified at the top of this subunit. K2 is thinning out to the south and southwest, and is more restricted in thickness around 20 ms (twt) in the center of the study area (Fig. 5.1.2). This erosion may be related to currents with relatively high flow velocity that erode subunit K2 in the middle and southern part of the area, and deposition in the northern part. This could imply that stronger currents have been flown into the south and further to the western part of the study area, following the topographical high negative relief (Fig. 5.1.2).

These current patterns may have been influenced by elevated local anticlinal highs, ocean currents were following the flanks of the Helland-Hansen and Modgrunn arches, located southeast and south of the study area, respectively. This interpretation is in conformity with Hjelstuen et al. (2005); the contouritic sediments deposited on the southern Vøring Margin have been influenced by uplifted anticlinal structures. Laberg et al. (2005b) suggested that the Miocene sediments deposited on the inner Vøring Marginal High, could be identified as contour-current controlled sedimentation. From the observation in the study area, an

increasing in contourite sedimentation within K1 and K2 with variation of depocenter, could be a consequence of changes in the bottom current related system.

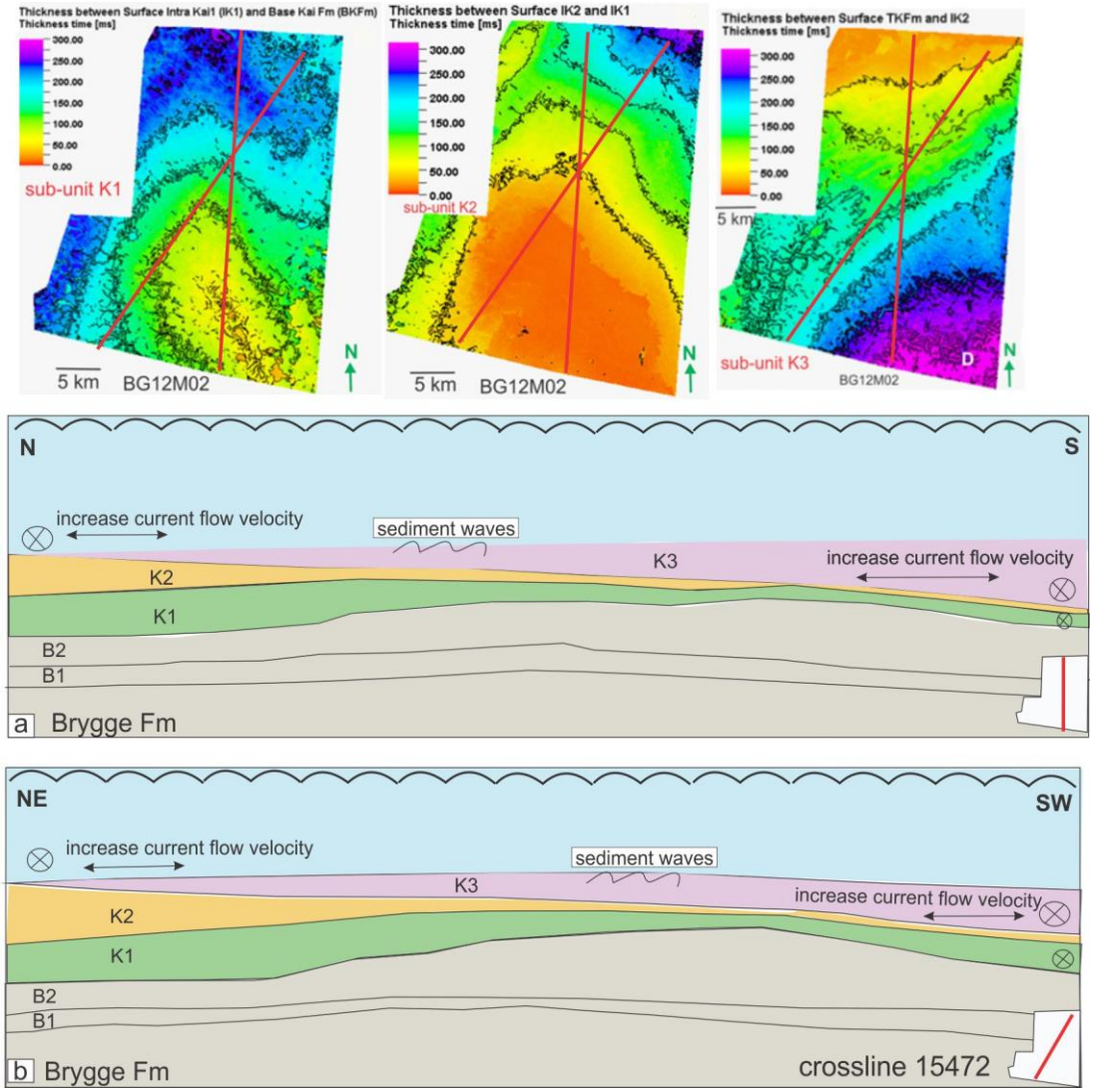

***Figure 5.1.2**: Thickness map of subunit K1, K2 and K3 in the Kai Formation in the study area, with seismic composite. a-b) Illustration of the seismic composite line with the distribution of upper Brygge Formationin a N-S and NE/SW orientation throughout the study area, and ocean current flow direction.*

Subunit K3

K3 is the youngest sub-unit in the study area. It has internal reflections slightly downdipping to the south, but their reflection terminations are located outside the study area. A few onlapping reflection terminations onto the underlying sub-unit K2 can be observed. This may suggest sediment migration upslope towards the north and northeast. A depocenter is located at the lower slope in the southeastern part of the study area (Fig. 5.1.2). Erosional truncations

were indicated both at the top and the base of the subunit boundaries. At the top surface sediment waves have developed (Fig. 5.1.2). This sedimentation pattern imply deposition from bottom currents (Stow et al, 2009). Eidvin et al. (2014) suggested that a shifting position of local depocentres is indicative of changes in the paleogeography in the source area.

K3 do not follow the same depositional pattern as the underlying subunit K2. This may suggest that the currents have varied in flow direction and velocity. During the time of deposition of subunit K3, currents may have flown along the Vøring Escarpment, located at the western side of the study area, and towards the north with high flow velocity. Some branches of currents may also have flown into the study area from the north, resulting in erosion in this area (Figs. 5.1.2, 5.1.3). The strength of the currents was decreasing towards the southeast. That could be identified by the depositional features of the sediment waves, which have NE-SW orientation with a change from symmetric to sinusoidal waveforms upward-slope, and they became larger in waveforms (Figs 4.1.14 a, 4.1.15, and 8. in appendix).

Finally, the lowest velocity of the currents probably occurred in the area of the lower slope where there is a depocenter. Faults and polygonal fault system are observed to penetrate into some part of the sediment waves (Fig. 8, appendix). From this it is suggested that the sediment waves were formed before the development of the fault structures.

The reflection termination of the upper part of K3 located outside the study area, while internal seismic reflection configuration is gently divergent to the south and southwest. However, this could be an alternatively of sedimentation pattern, which deposited by less effect of bottom currents, but could be deposited by suspension.

As shown in the studies of Eidvin et al. (2014), it is still no sediment sampling in the Brygge Formation and upward into the middle part of Kai Formation on the Gjallar Ridge. Therefore, samples from nearby areas was used. Correlation of fossil assemblages between wells from the North Sea, the Norwegian Sea continental shelf (Trøndelag Platform and Nordland Ridge), and the Vøring Plateau show the *Balboforma* (*B. badeensis*, *B. reticulata*) assemblage found in the Nordland group in the deep-marine Kai Formation on the Vøring Plateau is interpreted to be of middle Miocene age. These formations were deposited as a result of

mainland Norway uplift and erosion in mid Miocene time. The Kai Formation on the Vøring Plateau consist mainly of glauconitic sand, silt and clay (Eidvin et al., 2007). The fossil record consist mainly of calcareous microfossils, and dated at middle Miocene age (ca. 11.5-14 Ma). This could strengthen the interpretation that the K3 sediments were deposited during a period of changing sediment source area as a result of uplift of the mainland, deposited from ocean bottom currents.

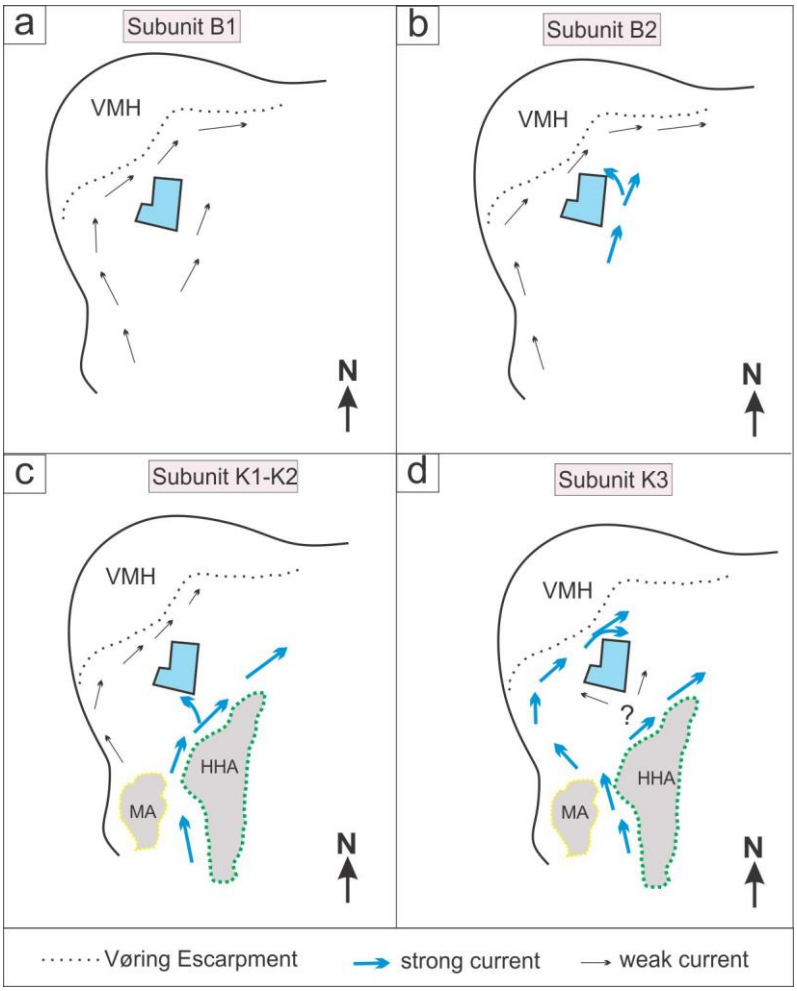

Figure 5.1.3: *Drawing shows evolution of the interpreted ocean circulation in the study area. Strong current indicated area with high flow velocity causing erosion. Weak currents indicate the area of minor branches of low velocity and/or less effected by bottom currents.*

The Naust Formation

The top surface of sub-unit K3 is identified as the Base Naust Unconformity (BSU). The reflection of the top surface is almost horizontal, and overlain by gentle dipping internal reflections, indicating a progradational pattern of the Naust Formation. These reflections are dipping towards the north and the west in the study area. This may suggest that the Naust

sediments were deposited by progadation from the east/southeast. Hjelstuen et al. (2005) found the post-Miocene sediments to deposit from an easterly source area representing a westward prograding wedge.

5.1.3 Summary

The deposition of the upper part of the Brygge and Kai Formations have been influenced by bottom currents. Subunit B1 was mainly deposited from suspension, i.e. this unit comprise hemipelagic sediments. The first indication of mounded elongated drifts with associating onlap reflection termination are found in the uppermost part of the Brygge Formation (B2). The contour-current regime during deposition of the studied interval was generally flowing into the eastern part of the study area, and north and northeastern flowing system in the Vigird Syncline while the western part, have another bottom current pattern with a generally flowing as closely to the Vøring Escarpment.

For sub-unit K1 and K2 (Kai Formation) a similar contouritic deposition pattern is observed, Sub-units K1 and K2 are eroded by relative high velocity currents in the southern part, and deposition on the northern part of the area. During deposition of subunit K3 a change in flow direction from the southern to the western side of the study area is observed, resulting in erosion of subunit K3 in the north and deposition in the southeast. K3 is effected by bottom current-related system, as well as a change in the source area caused by the uplift of mainland Norway.

5.2 Structural and stratigraphic controls on fluid flow

5.2.1 Polygonal faulting within the Brygge and Kai Formations

Small cross-cutting faults forming a polygonal network, interpreted as polygonal faults have been observed in the uppermost Brygge, Kai, and the lower Naust Formations within the study area. Polygonal faulting is widespread in fine-grained depositional systems (Cartwright et al., 2003), and occurs in the upper Oligocene and Miocene successions in the Vøring Basin (Berndt et al., 2003). On the Vøring Plateau, polygonal faulting have been found within fine-gained sediment of the Kai (Berndt et al., 2003), and the upper Brygge Formations (Hansen et al., 2005), as well as in the lower Naust Formation (Gay and Berndt, 2007). The polygonal fault system is developed in relation to compaction, diagenesis and dewatering, and could be associated with the overburden caused by the deposition of the overlying Naust Formation (Berndt et al., 2003; Chand et al., 2011). According to Gay and Berndt (2007) the Kai Formation is dominated by clayey ooze with very high smectite content, which form a fine texture in the sediment, and a contraction of the mud-dominated Kai sediments could probable lead to the formation of the polygonal faults at the large scale.

Based on several surface and volume seismic attributes, which were extracted from the 3D seismic data, a high intensity of polygonal faulting have been identified. These are especially pronounced in the southern part of the study area, and they are observed to have an origin in the upper Brygge Formation. The fault throw is best developed within the interval between the intra Brygge 1 surface and the DBSR reflection. Gay and Berndt (2007) suggested that fault offsets increasing with depth is characteristic of the polygonal faulting process. Some intervals of the Kai Formation is observed to comprise fault throw decreasing in intensity, and some of them penetrate through to the overlying base of the Naust Formation. There were also observed some younger faults formed in the uppermost Brygge Formation offsetting the Naust Formation. These new faults are interpreted to represent reactivation of both deeper major faults and polygonal faults, inferred to be a result of rapid loading of the Naust Formation. Gay and Berndt (2007) suggest that the reactivated polygonal faults in the Kai Formation penetrated into the lower Naust Formationas a consequence of deposition of the overlying submarine debris-flow deposit. However, debris flow deposits have not been identified in the study area. This may a reason to assume that overpressure development in the study area, caused by early Naust deposition, may have had a major role in polygonal faulting and fluid migration.

According to Berndt et al. (2003), fluid expulsion in relation to the development of polygonal faulting in the Vøring Basin could have had an onset in early Miocene time. This may suggest that an initiation of the polygonal fault system in the study area could itself be a main source of fluid expulsion. Fluid movement along polygonal faults, which are found to be fluid conduits, has a high potential for fluid migration from deeper levels. This is a conformity with previous studies by Hansen al. (2005), and Gay and Berndt (2007) that imply that fluids are driven along intersections between three adjacent polygonal faults which cross-cut the whole interval in the study area.

5.2.2 Sediment remobilization and fluid migration pathway

Positive relief structures with a circular forms are observed in the study area, and these are divided into three types based on their geometry, seismic signature and surrounding seismic anomalies.

Type 1 circular forms are mainly observed and clearly seen in plain view in the upper Brygge Formation, associated with an underlying chaotic reflection pattern, interpreted as mound structures. Mound structures are formed when there is large overpressure developed though time, that cannot be released by diffuse fluid flow (Chand et al., 2011).

Type 1 indicate a clear relation to major faults in deeper strata. This may suggest that the faults have acted as fluid migration pathways from deeper levels. There is not observed fluid migration above these forms, which suggest that the overlying sediments have functioned as a barrier to vertical movement further up in the strata (Fig 5.2.1 a). Although continuous with varying amplitude, as weak reflections are observed beside the circular forms, the bedding is continuing unbroken, while the sediments affected by overpressure are deformed (Løseth et al., 2009). This is conformity with Hansen et al. (2005) who suggests that the Oligocene sediments at the Gjallar Ridge may have prohibited vertical migration from deeper strata, as well as Svendsen et al (2004) who have identified hydrothermal vent complexes, caused by sill intrusions in the Vøring and Møre basins, suggest that the hydrothermal vent complexes represent pipe-like structures with craters and mounds, which terminate at the top of Oligocene level (Fig 5.2.1 a).

According to studies of Løseth et al. (2003) on the Hordaland Group (North Sea) sediment mobilization is also found in sediments with high smectite content and these are also related to polygonal faulting. It was classified as mud mobilization developed at shallow burial, at a depth less than 1000 m, by injection of gas/fluid from an external source. According to another model, overpressure was formed in the deep Viking Graben as a result of chemical compaction and hydrocarbon degeneration. In the study area, Eocene sediments may have been mobilized, as indicated by the presence of chaotic reflection zones under the type 1 circular forms. V-shaped reflections that are characteristic of carbonate-cemented sand injection structures, as interpreted by Løseth et al. (2003), was not found in the study area. From the above it is assumed that sediment mobilization in the study area may have been associated with fluid migration from a deeper source, possibly the Eocene interval (Fig 5.2.1 a).

Type 2 circular forms are found at the intra Brygge 1 reflection in the upper Brygge Formation. Above this type, small clusters of bright spots or singular bright spots occurred at the top of the Kai Formation, above the polygonal faults. These were found at the exit of small, vertically oriented acoustic pipes, which has acted as fluid migration pathways from deeper to shallower levels (Fig 5.2.1 b). Some buried pockmarks were observed near the Top Kai Formation. This may suggest that type 2 circular forms are ongoing stage of fluid migration in the late Oligocene time, and may developed from type 1, without vigorous evidence of blow-out of large acoustic pipes.

Type 3 circular forms show fluid migration from deeper strata to the subsurface. Based on vigorous evidence for blow-out acoustic pipes, bright spots, and push-down effects were found. The evidence for shallow gas accumulation at the top Kai Formation have a connection to vertical movement of fluid, and mobilized sediments from deep strata (Fig 5.2.1 c and d) Hansen et al. (2005) found evidences of mud remobilization and fluid migration on the Gjallar Ridge, associated with the Gleipne sill complex, this hydrothermal activity could have resulted in an increase in the vertical migration of sediments, leading to the formation of mud diapirs at top of the Kai formation.

Based on the interpreted attributes of the 3D seismic data, Variance displays the faults present, whereas the Chaos attribute show partly faults, and those faults that are associated

with vertical fluid migration can be identified. Anyway, it is important to combine 3D attributes with vertical seismic sections in the interpretation of potential fluid migration. Ligtenberg (2005) suggested that fluid activities could be detected along faults, and this indicates potential leaking of faults and fractures. Faults lacking any detected fluid activity probably correspond to sealing faults. It may be reasonable to assume that the cluster of high-amplitude anomalies in the Kai Formation, bright spots, and fault zones linked to the underlying acoustic pipes, indicates leakage, thus major faults have been acting as conduits or leaking faults for gases and pore fluids migrate upwards along the faults. These leakages related to the identified paleo-surface expression of the Kai Formation, including the identified pockmarks, and may also relate to seabed depression. This may suggested to form by inducing of sediment deformation and gas accumulation at the top of Kai Formation. According to Gay et al. (2012) suggested that the deformation of sediment gradually increases towards the axis of the vertical migration. The next phase of pipe evolution may collapse, and then forming a depression at seafloor, as narrow, bend-down of high amplitude reflections in strata below the seafloor observed.

The overpressure development in the Vøring Basin caused by loading of early Naust sediments may have resulted in polygonal faulting and dewatering. The biogenic oozes of the Miocene succession could be the main sources of biogenic methane though chimney-like structures and polygonal faults along with additional thermogenic component from deeper sources, suggested by Chand et al. (2011).

5.2.3 Timing of circular forms evolution

The Miocene ooze in the Brygge and Kai formations have extremely low density, and is usually associated with pore fluid overpressure. Van Rensbergen et al. (2003) has found that this is a common location where overpressures could developed; due to the large sediment supply and/or that this is a region of compressional tectonic stresses. High pore-pressure can cause fluidization and stimulate sediment mobilization. According to well data information from NPD (2007) the reservoir sand in the upper Cretaceous Springar Formation was a sand unit, which could be a potential hydrocarbon reservoir in the study area. This could suggest that there was a source of methane for the circular forms, especially type 3 circular form.

I addition, Chand et al. (2011) suggested that the overpressure development in the Vøring Basin was caused by loading of early Naust sediments, resulting in polygonal faulting and dewatering moving in an upward direction. This support the hypothesis that the biogenic oozes of the Miocene succession could be the main sources of biogenic methane though acoustic pipes and polygonal faults along with additional thermogenic component from deeper sources.

Type 3 circular form

In the study area, the sediment remobilization was linked to vertical fluid migration from an underlying source. This could be observed from the type 3 circular forms. This type could have been formed by sediment remobilization during late Paleocene to early Oligocene time (Fig 5.2.2 c). The vertical fluid migration into zones at the top of the Kai Formation, where clusters of high amplitude anomalies were formed, is interpreted to be a second phase of fluid migration and occurred in late Pliocene (Fig 5.2.1 d). The remigration of gas to some degree parallel to the timing of gas generation, as suggested by Hansen et al. (2000). Type 3 includes the accumulation of bright spots, indicating the presence of hydrocarbons, and this type also represent the best indication of vertical fluid migration (Fig 5.2.1 d).

Type 1 circular form should be formed at approximately late Palaeocene-early Eocene (~55 Ma) from sill intrusions (Fig 5.2.1 a), which intruded the Cretaceous Vøring and Møre basins during this time (Brekke 2000; Svensen et al., 2004; Lundin et al. 2013). Hydrothermal vent complexes correspond to capable for vertical fluid migration, was caused by gas methane

releasing and fluid expulsion from the metamorphic aureoles (Svensen et al., 2004; Aarnes et al., 2015). The restricted vertical movement of fluid and sediments are approximately located in the early Oligocene time, observed by no any evidence of fluid migration above type 1 circular form.

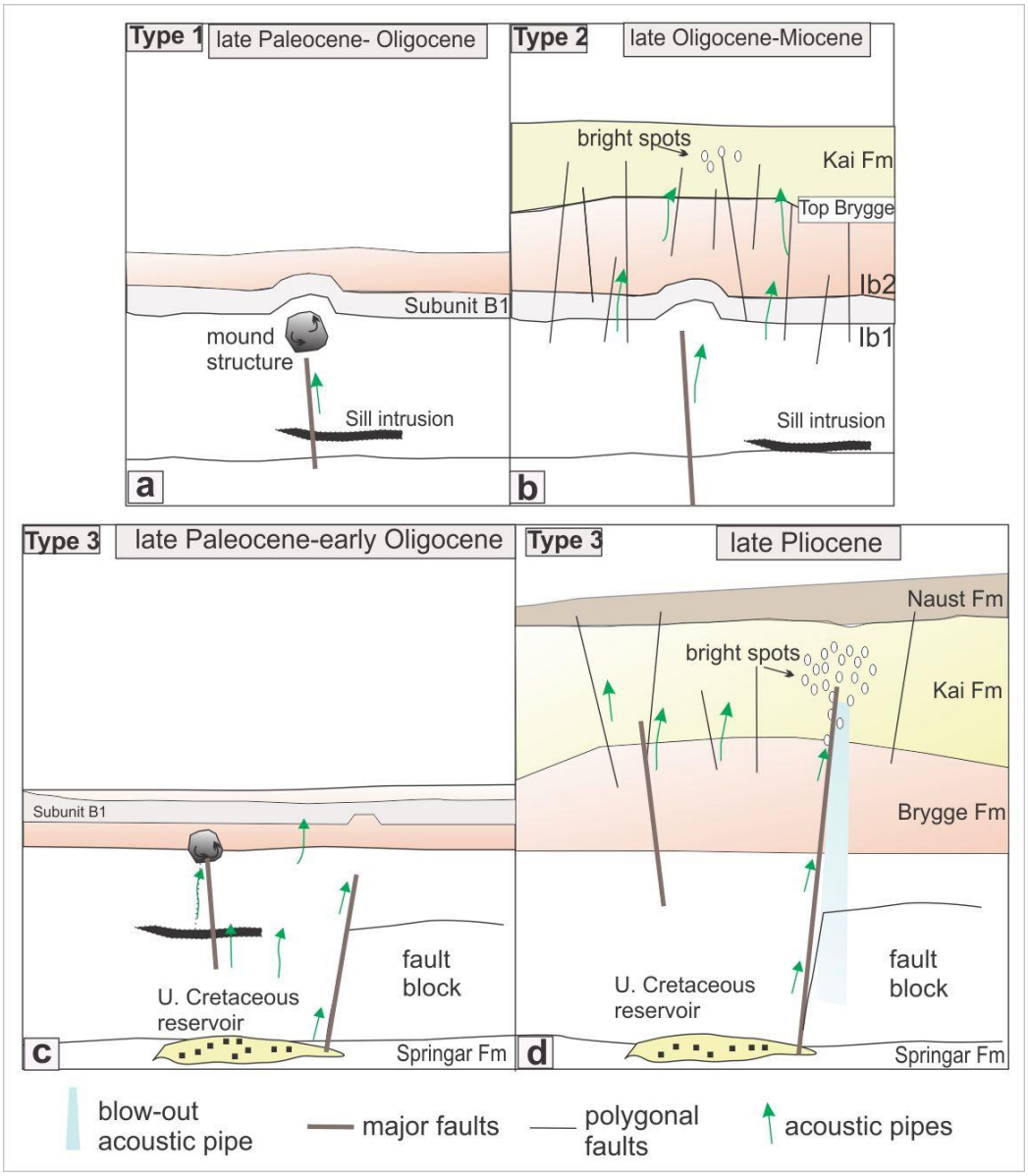

Figure 5.2.1: *Summary illustration showing the origin of the different types of circular forms in relationship to fluid migration the study area.* ***a)*** *Type 1 was related to mound structure development, caused by sill intrusion.* ***b)*** *Type 2 was caused by overpressure and fluid expulsion of the polygonal fault system.* ***c)-d)*** *Type 3 represent sediment remobilization in the same time as type 2, and then remigration occurred in the late Pliocene time, caused by overloading of the sediments of the Naust Formation*

Type 2 circular forms are interpreted to be related to underlying mound structures, as well as type 1, which were formed by fluid and sediment mobilization of Eocene sediments, possible caused by fluid migration along deeper major faults (Fig 5.2.1 a, b). These two types could be formed in the same time or after sill and dyke intrusions. Svensen et al. (2004) suggested that the formation of fluid and gas releasing have been occurred shortly, approximately in tens of years after the emplacement of sill intrusions. However, type 2 circular forms have been continued to next stage of fluid migration, as acoustic pipes formed beside. These evidences should be affected by overpressure and fluid expulsion of polygonal fault system within the overlying Kai Formation. Type 2 circular forms should be formed at approximately late Oligocene - Miocene time (Fig 5.2.1 b).

5.2.4 Soft sediment deformation and surface anomalies

Pockmarks were observed in the northern part of the study area, located at the top of the Kai Formation surface, interpreted as paleo-seafloor pockmarks. These pockmarks have a typically diameter of hundreds of metres, and are tens of metres deep. They are located mainly near the clusters of high amplitude anomalies, and some pockmarks are located above or in the vicinity of polygonal faults. Løseth et al. (2009) suggested that pockmarks are generally formed in soft fine-grained sediments by a leakage of gas and/or fluid into the water column. Ligtenberg (2005) however, suggested that pockmarks are not necessary located directly above a prospective reservoir. Because hydrocarbons and/or pore water can migrate over longer distances from deeper part of the basin to shallower levels fluids may migrate upward along fault and/or flanks of diapirs to reach the seabed where pockmark may be formed if fluid flux is vigorous enough.

In summary, this suggest that the pockmarks in the northern part of the study area were formed mainly near the accumulation of gas and fluid in the Kai Formations, and linked to gas and/or fluid migration from deeper strata. The pockmarks were likely formed due to fluid expulsion though polygonal faults in the Kai Formation. There was a few pockmarks spread around in the middle and southern part, while polygonal faults of high intensity play a major role in this area. This may suggest that the location of pockmarks could be strongly related to the clusters of high amplitude anomalies and major faults, rather than polygonal faults. However, the development and distribution of pockmarks in the study area in relationship to

fault and fractures is generally difficult to explain, due to absence of seismic evidence of the continuation of these fault and fractures in the shallow sediment succession.

5.2.5 A model for fluid migration

A model for fluid migration in the study area is created based on the observation and interpretation from 3D seismic data. Circular forms, pockmarks and seismic signatures are here seen in relation to focussed fluid and/or gas migration (Fig 5.2.2). The model is relevant for the Gjallar Ridge area in the western part of the Vøring Plateau.

(i)Type 1 and 2 circular forms in the upper Brygge Formation was developed by fluid injection and sediment mobilization, which have associated by sill and dyke intrusion during Palaeocene and Eocene time; (ii) Mound structures are formed below type 1 circular forms; (iii) Acoustic pipes, polygonal faults located have been found beside, and above type 2 circular forms, with/without bright spots indication; (iv) Type 3 circular forms originated by sediment mobilization within Brygge Formation, and deeper level during late Paleocene to early Oligocene. A reactivation of vertical fluid and sediments migration upwards the Top Kai formation occurred during late Pliocene; (v) Acoustic pipes, chaotic reflection pattern, bright spots are totally types of bypass structures of fluid migration; (vi) Push down effect indicate to the area comprises high concentration of gaseous fluid, related to adjacent strata; (vii) Major fault from deep strata, and polygonal faults are present in the Brygge, Kai and lower Naust Formations act as a conduit, and (viii) Sea-bed depression at the seafloor surface and paleo-seafloor pockmarks represent a termination of migration pathway.

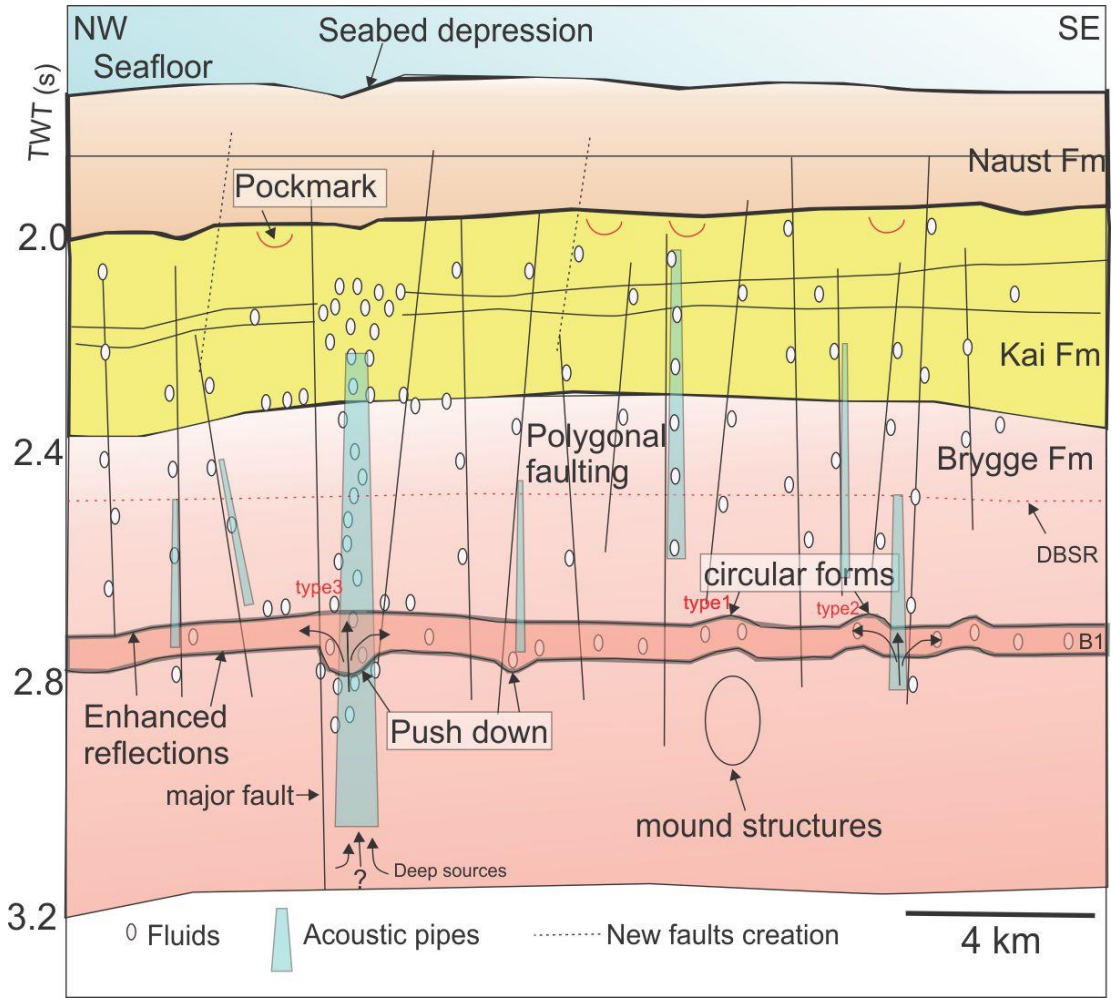

Figure 5.2.2: *A model of fluid migration showing an interconnection between deep geological structures, as circular forms, mound structures in the Brygge Formation and shallower fluid migration pathways.*

6 SUMMARY AND CONCLUSION

The upper part of the Brygge Formation and the Kai Formation have been studied on the western part of the Vøring Plateau, located on the northern part of the Mid-Norwegian continental shelf. The study is based on 3D seismic data and logs of well 6604/2-1. The main findings from this study are:

- The seismic reflection pattern of the subunits of the upper Brygge Formation (Oligocene to early Miocene) suggest a sedimentary environment influenced by a bottom current system.
- From the mid Miocene, the Kai Formation was dominated by ocean current influenced by erosion in the southern part and deposition in the northern part of the study area. The ocean current patterns was influenced by the local anticlinal highs (Helland-Hansen Arch and Modgunn Arch) near the study area.
- During the deposition of the uppermost part of the Kai Formation (late Miocene to early Pliocene), a change of the ocean current pattern led to erosion in the northern part, and deposition in the southeastern part of the study area.
- Seismic anomalies identified within the studied succession and are classified into three types.
- Type 1 and 2 circular forms developed in mud-dominated sediments and oozes in the upper Brygge Formation, and were affected by sediment mobilization and fluid migration along major faults from deeper levels.
- Type 3 circular forms was initially sediment mobilization within the Brygge Formation during late Paleocene to early Oligocene, related to fluid migration from deep strata during the Paleogene time. A second phase of sediments remobilization and vertical fluid migration upward into the top of the Kai Formation occurred in the late Pliocene.
- The polygonal faults in the study area associated with ooze-rich sediments are interpreted to have caused fluid expulsion and major overpressure during the rapid deposition of Naust Formation.

- Paleo-seafloor pockmarks formed mainly by fluid migration along deep major faults, together with fluid expulsion from the formation of polygonal faults and probably rapid deposition of the Naust Formation.

7 REFERENCES

Aarnes, I., Planke, S., Trulsvik, M., & Svensen, H. (2015). Contact metamorphism and thermogenic gas generation in the Møre and Vøring basins, offshore Norway, during the Paleocene-Eocene thermal maximum. *Journal of the Geological Society*, 172, 588-598.

Andreassen, K., Laberg, J., & Vorren, T. O. (2008). Seafloor geomorphology of the Barents Sea and its glaci-dynamic implication. *Geomorphology*, 97 (1-2), 157-177.

Andreassen, K., Nilssen, E., & Ødegaard, C. (2007). Analysis of shallow gas and fluid migration within the Plio-Pleistocene sedimentary succession of the SW Barents Sea continental margin using 3D seismic data. *Geo-Mar Lett*, 155-171.

Arntsen, B., Wensaas, L., Løseth, H., & Hermanrud, C. (2007). Seismic modeling of gas chimneys. *Geophysics*, 5, 251-259.

Berndt, C., Bunz, S., & Mienert, J. (2003). Polygonal fault ysytems on the mid-Norwegian margin: a long term source of fluid flowSubsurface Sediment Mobilization. In P. Van Rensbergen, R. R. Maltman, A.J., & C. K. Morley (Eds.), *Subsurface Sediment Mobilization* (pp. 283-290). London: Geological Society.

Brekke, H. (2000). The Tectonic Evolution of the Norwegian Sea Continental Margin with the Emphasis on the Voring and More Basins. *Geological Society Special Publications*, 167, 327-378.

Brown, A. (1999). Interpretation of three-dimentional seismic data, 5th. *The American Association of Petroleum Geologist and the Society of Exploration Geopgysicists*(AAPG memoir 42, SEG investigations in geophysics, 9, 233-307.

Bryn, P., Berg, K., Forsberg, C., Solheim, A., & Kvalstad, T. J. (2005). Explaining the Storegga Slide. *Marine and Petroleum gology*, 22, 11-19.

Cartwright, J., James, D., & Bolton, A. (2003). The genesis of polygonalt fault systems. . *Subsurface Sediment Mobilization. The Geological Society of London, 2003*(216), 223-243.

Chand, S., Rise, L., Knies, J., Haflidason, H., Hjelstuen, B., & Bøe, R. (2011). Stratigraphic development of the south Vøring margin (Mid-Norway) since early Cenozoic time and its influence on subsurface fluid flow. *Marine and Petroleum Geology*, 28, 1350-1363.

Collinson, J., Mountney, N., & Thompson, D. (2015). *Sedimentary Structure* (3. ed.). Dunedin Academic Press.

Dahlgren, K., Vorren, T. O., Stoker, M. S., Nielsen, T., Nygård, A., & Sejrup, H. P. (2005). Late Cenozoic prograding wedges on the NW European continental margin: their formation and relationship to tectonic and climate. *Marine and Petroleum Geology*, 22, 1089-1110.

Dowdeswell, J. A., Ottesen, D., Rise, L., & Craig, J. (2007). Identification and preservation of landforms diagnostic of past ice-sheet activity on continental shelves from three-dimentional seismic evidence. *Geology*, 35, 359-362.

Eidvin, T., Bugge, T., & Smelror, M. (2007). The Molo Formation, deposited by coastal progradation on the inner Mid-Norwegian continental shelf, coeval with the Kai Formation to the west and the Utsira Formation in the North Sea, *Norwegian Journal Of Geology*, 87, 75-142.

Eidvin, T., Riss, F., & Rasmussen, E. S. (2014). Oligocene to LOwer Plitocene deposits of the Norwegian continental shelf, Norwegian Sea, Svalbard, Denmark and their relation to the uplift of Fennoscandia. *Marine and Petroleum Geology*, 56, 184-221.

Evans, D., McGiveron, S., McNeill, A. E., Harrison, Z. H., Østmo, S. R., & Wild, J. (2000). Plio-Pleistocene deposits on the mid-Norwegian margin and their impilcations for late Cenozoic uplift of the Norwegian mainland. *Global and Planetary Change*, 24, 233-237.

Faleide, J. I., Bjørlykke, K., & Grabrielsen, R. H. (2015). Geology of the Norwegian Continental Shelf. In B. K. (Ed.), *From Sedimentary Environments to Rock Physics* (pp. 603-637). Berlin: Springer-Verlag Berlin Heidelberg.

Faleide, J., Tsikalas, K., Breivik, A. J., Mjelde, R., Ritzmann, O., Engen, Ø., . . . Eldholm, O. (2008). Structure and evolution of the continental margin off Norway and Barents Sea. *Episodes*, 31(1), 82-91.

Gay, A., & Berndt, C. (2007). Cessation/reactivation of polygonal faulting and effects on fluid flow in the Vøring Basin, Norwegian Margin. *Journal of the Geological Society, London*, 164, 129-141.

Gay, A., Mourgues, R., Berndt, C., Bureau, D., Planke, S., Laurent, D., . . . Loggia, D. (2012). Anatomy of a fluid pipe in the Norway Basin: Initiation, propagation and 3D shape. *Marine Geology*, 333-334, 75-88.

Hansen, B., & Østerhus, S. (2000). North Altlantic-Nordic Sea exchanges. *Progress in Oceanography*, 45, 109-208.

Henriksen, S., & Vorren, T. (1996). Late Cenozoic sedimentation and uplift history on the mid-Norwegian continental shelf. *Global and Planetary Change*, 12(1-4), 171-199.

Hjelstuen, B. O., Sejrup, H. P., Haflidason, H., Nygård, A., Ceremicola, S., & Bryn, P. (2005). Late Cenozoic glacial history and evolution of the Storegga Slide area and adjacent slide flank regions, Norwegian continental margin. *Marine and Petroluem Geology*, 22, 57-59.

Hjelstuen, B., Eldholm, O., & Skogseid, J. (1999). *Cenozoic evolution of the northern Vøring margin*, pp. 1792-1807.

Hjelstuen, B., Haflidason, H., Kuijpers, A., Nygård, A., Dahlgren, K., Praeg, D., . . . Dahlgren, T. (2005). Pleistocene glacial history of the NW European continental margin. *Marine and Petroleum Geology*, 22, 1111-1129.

Hjelstuen, B., Sejrup, H., Haflidason, H., Berg, K., & Bryn, P. (2004). Neogene and Quaternary depositional environments on the Norwegian continental margin, 62 degrees N- 68 degrees N. *Marine Geology*, 213(1-4), 257-276.

Jordt, H., Thyberg, B., & Nøttvedt, A. (2000). Cenozoic evolution of the central and the northern North Sea with focus on differential vertical movement of the basin floor and surrounding clastic source areas. In A. Nøttvedt (Ed.), *Dynamics of the Norwegian Margin* (pp. 219-243). Oxford: The Alden Press.

Laberg, J., & Vorren, T. (2000). The Trænadjupet Slide, offshore Norway- morphology, evacuation and triggering mechanisms. *Marine Geology*, 171, 95-114.

Laberg, J., Dahlgren, K., & Vorren, T. (2005a). The Eocene-late Pliocene paleoenvironment in the Vøring Plateau area,. Norwegian Sea- paleoceanographic implications. *Marine Geology*, 214 (1-3), 269-285.

Laberg, J., Stoker, M. S., Dahlgren, K., de Haas, H., Haflidason, H., Hjelstuen, B. O., . . . Ceramicola, S. (2005b). Cenozoic alongslope processes and sedimentation on the NW European Atlantic margin. *Marine and Petroleum Geology,* 22(9-10), 1069-1088.

Løseth, H., & Henriksen, S. (2005). A Middle to Late Miocene compression phase along the Norwegian passive margin. *In: Dorè, A.G., Vining, B.A., (Eds.), Petroleum Geology: North-West Europe snd Global Perspectives-proceedings of the 6th Petroleum Conference*, 845-859.

Løseth, H., Gading, M., & Wensaas, L. (2009). Hydrocarbon leakage interpreted on seismic data. *Marine and Petroleum Geology*, 26, 1304-1319.

Løseth, H., Wensaas, L., Arntsen, B., Hanken, N., Basire, C., & Graue, K. (2011). 1000 m long gas blow-out pipes. *Marine and Petroleum Geology*, 28, 1047-1060.

Mangerud, J., Gyllencreutz, R., Lohne, Ø., & Svendsen, J. I. (2011). Glacial History of Norway. *Developments in Quaternary Science*, 15, 279-297.

Mitchum, R. M., Vail, P. R., & Sangree, J. B. (1977). Seismic Stratigraphy and Global Changes of Sea Level, Part 6: Stratigraphic Interpretation of Seismic Reflection Patterns in Depositional Sequence. In C. E. Payton (Ed.), *Seiemic Stratigraphy-applications to hydrocarbon exploration* (pp. 117-133). The American Association of Petroleum Geologists.

Mogensen, T. E., Nyby, R., Karpuz, R., & Haremo, P. (2000). Late Cretaceous and Tertiary structural evolution of the northeastern part of the Vøring Basin, Norwegian Sea. In A. Nøttvedt (Ed.), *Dynamics of the Norwegian Margin* (pp. 379-398). Oxford: The Alden Press.

Neagu, R., Cartwright, J., Davies, R., & Jensen, L. (2010). Fossilisation of a silica diagenesis reaction front on the mid-Norwegian margin. *Marine and Petroleum Geology,* 27, 2141-2155.

Neilsen, T., Knuyz, P. C., & Kuijpers, A. (2008). Seismic Expression of Contourite Depositional System. In *Developments in Sedimantology* (pp. 301-321). Øster Voldgade, Copenhagen, Denmark: Gelogical Survey of Denmark and Greenland (GEUS).

Nichols, G. (2009). *Sedimentalogy and Stratigraphy* (2. ed.). Backwell, Oxford.

Nygård, A., Sejrup, H., Haflidason, H., & Bryn, P. (2005). The glacial North Sea Fan, southern Norwegian Margin: architecture and evolution from the upper continental slope to the deep-sea basin. *Marine and Petroleum Geology,* 22, 71-84.

Ottensen, D., Leif, R., Andersen, E. S., Bugge, T., & Eidvin, T. (2009). *Geological evolution of the Norwegian continental shelf between 61 N and 68 N during the last 3 million years.Norwegian Journal of Geology,* 89, 251-265.

Planke, S., & Alvestad, E. (1999). Seismic volcanostratigraphy of the extrusive breakup complexes in the northeast Atlantic: Implications from ODP/DSDP Drilling. *Scientific Resaults*.

Rebesco, M., & Stow, D. (2001). Seismic expression of contourites and related deposits. *Marine geophysical Reseaches,* 22, 303-308.

Reynolds, J. M. (2011). Seismic Reflection Surveying. In *An introduction to applied and Environmental Geophysics* (pp. 217-286). Oxford, UK: Wiley-Blackwell.

Rider, M., & Kennedy, M. (2011). *The Geological Interpretation of Well Logs* (3. ed.). Glasgow: Bell and Bain.

Riis, F., Berg, K., Cartwright, J., Eidvin, T., & Hansch, K. (2005). Formation of large, crater-like evacuation structures in ooze sediments in the Norwegian Sea. Possible implications for development of the Storegga Slide. *Marine and Petroleum Geology 22*, 257-273.

Rise, L., Chand, S., Hjelstuen, B. O., & Bøe, R. (2010). Late Cenozoic geological development of the south Vøring margin, mid-Norway. *Marine and Petroleum Geology*, 27, 1789-1803.

Rise, L., Ottesen, D., Berg, K., & Lundin, E. (2005). Large-scale development of the mid-Norwegian margin during the last 3 million years. *Marine and Petroleum Geology*, 22, 33-44.

Sangree, J., & Widmier, J. (1977). Seismic Stratigraphy and Global Changes of Sea Level, Part 9. In C. Payton (Ed.), *Seismic Interpretation of Clastic Deposition Facies* (pp. 165-183). Oklahoma: The American Association of Petroleum Geologists.

Sejrup, H., Hjelstuen, B. O., Dahlgren, K., Haflidason, H., Kuijpers, A., Nygård, A., . . . Vorren, T. O. (2005). Pleistocene glacial history of the NW European continental margin. *Marine and Petroleum Geology*, 22, 1111-1129.

Sheriff, R. E. (1977). Limitations on Resolution of Seismic Reflection and Geologic Detail Derivable from Them. In C. E. Payton (Ed.), *Seiemic Stratigraphy-applications to hydrocarbon exploration* (pp. 3-14). The American Association of Petroleum Geologists.

Sheriff, R. E. (1985). Aspects of Seismic Resolution. *Seismic Stratigraphy II: An Integrated Approach To Hydrocarbon Exploration*, pp. 1-13.

Solheim, A., Berg, K., Forsberg, C. F., & Bryn, P. (2005). The Storegge Slide complex: repetative large scale sliding with sililar cause and development. *Marine and Petroleum Geology*, 22, 97-107.

Stoker, M., Hoult, R., Nielsen, T., Hjelstuen, B., Laberg, J., Shannon, P., . . . MaDonnell, A. (2005b). *Sedimentary and oceanographic responses to early Neogene compression on the NW European margin*, 22, 1031-1044.

Stoker, M., Praeg, D., Hjelstuen, B., Laberg, J., Nielsen, T., & Shannon, P. (2005a). Neogene stratigraphy and the sedimentary and oceanographic development of the NW European Atlantic margin. *Marine and Petroleum Geology*, 22, 977-1005.

Storvoll, V., Bjørlykke, K., & Mondol, N. (2006). Velocity-depth trends in Mesozoic and Cenozoic sediments from the Norwegian Shelf. *AAPG Bulletin*, 90, 1145-1148.

Stow, D., Faugères, J., H., J., Pudsey, C., & Viana, A. (2002). Bottom currents, contourites and deep-sea sediment drifts: current state-of-the-art. *The Geological Society of London*, 22, 7-20.

Stow, D., Hernàndez-Molina, F., Llave, E., Sayago-Gil, M., Dìaz del Rìo, V., & Branson, A. (2009). Bedform-velocity matrix: The estimation of bottom current velocity from bedform observations. *The Geological Society of America*, 37, 327-330.

Svensen, H., Planke, S., Malthe-Sørenssen, A., Jamtveit, B., Myklebust, R., Eidem, T., & Rey, S. (2004). Release of methane from a volcanic basin as a mechanism for initial Eocene global warming. *Nature*, 429, 542-545.

Vail, P. R. (1987). Seismic stratigraphy interpretation using seismic sequence, Part 1. In A. W. Bally (Ed.), *Atlas of Seismic Stratigraphy* (pp. 1-10). AAPG studies in Geology No.27, Vol.1.

Vorren, T. O. (2003). Subaquatic Landsystems: Continental margins. In D. J. Evans (Ed.), *Glacial Landsystems* (pp. 289-312). New York: Routledge.

8 APPENDIX

8.1 The resolution of the data

Top of the Kai formation

Wavelength: $\lambda = \frac{V}{f} = \frac{2{,}400\ m/s}{38.16\ Hz} = 62.89$ m.

Vertical resolution: $\frac{\lambda}{4} = \frac{62.89\ m}{4} = 15.72$ m.

Fresnel zone before migration: $r(f) = \frac{V}{2}\sqrt{\frac{t}{f}} = \frac{2{,}400\ m/s}{2}\sqrt{\frac{1.959\ s}{38.16\ Hz}} = 272$ m.

Fresnel zone after migration: $Hr = \frac{\lambda}{4} = \frac{V}{4f} = \frac{2{,}400\ m/s}{4*38.16\ Hz} = 15.72$ m.

The vertical resolution of the top of the Kai formation is 15.72 m., the radius of the Fresnel zone before migration is 272 m. and the radius of the Fresnel zone after migration is 15.72 m.

Base of the Kai formation

Wavelength: $\lambda = \frac{V}{f} = \frac{2{,}200\ m/s}{40.46\ Hz} = 54.37$ m.

Vertical resolution: $\frac{\lambda}{4} = \frac{54.37\ m}{4} = 13.6$ m.

Fresnel zone before migration: $r(f) = \frac{V}{2}\sqrt{\frac{t}{f}} = \frac{2{,}200\ m/s}{2}\sqrt{\frac{2.187\ s}{40.46\ Hz}} = 255.7$ m.

Fresnel zone after migration: $Hr = \frac{\lambda}{4} = \frac{V}{4f} = \frac{2{,}200\ m/s}{4*\ 40.46\ Hz} = 13.6$ m.

The vertical resolution of the base of the Kai formation is 13.6 m, the radius of the Fresnel zone before migration is 255.7 m, and the radius of the Fresnel zone after migration is 13.6 m.

Intra Brygge 2

The velocity can be calculated from the applying equation 3.5 by taking the slowness value from the P-sonic log.

$$\text{Velocity ft/sec} = \frac{1}{\Delta t\mu s/ft * 10^{-6}} \qquad (3.5)$$

So for a Δt = 158.19 μs/ft from the P-sonic log: Velocity = $\frac{1}{158.19 * 10^{-6}}$ = 6,322 ft/sec

= 6,322 / 3.281 = 1,927 m/s

Wavelength: $\lambda = \frac{V}{f} = \frac{1{,}927\ m/s}{41.45\ Hz}$ = 46.5 m.

Vertical resolution: $\frac{\lambda}{4} = \frac{46.5\ m}{4}$ = 11.63 m.

Fresnel zone before migration: $r(f) = \frac{V}{2}\sqrt{\frac{t}{f}} = \frac{1{,}927\ m/s}{2}\sqrt{\frac{2.583\ s}{41.45\ Hz}}$ = 240.52 m.

Fresnel zone after migration: $Hr = \frac{\lambda}{4} = \frac{V}{4f} = \frac{1{,}927\ m/s}{4 * 41.45\ Hz}$ = 11.62 m.

The vertical resolution of the intra Brygge 2 is 11.63 m, the radius of the Fresnel zone before migration is 240.52 m, and the radius of the Fresnel zone after migration is 11.62 m.

Intra Brygge 1

The velocity can be calculated from the applying equation 3.5 by taking the slowness value from the P-sonic log.

$$\text{Velocity ft/sec} = \frac{1}{\Delta t\mu s/ft * 10^{-6}} \qquad (3.5)$$

So for a Δt = 144.37 μs/ft from the P-sonic log: Velocity = $\frac{1}{144.37 * 10^{-6}}$ = 6,927 ft/sec

= 6,927 / 3.281 = 2,111 m/s

Wavelength: $\lambda = \frac{V}{f} = \frac{2{,}111\ m/s}{45.39\ Hz}$ = 46.51 m.

Vertical resolution: $\frac{\lambda}{4} = \frac{46.51\ m}{4}$ = 11.63m.

Fresnel zone before migration: $r(f) = \frac{V}{2}\sqrt{\frac{t}{f}} = \frac{2{,}111\ m/s}{2}\sqrt{\frac{2.648\ s}{45.39\ Hz}}$ = 254.94 m.

Fresnel zone after migration: $Hr = \frac{\lambda}{4} = \frac{V}{4f} = \frac{2{,}1111\ m/s}{4 * 45.39\ Hz}$ = 11.63 m.

The vertical resolution of the intra Brygge 1 is 11.63 m, the radius of the Fresnel zone before migration is 259.94 m, and the radius of the Fresnel zone after migration is 11.63 m.

8.2 Sediment wave at the top oof the Kai Formation surface

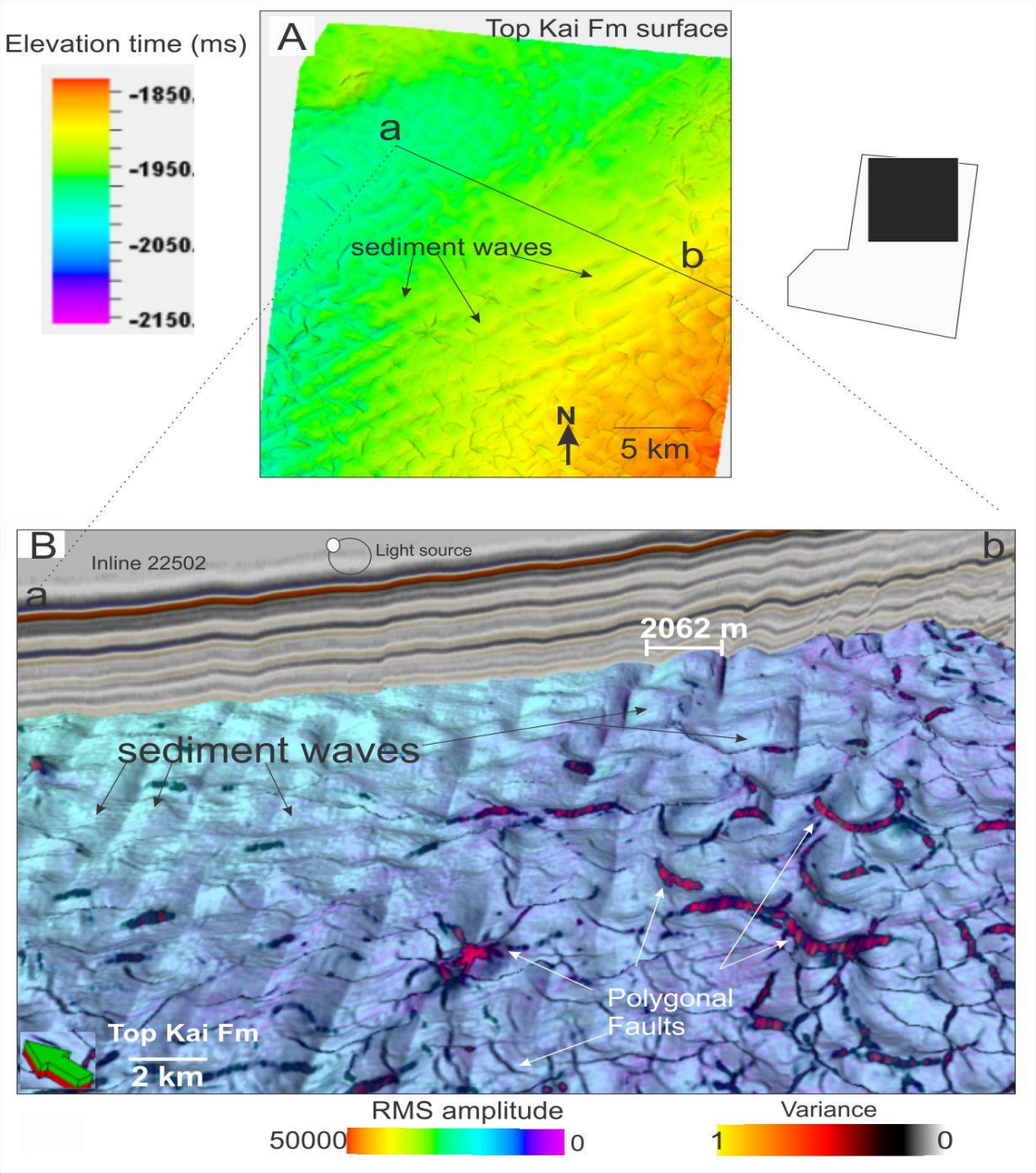

Figure 8: *The top of the Kai Formation shown* ***A)*** *A Isochrone map of Top Kai Formation showing depth and morphology of the paleo-surface (ms: millisecond TWT), vertical exaggeration 7.5, the depositional features are observed, and interpreted as sediment waves.* ***B)*** *A combination between a vertical seismic section and a RMS amplitude map with a superimposed variance map showing the development of faults penetrate upwards the overlying of sediment waves.*